Selective Homogeneous Catalysis in Asymmetric Synthesis

Fristrup, Peter

Publication date:
2006

Document Version
Publisher's PDF, also known as Version of record

Peter Fristrup

Selective Homogeneous Catalysis in Asymmetric Synthesis

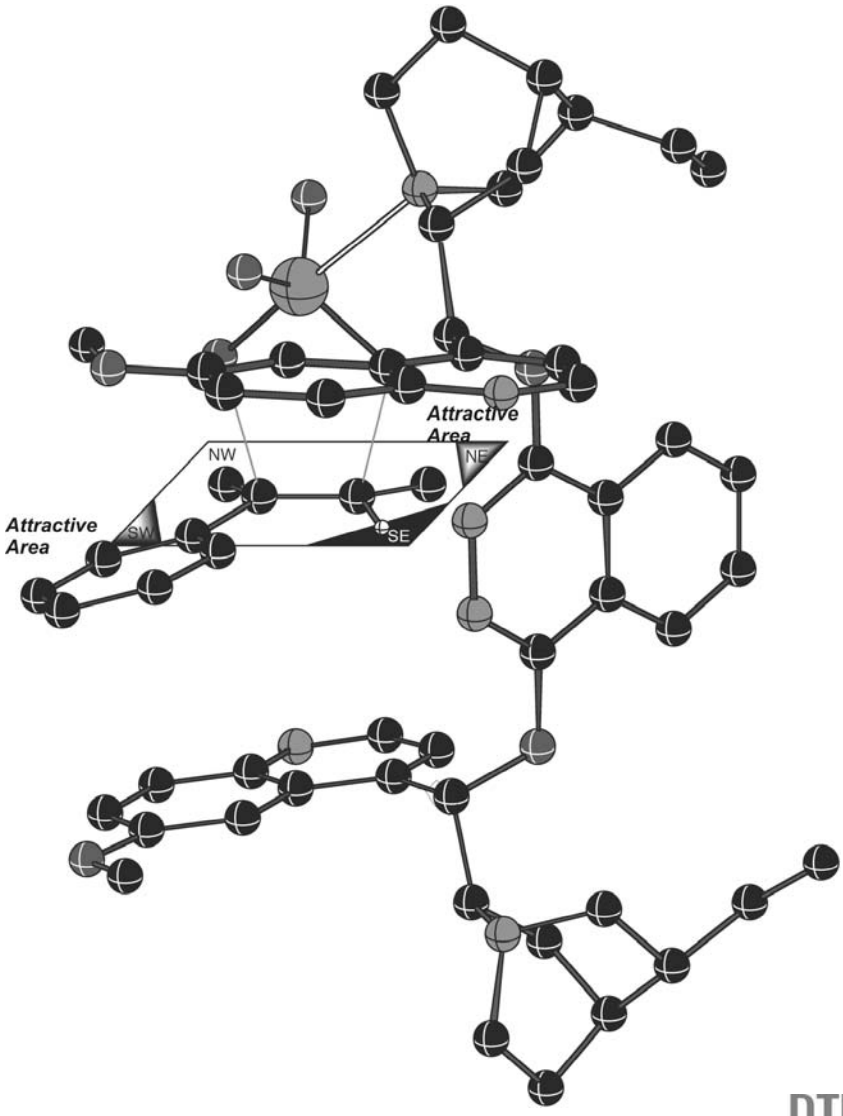

Ph. D. Thesis

DTU, Lyngby, February 2006.

Cover: Illustration of the new mnemonic device for prediction of absolute configuration in the osmium-catalyzed asymmetric dihydroxylation. A transition state structure incorporating one of the substrate probes is used to illustrate the molecular structure.

Peter Fristrup

Selective Homogeneous Catalysis in Asymmetric Synthesis

Ph.D. Thesis, February 2006

Department of Chemistry

Technical University of Denmark

Preface

This thesis is submitted in candidacy for the Ph.D. degree from the Technical University of Denmark (DTU). The work presented herein has been carried out at the Department of Chemistry, DTU from March 2003 to February 2006 under the joint supervision of Assoc. Prof. Per-Ola Norrby and Prof. David Tanner. This Ph.D. scholarship was sponsored by DTU. Along with the thesis are included six papers as appendices. This thesis is based on the work reported in the scientific papers, which in some parts of the thesis have necessitated some repetitions. Additional papers or manuscripts to which I have contributed during my education is listed in section 1.3 (Additional Publications).

First and foremost, I would like to thank my two supervisors for their exceptional patience with me. I started out working with them four years ago, and back then I was a "rookie" both in the lab and with computational chemistry, but in spite of this, they always allowed me to make my own mistakes – in some cases more than once...

In particular, I admire Per-Ola's ability to constantly come up with new ideas – something that I found especially pleasing in the first couple of years and perhaps not quite as pleasing here in the writing process. Also, David's unparalleled efficiency in the writing process is highly admirable, and with just a little bit more time we could actually have finished up all of Per-Ola's projects!

As part of the Ph.D. education I have been on two external stays. In October 2004 a one-month external stay took place at Ecole Normale Superieure, Departement de Chimie, Paris, France under the supervision of Prof. Anny Jutand. I am indebted to the European Science Foundation for giving financial support by accepting the visit as a "Short Term Scientific Mission" (STSM) under the COST D24 action.

In June-July 2005 a two-month external stay took place at Organic Chemistry 1, Lund University, Sweden under the supervision of Kenneth Wärnmark. On both occasions the students and supervisors were excellent partners in theoretical discussions and with regard to practical issues.

I would like to thank Sebastian Le Quement for sharing lab with me in the "early days", teaching me the tricks of practical organic synthesis. Furthermore, Sebastian did a great job working together with me on the Hammett study of the Heck reaction. Also a warm thank to Sebastian's successor, Mårten Ahlquist, who has been a never-ending source of inspiration with regards to the chemistry of palladium, a critical reviewer of my writing, and in particular for the team-work we have carried out recently. My "office-mate" Henriette Holm is credited for always keeping up a good spirit, for her organizing abilities in general, and for discussions on the Mn(salen)-catalyzed epoxidation. The remaining Ph.D. students and one Post. Doc. are

acknowledged for many interesting scientific discussions and for the nice breakfast and afternoon-cake sessions. A special thanks to the members of the Tanner group in which I have participated as a "guest member" when performing synthetic chemistry.

I have been very fortunate to have talented, skilful and hard-working students with whom I have collaborated on various projects throughout the last three years. Maria Vinther Juhl, Pernille B. Tofteng, Gitte Holm Jensen, Marie Louise Nygaard Andersen, Thomas Jensen, Jakob Hoppe, and Brian B. Dideriksen I enjoyed working together with all of you!

I would like to thank all the people at the department and in building 201 in particular for making my time here enjoyable. Last, but not least I want to express my deepest gratitude to my wife for always believing in me.

Peter Fristrup

DTU, Lyngby, February 21st, 2006

Abstract

The subject of this thesis is selectivity in homogeneous asymmetric transition metal-catalyzed reactions. Four different reactions within organic chemistry have been studied by kinetic measurements, computational chemistry (modelling) or both of them in parallel.

A Hammett study was performed on the Heck reaction between phenyl triflate and a series of *para*-substituted styrenes. A linear correlation was obtained only for substitution in the α-position, where the developing positive charge is in direct conjugation with the group in the *para*-position.

The palladium-catalyzed allylic alkylation has been the subject of several smaller projects. With bidentate nitrogen-based ligands experimental selectivities were used as a benchmark for a computational study. When a large enough part of the experimental system was included, the selectivity could be predicted with reasonable accuracy.

When using PPh_3 as ligand, the effect of chloride has been the subject of both experimental and computational studies. The effect on the regioisomeric distributions resulting from allylic alkylation of a branched starting material was investigated experimentally and could be rationalized computationally. A thorough computational study succeeded in explaining the observed results, although other significant results were also obtained during this study. Finally, an intramolecular reaction was studied computationally, and the rate increase observed under phase transfer catalysis conditions could be related directly to the absence of Na^+. This explanation was supported by new experimental investigations.

A kinetic study was conducted on the Mn(salen)-catalyzed asymmetric epoxidation reaction employing a series of methyl-substituted styrenes. The observed reactivities and selectivities could be rationalized by the existence of two different approach vectors, which are both favoured for these substrates. In addition, the study could serve as a testing ground for the development of new theoretical methods.

The reactivity and selectivity in the osmium-catalyzed asymmetric dihydroxylation was studied using a series of twelve "substrate-probes", which were designed and synthesized specifically for this purpose. Both the stoichiometric reaction with OsO_4 in toluene and the more environmentally benign catalytic reaction in a two-phase system were studied. The obtained experimental results were in good agreement with predictions based on computational modelling of the transition states. Visualization of the determined transition states allowed for the construction of the new mnemonic device for prediction of absolute configuration, which also included a mapping of the important features onto an overlaid transition state.

Dansk resumé

Emnet for denne afhandling er selektivitet i homogene asymmetriske overgangsmetal-katalyserede reaktioner. Fire forskellige reaktioner indenfor organisk kemi er blevet studeret ved kinetiske målinger, computer-baseret modellering eller en kombination af dem begge.

Et Hammett studie blev udført på Heck reaktionen mellem phenyl triflat og en række *para*-substituerede styrener. En lineær korrelation blev kun observeret for substitution i α-positionen, hvor den øgende positive ladning er i direkte konjugation med gruppen i *para*-positionen.

Den palladium-katalyserede allyliske alkylering har været underlagt en række mindre studier. Med bidentate nitrogen-baserede ligander er eksperimentelt observerede selektiviteter blevet brugt som benchmark for et computer-baseret modelleringsstudie. Når en tilstrækkelig stor del af det eksperimentelle system blev inkluderet, kunne selektiviteten i reaktionen forudsiges med god præcision.

Med PPh_3 som ligand blev effekten af chlorid-ioner studeret både eksperimentelt og med computer-baseret modellering. Den observerede effekt på fordelingen mellem de mulige regio-isomerer ved alkylering af tre allyliske acetater blev studeret eksperimentelt, og kunne forklares ved beregninger. Et grundigt beregningsstudie kunne forklare de observerede resultater, og desuden blev der opnået flere andre signifikante resultater i dette studie. Endelig blev også en intramolekylær reaktion studeret ved beregninger, og den observerede øgning af reaktionshastigheden under "phase transfer catalysis" blev forklaret udelukkende ved fravær af Na^+. Denne forklaring blev senere underbygget af nye eksperimentelle forsøg.

Et kinetisk studie af den Mn(salen)-katalyserede asymmetrisk epoxideringsreaktion blev udført på en serie af methyl-substituerede styrener. Den observerede reaktivitet og selektivitet kunne forklares ved eksistensen af to favoriserede reaktionsveje for disse substrater. Desuden kan det rapporterede studie være nyttigt som test ved udviklingen af nye teoretiske metoder.

Reaktiviteten og selektiviteten i den osmium-katalyserede asymmetriske dihydroxylering blev studeret med en serie af tolv alkener som blev specielt designet og syntetiseret til dette formål. Både den støkiometriske reaktion med OsO_4 i toluen samt det miljømæssigt mere fordelagtige katalytiske tofase system blev undersøgt. De opnåede eksperimentelle resultater var i god overensstemmelse med forudsigelser baseret på beregninger af de tilhørende "transition states". Visualisering af de beregnede "transition states" resulterede i konstruktionen af et nyt mnemoteknisk værktøj til forudsigelse af absolut konfiguration, som også inkluderer en af de beregnede "transition state" strukturer med de vigtigste fysiske interaktioner indikeret.

Contents

1.1 List of Abbreviations

AAA	Asymmetric Allylic Alkylation
Ac	Acetate
AD	Asymmetric Dihydroxylation
AQN	Antraquinone
B3LYP	Becke 3 parameter functional with Lee Yang Parr correlation functional
BINAP	2,2'-bis(diphenylphosphanyl)-1,1'-binaphthyl
BSA	*N*,*O*-Bis(trimethylsilyl)acetamide
Bu	Butyl
COST	European Cooperation in the field of Scientific and Technical Research
Cy	Cyclohexyl
DFT	Density Functional Theory
DHQ	Dihydroquinine
DHQD	Dihydroquinidine
DIOP	(2,2-dimethyl-1,3-dioxolane-4,5-diylbis(methylene)) bis(diphenylphosphane)
DME	Dimethoxyethane
DMF	Dimethylformamide
DMM	Dimethoxymethane
DMSO	Dimethylsulfoxide
DNA	Deoxyribonucleic Acid
DPPP	1,3-Bis(diphenylphosphino)propane
DTU	Technical University of Denmark
ECP	Effective Core Potential
EDG	Electron-donating Group
ee	Enantiomeric Excess
EWG	Electron-withdrawing Group
FID	Flame Ionization Detector
GB/SA	Generalized Born/Surface Area
GC	Gas Chromatography
GTO	Gaussian Type Orbital
HF	Hartree-Fock
HWE	Horner-Wadsworth-Emmons reaction
LAC	Ligand-Accelerated Catalysis
Me	Methyl
MM	Molecular Mechanics
MS	Mass Spectrometry
NMP	N-Methyl Pyrrolidine
NMR	Nuclear Magnetic Resonance
PB	Poisson-Boltzmann

PES	Potential Energy Surface
Ph	Phenyl
PHAL	Phthalazine
Pr	Propyl
PYR	Diphenylpyrimidine
Q2MM	Quantum to Molecular Mechanics (a method using QM to derive MM parameters for TS)
QM	Quantum Mechanics
SAD	Sharpless Asymmetric Dihydroxylation
SCF	Self-Consistent Field
SCRF	Self-Consistent Reaction Field
SEAM	a method for determining TS on the intersection between two force fields
STO	Slater Type Orbital
STSM	Short Term Scientific Mission
THF	Tetrahydrofuran
TON	Turnover Number
TS	Transition State
TSFF	Transition State Force Field
TST	Transition State Theory

1.2 Publications Included in Appendix

1. "Reactivity and Regioselectivity in the Heck Reaction - A Hammett Study of 4-Substituted Styrenes" Peter Fristrup, Sebastian Le Quement, David Tanner and Per-Ola Norrby *Organometallics* **2004**, *23*, 6160.
2. "Deconvoluting the Memory Effect in Pd-Catalyzed Allylic Alkylation; Effect of Leaving Group and Added Chloride", Peter Fristrup, Thomas Jensen, Jakob Hoppe, and Per-Ola Norrby, *submitted to Chem. Eur. J.*
3. "Surprisingly Mild Enolate-Counterion-Free Pd(0)-Catalyzed Intramolecular Allylic Alkylations" David Madec, Guillaume Prestat, Elisabetta Martini, Peter Fristrup, Giovanni Poli, and Per-Ola Norrby, *Org. Lett.* **2005**, *7,* 995.
4. "Probing Competitive Enantioselective Pathways Operating in the Jacobsen-Katsuki Epoxidation: A Kinetic Study of Methyl-substituted Styrenes" Peter Fristrup, Brian B. Dideriksen, David Tanner, and Per-Ola Norrby, *J. Am. Chem. Soc.* **2005**, *127,* 13672.
5. "Updating the Asymmetric Osmium-Catalyzed Dihydroxylation (AD) Mnemonic. Q2MM Modeling and New Kinetic Measurements" Peter Fristrup, David Tanner and Per-Ola Norrby, *Chirality*, **2003**, *15*, 360.
6. "Combining Q2MM Modeling and Kinetic Studies for Refinement of the Osmium-catalyzed Asymmetric Dihydroxylation (AD) Mnemonic" Peter Fristrup, Gitte Holm Jensen, Marie Louise Nygaard Andersen, David Tanner, and Per-Ola Norrby, *J. Organomet. Chem.* **2006**, *in press.*

1.3 Additional Publications

The following list of publications includes work carried out during the Ph.D. study which has not been included in the final thesis.

7. "A Nonradical Zinc-Barbier Reaction for Diastereoselective Synthesis of Vicinal Amino Alcohols" Lise Keinicke, Peter Fristrup, Per-Ola Norrby, and Robert Madsen, *J. Am. Chem. Soc.* **2005**, *127,* 15756.
8. "Direct Determination of Absolute Configuration of Methyl-Substituted Phenyloxiranes: A Combined Experimental and Theoretical Approach" Peter Fristrup, Peter R. Lassen, Christian Johannessen, David Tanner, Per-Ola Norrby, Karl. J. Jalkanen, and Lars Hemmingsen, *submitted to J. Phys. Chem. A.*.
9. "Direct Determination of Absolute Configuration: a Vibrational Circular Dichroism Study on Dimethyl-Substituted Phenyloxiranes Synthesized by Shi Epoxidation" Peter Fristrup, David Tanner, and Karl J. Jalkanen, *manuscript.*
10. "Theoretical Evidence for Low-Ligated Palladium(0): [Pd-L] as the Active Species in Oxidative Addition Reactions." Mårten Ahlquist, Peter Fristrup, David Tanner, and Per-Ola Norrby, *Organometallics* **2006**, *accepted.*

2 Introduction

This thesis revolves around selectivity – regioselectivity, diastereoselectivity or enantioselectivity. Why is there selectivity for a given reaction? How can the selectivity be determined as a function of the reaction mechanism? And, finally, how accurate is the determination when compared to experimental results? At present most computational investigations are carried out *after* the experimental investigation, which means they must be considered as *rationalizations*. An accurate *prediction* of the selectivity for a given reaction could be used to determine whether or not the reaction should be carried out, and can be considered to be the ultimate goal of computational chemistry.

The thesis is divided into two main parts, which both belong to the very "heart" of synthetic organic chemistry – palladium-catalyzed coupling reactions and transition metal-catalyzed, asymmetric oxidations. The first half is entitled Palladium-Catalyzed Coupling Reactions and consists itself of two separate chapters. The first of these concerns the Heck reaction (chapter 4.1), which is one of the Pd-catalyzed cross coupling reactions where incorporation of chirality is available. The second chapter in part concerns the palladium-catalyzed allylic alkylation (chapter 4.2), for which there exists a powerful asymmetric variant, and in this chapter several small projects and collaborations are described (chapters 4.3-4.6).

The second half of the thesis is devoted to transition metal-catalyzed asymmetric oxidations, with the Mn(Salen)-catalyzed epoxidation (chapter 5.1) and the Os-catalyzed dihydroxylation (chapter 5.2) as examples. The epoxidation reaction is studied experimentally by a kinetic study and the results are interpreted mechanistically. The dihydroxylation has been studied using a combination of kinetics and molecular modelling, which also allowed an evaluation and bench-marking of the computational method along with an improved understanding of the selectivity-determining features of the reaction.

To make the thesis interesting to a broader audience some of the most important basic concepts are introduced in chapter 3, including catalysis (chapter 3.1), chirality (chapter 3.2) and computational chemistry (chapter 3.6). In these introductory chapters, the Nobel Prize has been used as a light-beacon to select the most important achievements in the 20th century – interested readers are referred to the Nobel web site, where all Nobel laureates and their lectures are available.[1]

2.1 Outline of the thesis

The first part of the thesis is entitled "Basic Concepts" and consists of an introduction to catalysis with special emphasis on homogeneous, asymmetric reactions in organic chemistry. Some of the basic concepts in computational chemistry: Molecular mechanics, potential energy surfaces, molecular ensembles, quantum mechanics and density functional theory along with various ways of describing the effect of solvent will be introduced in this chapter.

2.1.1 Palladium-Catalyzed Coupling Reactions

This first half of the thesis with the title "Palladium-Catalyzed Coupling Reactions" consists itself of several chapters. Chapter 4 begins with a brief introduction to the most important palladium-catalyzed coupling reactions. In chapter 4.1 the Heck reaction is introduced with emphasis on the cationic, asymmetric version, and the motivation for conducting a Hammett study is given. The obtained kinetic results are discussed along with the implications for the mechanism of the cationic Heck reaction. The results have been published in paper 1.

In chapter 4.2 a general introduction to the palladium-catalyzed allylic alkylation is given with a discussion of the different ways of achieving asymmetric induction. The subject of chapter 4.3 is the regioselectivity of the nucleophilic addition, depending on the ligand used for palladium. A computational study was performed and compared to experimental results from the literature. In a co-operation with two students (Thomas Jensen and Jakob Hoppe) a mechanistic study was performed, which explored the influence of additional chloride ions and the results were rationalized by quantum mechanical calculations (paper 2). In chapter 4.4 those of the results which were most relevant to this thesis are presented, namely the effect of added chloride in the Pd-catalyzed allylic alkylation.

To further elucidate the effect of chloride, an extensive computational study has been conducted (chapter 4.5). The study focused on locating which step in the catalytic cycle was selectivity-determining, and furthermore elucidated the importance of the choice of model phosphine ligands on palladium.

In co-operation with Prof. Poli's group in Paris, a ring-closing Pd-catalyzed allylic alkylation has been studied (chapter 4.6). The results have been published in paper 3.

2.1.2 Transition Metal-Catalyzed Asymmetric Oxidations

A short introduction to transition metal-catalyzed asymmetric oxidations is given in chapter 5. The first chapter of this part of the thesis concerns the Mn(salen)-catalyzed epoxidation of unfunctionalized alkenes (chapter 5.1). An introduction to the reaction mechanism is given and the selection of kinetic study is motivated. The obtained kinetic results are discussed and the

implications for the general mechanism of the Mn(salen)-catalyzed epoxidation are commented upon. The results have been published (paper 4).

The investigation of the osmium-catalyzed, asymmetric dihydroxylation is reported in chapter 5.2. A kinetic study was performed employing stoichiometric amounts of OsO_4 in toluene along with calculations using a tailored molecular mechanics method (paper 5). In addition, two students (Gitte Holm Jensen and Marie Louise Nygaard Andersen) conducted a kinetic study using only catalytic amounts of osmium in a biphasic system. The two studies were compared to each other and to additional calculations and published together as paper 6.

Numbering of the compounds discussed in the text is restarted in each chapter, thus allowing a logical numbering within each of the studies reported herein. When experiments from the literature are described the compounds have not been given specific numbers.

3 Basic Concepts

The focus of this thesis is homogeneous, transition metal-catalyzed reactions, which belong to the area of "asymmetric synthesis" – generally considered to be one of the most important research areas within chemistry. The reactions considered in this thesis are all catalytic reactions and in chapters 3.1-3.3 different types of catalytic reactions are introduced. This is followed by an introduction to chirality (chapter 3.4), and finally historic examples from the development of catalytic asymmetric reactions are given (chapter 3.5).

The remaining part of this chapter is devoted to the introduction of computational chemistry (chapters 3.6-3.12) and finally some quotes on the use of computational methods in chemistry are given (chapter 3.13).

3.1 Catalysis

3.1.1 Introduction

A catalyst is a chemical substance which acts to increase the rate of a chemical reaction, but does not affect the position of the chemical equilibrium, nor is consumed during the course of the reaction. This concept was formulated by Ostwald in 1902, who later received the Nobel Prize in chemistry 1909,[2] whereas the word "catalysis" dates back to the Swedish chemist Berzelius, who coined it as early as 1836.[3] Catalysis is of major importance to our society as we rely on catalytic reactions in all parts of the chemical community, a few of the most important examples being: production of fertilizers, plastics, cracking of oil, automotive exhaust control and in the synthesis of pharmaceuticals.

Traditionally, catalysis is divided into two sub-classes depending on the physical state of the reaction mixture. If the catalyst and reactants are not in the same phase, the reaction is termed a "heterogeneous" reaction and thus involves a heterogeneous catalyst (chapter 3.2). The most important branch of heterogeneous catalysis consists of solid catalysts operating with gaseous reactants at elevated temperatures. Homogeneous catalysts operating in solution phase have been the most successful ones for incorporation of chirality (*i.e.* asymmetric synthesis) – a concept which will be introduced later (chapter 3.4). The uses of homogeneous catalysis in asymmetric synthesis have found wide-spread use in the synthesis of pharmaceuticals.[4]

3.2 Heterogeneous catalysis

Heterogeneous catalysis is characterized by the reactants and the catalyst being in different physical phases. The majority of the important examples of heterogeneous catalysis reported to

date have a solid-phase catalyst operating with gaseous reactants and products. The catalytic transformation takes place on the surface of the catalyst, thus a high surface area is advantageous.

The most prominent example is the well-known Haber-Bosch process,[5] in which gaseous N_2 and H_2 combine to give ammonia while passing over an iron catalyst at high pressure and temperature (200 atm. and 450°C). This process has been elected the most important invention of the last century,[6] and it produces ammonia which is converted into 500 million tons of artificial fertilizer each year. This tremendous amount sustains roughly 40% of the world's population, while using 1% of the world's energy supply to do so.[7]

Another important example of heterogeneous catalysis is the Ziegler-Natta process, which produces polyethylene and polypropylene from their respective monomers. The catalyst formes spontaneously when mixing $TiCl_4$ and $AlEt_3$ and its reactivity was discovered by Karl Ziegler in 1955.[8] This catalyst effects polymerization of ethylene at normal pressure, whereas the similar uncatalyzed transformation requires high pressure and heat (1000-2000 atm. and 200ºC).[9] Simultaneously, Giulio Natta discovered a similar polymerization reaction with propylene, and for their discoveries Ziegler and Natta were awarded the 1963 Nobel Prize in chemistry together. Recently, monomeric and well-defined Zr-based catalysts have been developed by Kaminsky and co-workers,[10] which exhibit a high reactivity (higher than the original Ziegler-Natta catalysts) and a simultaneously high selectivity for different isomers of substituted ethylenes (for example propylene and styrene).

One important advantage of heterogeneous catalysis is the facile separation of the catalyst from the reaction mixture, something which can be quite troublesome in homogeneous catalysis. Furthermore, heterogeneous catalysts are usually very robust, allowing very high turn over numbers[a] (TON) often in the order of 10^6 or even higher.

3.3 Homogeneous catalysis

In homogeneous catalysis the reactants and the catalyst are in the same phase, with the typical example being a liquid solution. Homogeneous catalysts are often less robust than their heterogeneous counter-parts, with typical catalyst loadings ranging between 0.5 mol% and 5 mol%, although recently highly active and robust catalysts have been developed for Pd-catalyzed cross-coupling reactions, allowing for TON>100.000 in some simple Heck or Suzuki reactions.[11] The most important class of homogeneous catalyst consists of a metal atom associated with a chiral ligand (Figure 1).

[a] The turnover number is the average amount of product (mole) generate by each mole of catalyst.

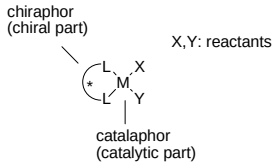

Figure 1 General construction of many chiral metal catalysts.

Usually, the reaction takes place in the inner coordination sphere of the metal-atom (catalaphor), which is rendered chiral due to the presence of the chiral ligand (chiraphor). Examples of efficient transfer of chirality with homogeneous catalysts have been far more widespread than in heterogeneous catalysis, where the introduction of a chiral environment is hampered by the presence of the inherently achiral metal surface.

The principle of a reactive metal centre surrounded by a chiral environment is a well-known construction derived from Mother Nature's own metalloenzymes. These enzymes have provided us with numerous examples of catalytic asymmetric reactions, where an enzyme transforms substrate to product in 100% yield and 100 % *ee*[b]. However, development of chiral catalysts for synthetic reactions is often a complex, time-consuming process which renders the approach of nature with one catalyst per substrate unappealing. Usually, a broader substrate range is preferred (*i.e.* substrate generality), and a concomitant slight decrease in selectivity for each individual substrate is accepted.

3.4 Chirality

In the previous section the concept of catalysis was introduced; however, to fully comprehend asymmetric synthesis the physical phenomenon "chirality" must also be introduced. Chirality is defined as follows: When a molecule cannot be superimposed on its own mirror image, the molecule is said to be chiral.[c] The relationship between the two mirror images is comparable to that of a person's right hand to the left hand. The two mirror images are termed enantiomers and they have identical physical properties (melting point, boiling point, NMR etc.) except when they are in a chiral environment. In nature, chirality is the rule rather than the exception with prominent examples being DNA, amino acids, carbohydrates and numerous natural products. Without any chiral components a reaction which turns an achiral[c] reactant into

[b] Enantiomeric excess (*ee*) is defined in chapter 3.4, "Chirality".

[c] Chiral is derived from ancient Greek "cheir", meaning hand. Achiral means "not chiral".

a chiral product will always form equal amounts of the two enantiomers. The resulting 50/50 mixture of enantiomers is designated a racemate.[12]

Chirality was first discovered by Pasteur in 1849 when he was able to separate the two enantiomers of tartaric acid - by hand! This exceptional achievement was only possible because the two enantiomers crystallize as separate enantiomers spontaneously, a phenomenon which only takes place at temperatures below 27 ºC (Figure 2).[12]

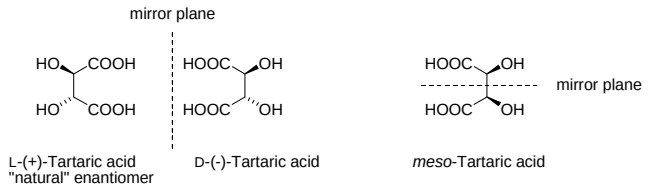

Figure 2 Left: The two enantiomers of tartaric acid, which were separated by Pastaur based on the visual appearance of the crystals. Right: The meso-form of Tartaric acid which is not a chiral compound (*i.e.* achiral).

Tartaric acids have two stereogenic centres, which is the designation used for carbon atoms with four different substituents. The configuration at each stereogenic centre can indicated using a chemical structure with stereochemically defined bonds, such as wedges (┣) for bonds pointing "up" and dashed lines (┋) for bonds pointing "down" as shown in Figure 2. Alternatively, an (*R*)- or (*S*)-prefix can be assigned using the Cahn-Ingold-Prelog priority system.[13] For many years only one general way of distinguishing between two enantiomers existed, which was based on the observed physical phenomenon that enantiomers rotate plane-polarized light by the same magnitude but in opposite directions. The enantiomer rotating the light in a clock-wise manner (termed dextrorotary) is assigned a (+)-prefix, whereas the enantiomer affecting a counter-clockwise rotation of the plane-polarized light is assigned a (-)-prefix. The last nomenclature uses a D- or L-prefix (Figure 3), which is particular popular for carbohydrates, and is based on relating unknown stereochemistry to the configuration in glyceraldedehyde using stereochemically "known" transformations (*i.e.* chemical correlation).

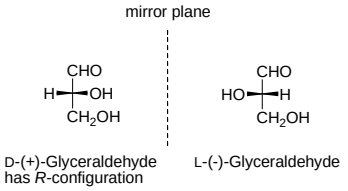

Figure 3 The two enantiomers of Glyceraldehyde from which all D- and L-configurations are based.

When a chiral catalyst is being used for a chemical reaction the possibility of obtaining chiral products from achiral reactants exists, and this will be the focus of chapter 3.5. The degree of induced chirality is expressed as enantiomeric excess (*ee*), and is defined from the amounts of each enantiomer as shown in eq. 1.

$$ee = \frac{\text{amount(major)} - \text{amout(minor)}}{\text{total amount}} * 100\% \quad (1)$$

The racemic mixture mentioned previously with equal amounts of each enantiomer can be assigned an *ee* of 0%, whereas if only one enantiomer is present, *ee* is 100%. A compound is said to be "enantiomerically pure" or "enantiopure" when only one enantiomer is present, and this is always the target aimed for by developers of asymmetric reactions. Although asymmetric synthesis is a relatively new branch of chemistry, chirality is of fundamental importance in biology, where the majority of the biologically important molecules are themselves, chiral. As a consequence the human body constitutes a chiral environment, which results in enantiomers causing a different biological response. A good example is the terpene-derivative limonene, where one enantiomer (Figure 4, left) is naturally occurring and responsible for the smell in several citrus fruits, whereas the other enantiomer (Figure 4, right) has a somewhat sharper smell of lemons but is not naturally occurring.

R-(+)-limonene
smells of oranges

S-(-)-limonene
smells of lemons

Figure 4 The two enantiomers of limonene, with the different biological responses indicated. * indicates the stereogenic centre.

If the absolute configurations at all the stereogenic centres are known, each of the stereoisomers can be identified using the (*R*)/(*S*)-nomenclature. In the case of limonene the (+)-enantiomer has the *R*-configuration at the stereogenic carbon atom (* in Figure 4). Numerous other examples of the difference in biological response have been reported, with the most notorious example being the anti-nausea drug Thalidomide. The drug was administered in racemic form to pregnant women in the 1960s, but unfortunately the presumed inactive enantiomer caused deformities in the newborn babies. However, later studies revealed a rapid interconversion of the enantiomers (*i.e.* racemization), which also rules out the pure enantiomer as a viable drug.[4] In recent years several drugs, originally marketed as racemic mixtures, have

had their patents renewed on the basis that the pure enantiomers had improved drug characteristics.

The most elegant and efficient way of producing a single enantiomer of these drugs would be through use of catalytic asymmetric reactions. Some thirty years ago the perfect reaction was described by the 1975 Nobel laureate in chemistry, J. W. Cornforth[14]:

"It is, for example, no good offering an elegant, difficult, and expensive process to an industrial chemist whose ideal is something to be carried out in a disused bathtub by a one-armed man who cannot read, the product being collected continuously through the drain-hole in 100% purity and yield" **J.W. Cornforth (1975)**

At present, catalytic asymmetric reactions constitute the best candidates for "perfect reactions" and they will be discussed in more detail in the following chapter.

3.5 Asymmetric catalysis

The field of asymmetric catalysis constitutes one of the most active areas within synthetic organic chemistry. There exist a few monographs on the subject,[15] however due to the rapid expansion of the area review articles must frequently be consulted.

3.5.1 First examples

In the mid 1960s the first examples of catalytic asymmetric reactions using man-made chiral catalysts appeared in the chemical literature. Among the earliest discoveries was an asymmetric cyclopropanation,[16] which was reported by Nozaki and co-workers in 1966 (Figure 5).[17] By present standards the level of chiral induction was very low, but this is still considered to be the beginning of the era of asymmetric catalysis.

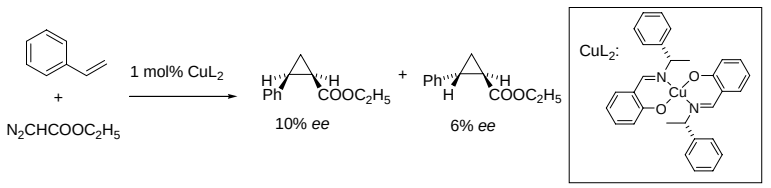

Figure 5 The catalytic asymmetric cyclopropanation reported by Nozaki and co-workers.

The first reaction to approach perfection (*i.e.* high *ee* and a broad substrate scope) was the catalytic asymmetric hydrogenation, where the first steps were taken by Knowles and Sabacky in 1968.[18] An optically active rhodium complex with chiral tertiary phosphines as ligands (69%

ee) was used to perform the asymmetric hydrogenation of α-phenyl acrylic acid in 15% *ee* (Figure 6).

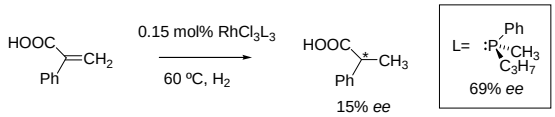

Figure 6 The first example of catalytic asymmetric hydrogenation using a chiral tertiary phosphine as ligand.

Subsequent optimizations by Knowles and co-workers at the Monsanto Company lead to an industrial application, with one of the key steps in the synthesis of the drug L-DOPA furnishing the desired product in astonishing 97.5% *ee* (Figure 7).[19] L-DOPA is decarboxylated enzymatically to the neurotransmitter dopamine in the human body, and was one of the first effective drugs in the treatment of Parkinson's disease – a condition caused primarily by dopamine deficiency.[20]

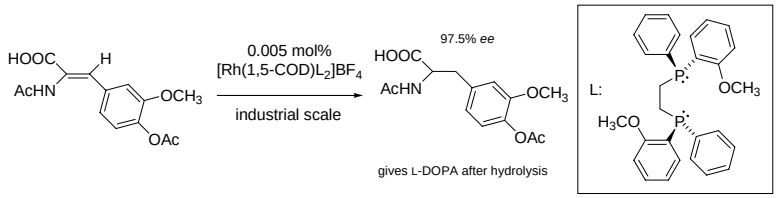

Figure 7 The industrial application of asymmetric hydrogenation as a key step in the production of L-DOPA at the Monsanto Company.

A massive breakthrough came with the introduction of the chiral ligand BINAP by Noyori and co-workers,[21] who were able to effect asymmetric hydrogenation of a wide range of α-(acylamino) acrylic acid derivatives in high yields (93-99%) and high enantioselectivities (79-100% *ee*) using Ru as the catalaphor.[22] This catalyst also found industrial use in 1984 when the Takasago International Co. started using it in a key asymmetric isomerization in the production of (-)-menthol. This process delivers the naturally occurring flavour in a quantity of 1000 tons per year, equal to one-third of the world demand. Impressively, the reaction is run on a 9 ton scale and the enantioselectivity is a staggering 99%, which supersedes that of the natural compound, citronellal itself (80% *ee*). The key asymmetric isomerization is shown in Figure 8 along with the chiral catalyst. For their achievements in the development of catalytic asymmetric

hydrogenation reactions Knowles and Noyori were awarded one half of the 2001 Nobel Prize in chemistry.[23]

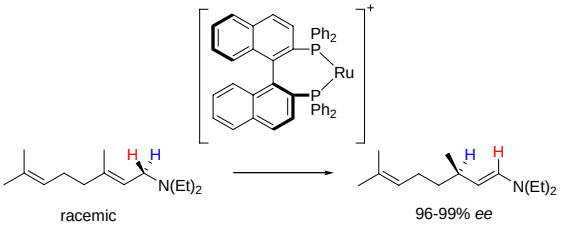

Figure 8 The asymmetric isomerization used by Takasago International Co. in synthesis of (-)-menthol.

The asymmetric hydrogenation reaction was also very interesting mechanistically since the major enantiomer was shown to arise from the *least* stable intermediate as suggested by Halpern in 1982 due to a significantly higher reactivity of this intermediate.[24] This is often referred to as the "Halpern mechanism" and is a consequence of the transition state (TS, more about this in chapter 3.7.1 Chemical Reactions) formed from the least stable intermediate being lower in energy than that of the more stable intermediate (Figure 9).

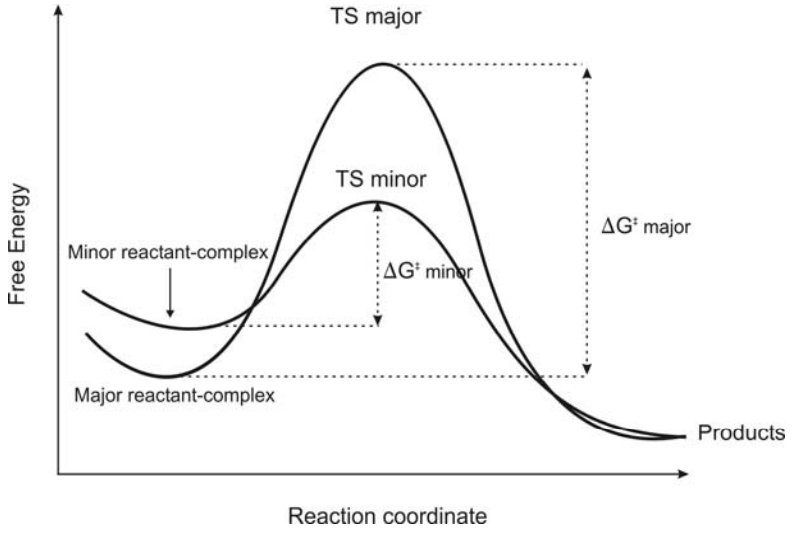

Figure 9 Illustration of the principles behind the "Halpern" mechanism.

The principles behind the Halpern mechanism for asymmetric hydrogenation are not limited to this particular reaction. Similar observations have been made in the asymmetric version of the

Mo/Ru-catalyzed ring-closing metathesis reaction,[25] which was recently celebrated by the 2005 Nobel Prize in chemistry to Chauvin, Shrock and Grubbs.[26] In Figure 10 is shown the first example of asymmetric induction using a Ru-based chiral catalyst.[27]

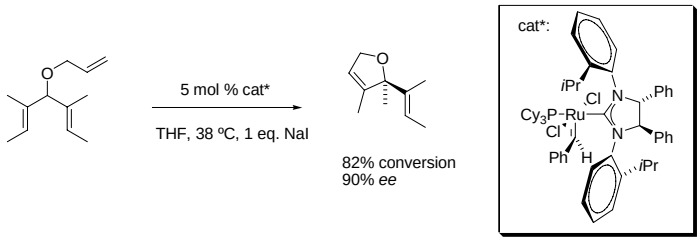

Figure 10 Example of an asymmetric ring-closing metathesis reaction from Grubbs and co-workers.

Also in the field of oxidation chemistry, asymmetric transition metal-catalyzed reactions have been approaching the "perfect reaction". The first major achievement was the asymmetric Ti-catalyzed epoxidation of allylic alcohols reported by Katsuki and Sharpless in 1980.[28] The reaction functioned with a wide range of allylic alcohols and delivered a predictable enantiomer of the epoxide depending on which enantiomer of the chiral ligand had been used (Figure 11).

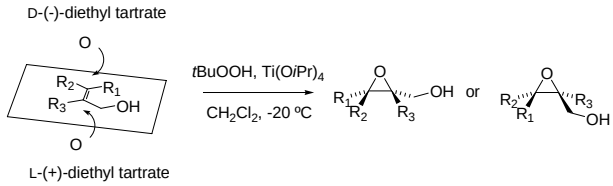

Figure 11 The Sharpless epoxidation reaction including a mnemonic device for prediction of the major enantiomer depending on the choice of chiral ligand.

The fact that the major enantiomer could be predicted from the choice of chiral ligand also characterized another major achievement by Sharpless and co-workers, namely the Os-catalyzed asymmetric dihydroxylation (Figure 12). This reaction was also developed in the 1980s, and will be covered in more detail in chapter 5.2.

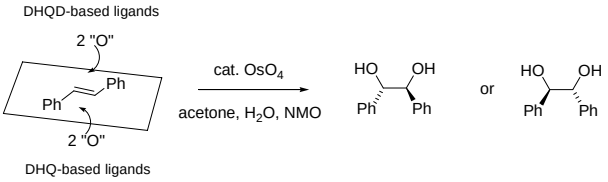

Figure 12 The Sharpless asymmetric dihydroxylation catalyzed by osmium. The enantiomer of the diol can be predicted from the choice of chiral ligands for osmium.

As mentioned previously, Knowles and Noyori were awarded the Nobel Prize for asymmetric hydrogenation and in the same year (2001) Sharpless was awarded the other half of the Nobel Prize for the development of his two catalytic asymmetric oxidation reactions.[23]

Since the Sharpless epoxidation is limited to allylic alcohols, where the OH-functionality provides complexation between the alkene and the catalyst, a more general catalyst for asymmetric epoxidation was desirable. One of the best solutions to this problem came in 1990, when Katsuki and Jacobsen independently reported the Mn(salen)-catalyzed epoxidation of "unfunctionalized" alkenes (Figure 13),[29] which will be the subject of chapter 5.1.

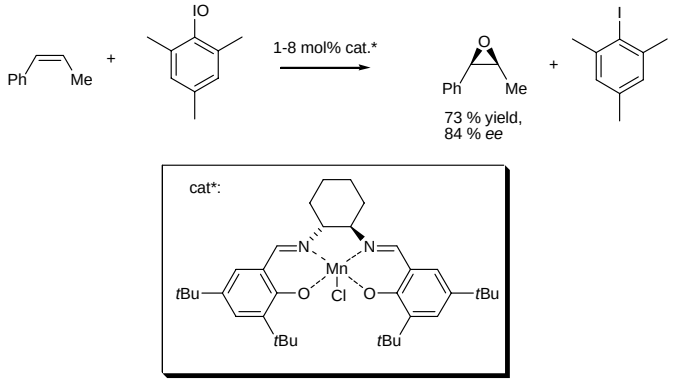

Figure 13 One of the examples of asymmetric, Mn(salen)-catalyzed epoxidation of alkenes reported by Jacobsen and co-workers.[29a]

In the following chapters an introduction to computational chemistry with special emphasis on the prediction of enantioselectivity for asymmetric metal-catalyzed reactions occurring in homogeneous phase is given.

3.6 Computational Chemistry

3.6.1 Introduction

Computational chemistry is the term used to describe the application of mathematics to solve problems in chemistry. This particular research area has expanded tremendously in the past decades, and at present time virtually every aspect of chemistry can be studied computationally. Obviously, such a large area of research is impossible to fully cover in this text, so the main focus will be on theoretical models and techniques, which have been used in the following parts of this thesis. In this first chapter I will introduce some of the most common methods and also comment on their individual strengths and weaknesses. The text is based on a collection of text books,[30] which are recommended for readers with special interests in this area. The importance of the area is underlined by the relatively recent Nobel Prize (1998) to Kohn and Pople for developments within density functional theory (DFT) and wavefunction based methods, respectively.[31]

3.6.2 Molecular Mechanics (MM)

Molecular mechanics is the simplest possible method for calculating the structural properties of molecules. Atoms are treated as being balls and the bonds connecting them are treated as springs. The total energy of the molecule is calculated as a sum of different components resulting from bond stretching, bending etc. In the following section each of these components will be described in turn and examples will be given to illustrate the principles.

3.6.2.1 Bond stretching

The most realistic description of bonding between atoms is represented by the Morse potential (eq. 2), which is able to describe dissociation at long bond lengths (Figure 14).

$$E = D(1 - e^{\alpha(r-r_0)^2}) \qquad (2)$$

D is the dissociation energy, the parameter α determines the width of the well and $(r\text{-}r_0)$ is the displacement from equlibrium.

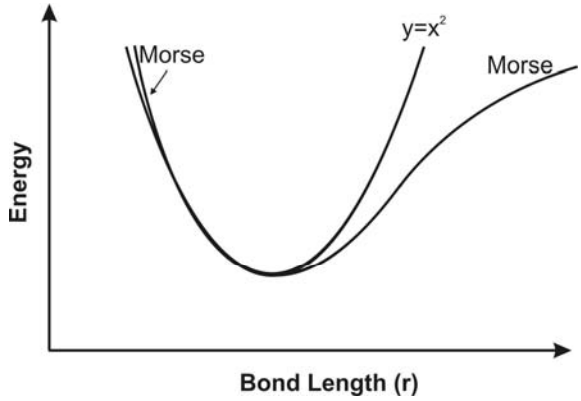

Figure 14 Comparison between the realistic Morse potential and a simple harmonic potential.

In molecular mechanics bonding is usually described using springs (Figure 15, left), which in the simplest form reduces to the well-known Hookes law expressions for force (eq. 3) and energy (eq. 4), as functions of the displacement from equilibrium (r-r_0):

$$F_{Bond} = -k_{Bond}(r - r_0) \tag{3}$$

$$E_{Bond} = \frac{1}{2}k_{Bond}(r - r_0)^2 \tag{4}$$

The stiffness of the each particular bond is contained in the force constant, k_{Bond}. In most popular force fields the simple harmonic expression is replaced with a higher polynomial (*e.g.* to third and fourth order with the MM2 and MM3 force fields, respectively) to allow fit to experimental data over a wider range of values. The equilibrium bond length (r_0) and force constant (k_{Bond}) can be derived from experimental data or from quantum mechanical data.

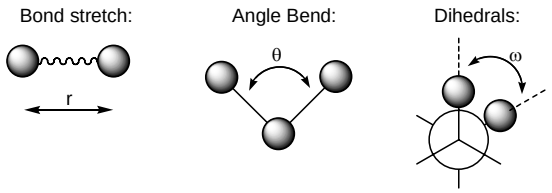

Figure 15 Illustration of some of the basic energy terms used in molecular mechanics.

Using a polynomial function results in a sharp rise in energy for long bond distances, which effectively limits the use of molecular mechanics to molecular geometries close to their equilibrium. Gratifyingly, this rapid rise in strain energy is actually very convenient when building up structures, where a physically unreasonable geometry is rapidly energy minimized.

If the more realistic Morse potential was used, the force acting on the atoms at long distances would be almost zero, leading to a very slow convergence.

3.6.2.2 Angle bending

When one atom is connected to two other atoms, the two terminal atoms can exhibit a bending motion (Figure 15, centre). The energy required to bend the bond can be handled by a simple harmonic expression (eq. 5), but also here higher polynomials are often preferred. The equilibrium bending angle (Θ_0) can usually be estimated from the hybridization of the central atom (*e.g.* 109.5° in CH_4), whereas the force constant (k_{Angle}) is often dependant on all three atoms.

$$E_{Angle} = \frac{1}{2} k_{Angle} (\theta - \theta_0)^2 \tag{5}$$

3.6.2.3 Dihedral angles

When four atoms are connected contiguously the two terminal atoms can "twist" with respect to the line connecting the two central atoms (Figure 15, right). The energy change upon twisting is periodic, and can be modelled by cosine functions (eq. 6).

$$E_{Dihedral} = \sum_{n=1} k_{dihr,n} \cos(n\omega) \tag{6}$$

The number of minima (denoted *n* in eq. 6) can usually be predicted from the hybridization of the two central atoms. The necessary energy required to rotate is dependent on the force constant ($k_{dihr,n}$), which in turn depends on the nature of the interacting atoms as well as the hybridization. Illustrative examples are the simple hydrocarbons ethane and ethene, where the former has a three-fold symmetry with a rotational barrier of only 10 kJ/mol while the latter requires as much as ~150 kJ/mol to interconvert between the two minima.[d]

3.6.2.4 Non-bonded Interactions

There also exist forces between atoms *not* connected by bonds – either due to van der Waals forces or electrostatic interactions. In common these are referred to as "non-bonded" interactions, and should in principle be calculated pair-wise for all atoms in a molecule. Often a certain "cut-off" radius is set to limit the computational demand. Electrostatic interactions are

[d] Energies were obtained using the MM3* force field in Macromodel v. 8.0 in gas phase.

usually accounted for by using Coulomb's law, where each atom is assigned a partial charge (eq. 7).

$$E_{Coulomb} = \frac{q_a q_b}{\varepsilon r} \tag{7}$$

The partial charges (q_a, q_b) can be derived from quantum mechanical calculations or they can be fitted to the experimentally observable dipole moment. The dielectric constant (ε) is usually set equal to one in order to simulate gas phase, although a higher value can be used to decrease the effect of long-range electrostatic interactions. This can be seen as a first, very crude attempt to account for the effect of solvation.

In the original development of the popular MM2 and MM3 force fields Allinger and co-workers used dipole moments instead of partial charges,[32] but this was changed to partial charges when these two force fields were implemented in Macromodel.[33]

A representation of the van der Waals forces requires a complicated and computationally "expensive" method.[e] At long distances the interaction is weakly attractive, but at short distances there is strong repulsion. In the literature several equations have been suggested, each with its own advantages and disadvantages. One of the most accurate ones is the Buckingham potential (eq. 8), but for historic reasons the Lennard-Jones potential is usually preferred (eq. 9).

$$E_{Buckingham} = Ae^{-Br} - \frac{C}{r^6} \tag{8}$$

$$E_{Lennard-Jones} = \varepsilon\left[\left(\frac{r_0}{r}\right)^{12} - \left(\frac{r_0}{r}\right)^{6}\right] \tag{9}$$

With the Buckingham potential A, B, and C are constants which can be selected to give the desired fit to the data at hand, whereas ε corresponds to the well depth and r_0 is the distance corresponding to the energy minimum with a Lennard-Jones potential.

Finally, most force fields have extra terms to compensate for known deficiencies. These are noted "cross-terms" and used when there is a known coupling between some of the "fundamental" terms already mentioned. An example is the stretch-bend term, which compensates for the observation that compressing an angle frequently leads to a change in the optimal bond lengths to the central atom – an elongation is often favoured due to reduction of steric interactions.

[e] In computational chemistry, the term "expensive" means time-consuming.

3.6.2.5 Exceptions to the rule

In this work I have mainly used the MM3* force field as implemented in the Macromodel program package.[33] In this force field the additional information about "special cases" is handled by substructures. The substructure contains a recognition pattern, which allows the program to detect special substructures such as a strained ring (cyclopropane, cyclobutane or cyclopentane) or an aromatic structure like benzene or pyridine. These molecules have a structure which cannot be predicted correctly from the default parameters but have been deemed important enough to warrant the development of an extra set of parameters. A good example is the benzene ring, where the conjugation makes all the C-C bonds equivalent but neither equal to a carbon-carbon single bond nor a double bond. By simply deleting the substructure for benzene its actually possible to energy minimize the Kekule structure, which corresponds to the "unknown" compound 1,3,5-cyclohexatriene (Figure 16). Probably (or should I say hopefully...) most other computational methods would quickly minimize to benzene instead.

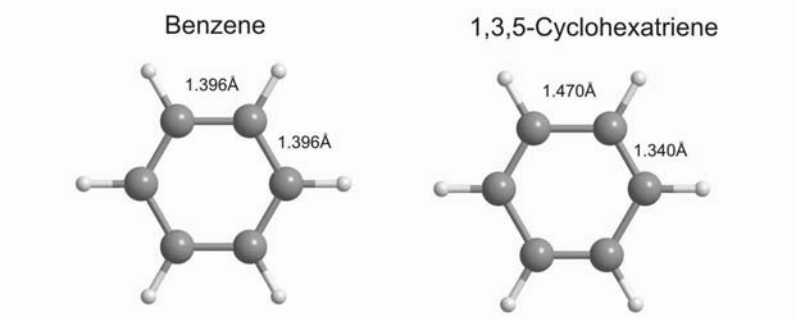

Figure 16 The minimized structure of benzene (left) and 1,3,5-cyclohexatriene (right). Both calculations were performed using MM3* as incorporated in Macromodel v. 8.0.

3.7 Potential Energy Surface

A potential energy surface (PES) is a hypothetical construction, which uniquely defines the energy associated with each particular arrangement of nuclei. In general the PES will have 3N coordinates (N: number of atoms) but for most reactions the dimensionality can be greatly reduced, usually to a single coordinate or two (*e.g.* the length of the forming/breaking bonds). When reduced to two coordinates the corresponding height (z-axis) is the potential energy for this particular arrangement of the nuclei, whereas the xy-coordinates determine the arrangement of nuclei.

A stable molecule can be considered as being a ball rolling around on the PES. With MM the position and type of each bond is fixed, and for a certain arrangement of bonds there exists a minimum energy conformation. On the PES this corresponds to a well and an energy minimization is simply a matter of moving the ball to the bottom of this well. Given a particular functional form for the energy as function of atomic positions there exists a number of different mathematical procedures capable of minimizing the energy. Molecular mechanics is an easy way of generating a PES – in principle all methods can be used as long as they can associate an energy to each arrangement of the nuclei. In the following sections quantum mechanical methods will be introduced, which are significantly more complex than MM; however, they can also be viewed upon as an alternative way of generating a PES.

3.7.1 Chemical Reactions

A chemical reaction can also be interpreted using the intuitively appealing concept of a ball rolling on a PES. A reaction can be viewed as a ball moving from one well to the neighbouring well.[f] At some point along the journey a ridge must be passed. In chemistry this point is called a transition state (TS) and is important since this is where the regio- and stereoselectivity is determined for an irreversible reaction.

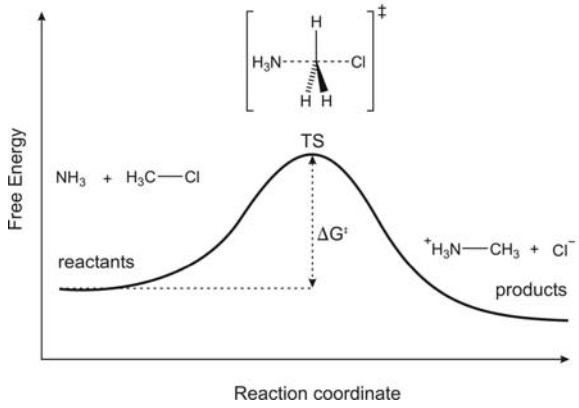

Figure 17 Illustration of the energy profile for the S_N2 reaction of ammonia with CH_3Cl (the Menschutkin reaction) .[34]

[f] Here I would like to acknowledge Frank Jensen, University of Southern Denmark for his inspiring lecture on PES in the course "Computational Chemistry".

In Figure 17 a one-dimensional energy profile for the Menschutkin reaction is shown,[34] the simplest of which is an S_N2 reaction of ammonia with methyl chloride. In this example the reaction coordinate (x-axis) is well represented by C-N or C-Cl distance but the reaction coordinate contains *all* geometrical changes occurring during the reaction. The TS can be characterized by being an energy maximum along the reaction coordinate but an energy minimum along all other degrees of freedom.

3.7.2 TS Optimization

Optimization to a TS is significantly more difficult than energy minimization and often a trial-and-error approach will have to be undertaken. With unknown reactions it can be beneficial to perform a "driver", which is a distortion of the molecule from reactant to product structure along a selected coordinate. The structure found to be highest in energy resembles the TS and a separate TS optimization can proceed from there. If this method fails, another driver can be performed using a smaller interval between the individual structures or by selecting a different coordinate to be fixed.

The TS optimization relies on a good starting guess of the Hessian, which is the matrix built up from the second derivatives of the energy with respect to nuclear positions. The search proceeds in the direction of the lowest vibrational mode, which in well-behaved cases will lead the search to the TS. On the PES this can be viewed as the ball situated close to the top of the ridge and moving uphill, finally arriving at the highest point.

The primary link between relative energies and experimentally observable quantities such as diastereoselectivity and enantioselectivity are through rate constants, which can be obtained using transition state theory (TST)[30b] and assuming Curtin-Hammett conditions, which states that interconversion between all isomers *before* the rate-determining step is fast and reversible.[30b,35] If the energy required to reach the TS is denoted $\Delta G^{\ddagger}$, the probability of a given molecule to possess this energy is proportional to $exp(-\Delta G^{\ddagger}/RT)$ when assuming a Boltzmann population. The corresponding rate constant can be shown to be equal to:[36]

$$k = \kappa \frac{k_B T}{h} e^{-\Delta G^{\ddagger}/RT} \tag{10}$$

κ: transmission coefficient, k_B: Boltzmann constant, h: Planck constant, R: gas constant.

The Gibbs free energy of activation ($\Delta G^{\ddagger}$) can be obtained from enthalpy and entropy using the standard expression (eq. 11):

$$\Delta G^{\ddagger} = \Delta H^{\ddagger} - T\Delta S^{\ddagger} \tag{11}$$

In many cases the inaccuracy involved in the calculation of the difference in enthalpy is similar to the contribution from $T\Delta S^{\ddagger}$, and in these cases the enthalpy can be used directly in eq. 10. For a given asymmetric reaction it is the *difference* in Gibbs free energy of activation for the two reaction paths leading to opposite enantiomers which is of interest ($\Delta\Delta G^{\ddagger}$, eq. 12). The expression connecting the relative reactivity to enantiomeric excess (*ee*) is shown in eq. 13.

$$k_{rel} = e^{-\Delta\Delta G^{\ddagger}/RT} \tag{12}$$

$$ee = 100\% \frac{k_{rel} - 1}{k_{rel} + 1} \tag{13}$$

In Figure 18 the calculated *ee* (%) as function of the energy difference between the two reaction pathways ($\Delta\Delta G^{\ddagger}$) is shown, and in Table 1 a selection of "intuitively" interesting energy differences and the corresponding ratio of the two products, the relative distribution of products (%), and the *ee* (%) if the two products are enantiomers. All values are calculated using eq. 12-13 with T=298 K but can easily be recalculated for a different temperature. In synthetic organic chemistry reactions are often run under cooling by dry-ice (-78ºC, 195K), which for a reaction proceeding with 80% *ee* at room temperature (298K) would lead to a substantial improvement to 93% *ee* at -78ºC.

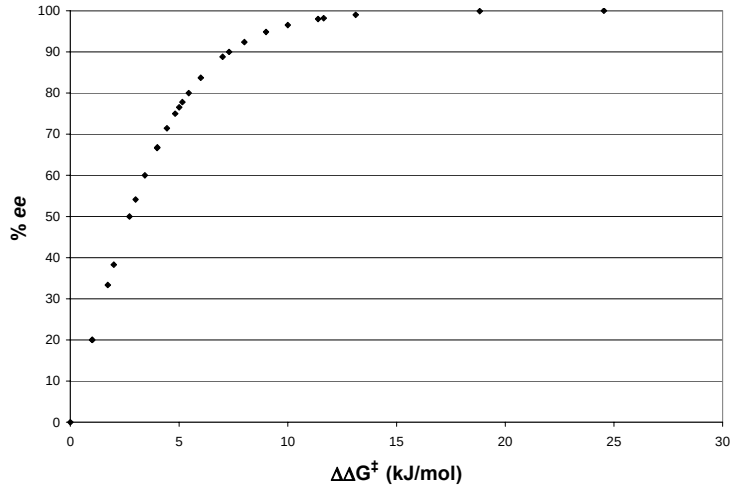

Figure 18 Relationship between difference in activation free energy for the two pathways leading to opposite enantiomers and the resulting % *ee* under Curtin-Hammett conditions.

Table 1 Differences in Gibbs free activation energy and the corresponding relative reactivities. Values have been obtained at 298K.

$\Delta\Delta G^{\ddagger}$ (kJ/mol)	Ratio (k_A/k_B)	% Major	% Minor	% ee
0.00	1.00	50.00	50.00	0.00
1.00	1.50	59.96	40.04	19.91
1.00	1.50	60.00	40.00	20.00
1.72	2.00	66.67	33.33	33.33
2.00	2.24	69.15	30.85	38.30
2.72	3.00	75.00	25.00	50.00
3.00	3.36	77.04	22.96	54.09
3.43	4.00	80.00	20.00	60.00
3.99	5.00	83.33	16.67	66.67
4.00	5.02	83.40	16.60	66.80
4.44	6.00	85.71	14.29	71.43
4.82	7.00	87.50	12.50	75.00
5.00	7.52	88.27	11.73	76.53
5.15	8.00	88.89	11.11	77.78
5.44	9.00	90.00	10.00	80.00
6.00	11.26	91.85	8.15	83.69
7.00	16.86	94.40	5.60	88.80
7.30	19.00	95.00	5.00	90.00
8.00	25.25	96.19	3.81	92.38
9.00	37.80	97.42	2.58	94.85
10.00	56.60	98.26	1.74	96.53
11.39	99.00	99.00	1.00	98.00
11.65	110.00	99.10	0.90	98.20
13.12	199.00	99.50	0.50	99.00
18.83	1999.00	99.95	0.05	99.90
24.54	19999.00	99.995	0.005	99.99

In asymmetric synthesis an *ee* of > 99% would satisfy most people, and from a mechanistic point of view the difference in energy for the two reaction paths leading to opposite enantiomers is then ~13 kJ/mol. An energy difference of this magnitude should be relatively straight-forward to predict computationally and would not provide a good test of the computational accuracy.

A much more interesting situation arises when a medium-range *ee* is observed; say 75%, which corresponds to an energy difference of 4.82 kJ/mol. If we assume that the accuracy in the

determination of the *ee* is ±1%, the corresponding accuracy in the determination of the energy is ±0.12 kJ/mol.[g]

The typical experimental error in determination of *ee* is very low, probably well below 1% when determined by chiral-GC which means that it is essentially accurate. For the typical theoretical calculation an error of 2 kJ/mol is acceptable, and usually it is extremely difficult to do much better than this. An energy difference of exactly 2 kJ/mol corresponds to 38% *ee*, and consequently, the entire interval from 0-38% *ee* essentially corresponds to no significant difference in energy between the two pathways.

[g] The interval 74-76% *ee* corresponds to 4.71-4.94 kJ/mol, which translates to 4.82±0.12 kJ/mol.

3.8 Molecular Ensembles

Up until this point only one TS for each reaction has been considered; however, in a typical small scale chemical reaction (1mmol) more than 10^{20} molecules will be converted from reactants to products. This massive number of similar molecules has important consequences for their behaviour and to account for this we must employ macroscopic quantities such as temperature, pressure and concentration. For an arbitrary chemical reaction (eq. 14) the rate can be expressed in terms of the concentration of the reacting molecules A and B (eq. 15, [] denotes concentration):

$$A + B \rightarrow C + D \tag{14}$$

$$\frac{d[C]}{dt} = k[A]^n[B]^m \tag{15}$$

The rate constant (k, eq. 15) can be calculated using the expression from the previous section and compared to experiment. Unfortunately, this only holds for the simplest of molecules since a more complex molecule exist as multiple conformers. In order to obtain the observable rate constant the reactivity of each of these conformers must be evaluated independently. When the system involves more than a few hundred atoms and/or more than 10-100 conformations molecular mechanics is the only method which at present is fast enough to allow a thorough investigation.

For several reasons we have chosen to employ only relative rate constants in this work. First of all, relative rate constants are easy to measure by simply reacting two substances simultaneously while measuring the rate of disappearance (see below). Second, in the computation of a relative rate constant, errors that are constant will disappear. This is important since the absolute accuracy of *any* computational method, which can be applied to large systems, is probably not good enough to be compared directly to experimental values.

Envision a competition reaction between two substrates (A and B) catalyzed by some active catalyst. Frequently, a first order dependence (n=m=1 in eq. 15) regardless of the exact nature of the reacting species can be assumed and with identical reaction orders in all other components, the rate of reaction of A and B are given by:

$$\frac{d[A]}{dt} = -k_A[cat][A] \tag{16}$$

$$\frac{d[B]}{dt} = -k_B[cat][B] \tag{17}$$

Division gives:

$$\frac{d[A]}{d[B]} = \frac{k_A}{k_B}\frac{[A]}{[B]} \tag{18}$$

The variables are separated and limits are introduced:

$$\int_{[A]_0}^{[A]} \frac{d[A]}{[A]} = \frac{k_A}{k_B}\int_{[B]_0}^{[B]} \frac{d[B]}{[B]} \tag{19}$$

Which upon integration gives:

$$\ln\left(\frac{[A]_0}{[A]}\right) = \frac{k_A}{k_B}\ln\left(\frac{[B]_0}{[B]}\right) \tag{20}$$

This expression can be recognized as a straight line with intercept at y=0 and by plotting $\ln([A]_0/[A])$ vs. $\ln([B]_0/[B])$ at different levels of conversion the relative reactivity (k_A/k_B) can be obtained as the slope of the line. If a straight line is *not* obtained the initial assumption does not hold for the system under investigation, or perhaps some of the compounds are unstable to the conditions employed. In principle the appearance of products (*C* and *D*, eq. 14) can also be used to determine k_A/k_B but on the systems studied here the disappearance of reactants consistently gave superior correlations.

The measured differences in reactivity from experiment can be compared directly to calculated reactivities (obtained from eq. 10) but frequently they are instead converted to differences in energy (in principle $\Delta\Delta G^{\ddagger}$) to avoid the exponential dependence. In Table 1 a selection of different reactivities along with the corresponding energy differences was listed and they also apply here.

3.9 Quantum Mechanics (QM)

In the beginning of the 20th century a new set of laws describing physical phenomena on atomic scale was developed based on contributions by brilliant physicists such as Planck, Einstein, Bohr, Heisenberg, Schrödinger, Born, Dirac and Pauli. The fundamental discovery was that energy is quantized (eq. 21) and the differences between the individual energy levels were equal to Planck's constant (*h*) times the frequency of the absorbed/emitted light:

$$\Delta E = hf \tag{21}$$

Applying this principle to an atom with electrons revolving around the nucleus in quantized energy levels, the Danish physicist Niels Bohr developed the "Bohr model".[37] This model successfully predicted the absorption spectra of hydrogen, which was a formidable achievement for such a crude theory. By elaborating the Bohr model in a more general mathematical form, Erwin Schrödinger in 1925 arrived at the formulation of the so-called Schrödinger equation (eq. 22):

$$H\Psi = E\Psi \tag{22}$$

The fundamental concept was the existence of a wave function, Ψ from which any desired property of the system could be extracted using the appropriate mathematical operator. The most important operator is the Hamiltonian operator (*H*), which returns the energy (*E*) of the system when applied to the wavefunction. In almost all cases the Born-Oppenheimer approximation is applied, which in principle states that electrons move significantly faster than the nucleus, and thus are able to relax instantaneously to changes in the positions of the nuclei. This permits a separation of the nuclear and electronic parts of the Schrödinger equation, which allows one to solve each of these equations independently. If the movements of the nuclei are solved using classical mechanics, this can be viewed upon as a theoretical basis for molecular mechanics. For one-particle systems such as the hydrogen atom or the helium cation, the Schrödinger equation can be solved analytically but for more complex systems a numerical solution is the only possibility. Fortunately, due to the ever increasing computational power it is possible to achieve a very high accuracy in the numerical solution.

3.9.1 Basis sets

The wavefunction is usually constructed from a sum of mathematical functions, and the type and number of these functions is called the "basis set". From the solution of the hydrogen atom the exact mathematical form is known and the corresponding three-dimensional shapes of these are easily recognizable by chemists as "orbitals". Mathematically they are known as Slaters or Slater-type orbitals (STO) but they can also be implemented as Gaussian-type orbitals (GTO), which is usually preferred due to improved computational efficiency. The functional form of the GTOs is however somewhat different from the "real" wavefunction but by using multiple GTOs (so-called "primitive"-GTOs) for every wavefunction a good accuracy can still be obtained. The majority of the calculations in this work have been performed with a 6-31G* basis set, where the core orbitals consist of a GTO constructed from 6 individual GTOs and the valence orbitals are described by a GTO constructed from 3 primitive GTOs and one additional GTO. These GTOs are multiplicated with angular terms in spherical coordinates to achieve spatial orientations

corresponding to s-type, p-type or d-type orbitals. The * indicates that one additional d-type polarization function (also a GTO) have been added to non-hydrogen atoms (** indicates that a p-type polarization function have been added also to hydrogen atoms).

Anions have large, delocalized electron clouds and require additional "diffuse functions" which are designed to account for electron-density far from the nucleus. Also here, a differentiation between non-hydrogen atoms (+) or all atoms is possible (++). Heavy atoms with many core electrons results in a huge number of basis functions and frequently an "effective core potential" (ECP) is used to account for all the core electrons using relatively few mathematical functions. An additional advantage of using an ECP is that they can be parameterized to include relativistic effects, which become important for the 2nd row transition metals and up. The resulting equations for all the atoms and electrons are usually solved using the Hartree-Fock self-consistent field method (HF-SCF).[30b]

3.10 Density Functional Theory (DFT)

In DFT the wavefunction is replaced with the electron density as the fundamental property, which is possible due to the existence of a connection between the wavefunction and the electron density.[38] This allows the computational chemist to do the calculations using density functional theory, which has recently surpassed the traditional Hartree-Fock based methods in terms of cost/accuracy.[30a]

The introduction of so-called "hybrid methods",[39] have lead to an increase in computational accuracy without increasing the computational demand. One of the most successful schemes is the B3LYP method,[40] where DFT is mixed with 20% Hartree-Fock. This method is considered very accurate for most purposes while *simultaneously* being applicable for even relatively large systems including transition metals.[41] The benefits of mixing these two methods can be understood intuitively since many of the systematic errors tend to cancel upon mixing. For example, reaction barriers are underestimated by DFT, whereas HF suffers from overestimation thus allowing a mixed method to be inherently more accurate.

However, one should be aware that with the increasing computational capacity in mind the "optimum" compromise between speed and accuracy is constantly shifting, allowing for the use of better (and more complex) computational methods in the future.

3.11 Solvation

In the early days of computational chemistry, all calculations were performed on systems in the gas phase but recently reliable and efficient solvation models have begun to appear. The

models can be divided into two sub-classes, depending on the presence ("explicit solvation") or absence ("implicit solvation") of solvent molecules.

3.11.1 Explicit solvation

Explicit solvation simply deals with adding a number of solvent molecules around the solute to simulate solvation and is a conceptually very simple method. There exists; however, several problems with this approach: 1) How many solvent molecules are "enough" – one layer, two layers or even more? 2) The complexity of the calculation increases dramatically – not only due to the increased number of atoms present, but also due to loosely bound solvent molecules, which inevitably results in multiple conformations. An illustration of explicit solvation is given in Figure 19 for the Menschutkin reaction of ammonia with methyl chloride, where the TS is shown solvated by four water molecules. The water molecules are positioned in an electrostatically favoured arrangement around the polarized TS.

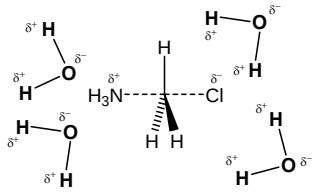

Figure 19 Illustration of explicit solvation with four H_2O molecules applied to the TS of the Menschutkin reaction of NH_3 with CH_3Cl.

3.11.2 Implicit solvation

The main influence a given solvent has on a molecule can be thought of as a reduction of the electrostatic interactions. This screening of charge can be handled by simply selecting a higher value for the dielectric constant (ε) as mentioned previously, but frequently a more sophisticated approach is necessary. Several different methods have been developed to account for the electrostatic interactions between the solute and the solvent. In the present work we have mainly relied on Poisson-Boltzmann self-consistent reaction field (PB-SCRF) solvation method as developed by Martens *et al.*[42] in combination with calculations using the B3LYP method. In essence, PB-SCRF models the effect of solvent by placing charges around the molecule in a way which minimizes the energy of the molecule. This will lead to a more polarized wavefunction for the molecule as illustrated schematically in Figure 20; however, it simultaneously diminishes the structural effects of these charges.

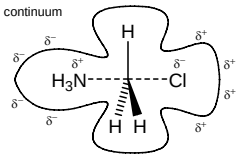

Figure 20 Illustration of how the charges are positioned on the solvent-accessible surface – exemplified with the TS from the Menschutkin reaction.

The main differences between the different methods available lie in the way the cavity is created and also in how the exact magnitudes of the charges are calculated. The PB-SCRF method is relatively fast[h] and gives results which are in good accordance with experimentally determined values as documented by a recent study on the solvation of chloride anions in THF.[43]

In connection with molecular mechanics calculations (chapter 5.2 Osmium-Catalyzed Dihydroxylation) we have used the GB/SA solvation model as reported by Still et al.,[44] which relies on contributions to the solvation energy from each atom or group of atoms exposed to the solvent based on the Born equation (eq. 23).

$$\Delta G = -\left(1-\frac{1}{\varepsilon}\right)\frac{q^2}{2a} \tag{23}$$

q: partial charge, a: surface area.

3.12 Fast methods

Up to this point several different computational methods have been discussed, each with its own strengths and weaknesses. MM is a very fast method, capable of handling large molecules or many small molecules (up to ~100.000 atoms) but is of limited use in the study of reactions (*i.e.* TS) without additional parameters or functionals. The study of the entire reaction profile is possible using QM (either HF or DFT) but this severely limits the size of the system (up to ~200 atoms). To predict the selectivity of a metal-catalyzed reaction we need the capability of calculating multiple TS's *and* the ability to include the full chiral ligand and all the reactants in the calculation. Several solutions to this dilemma have been suggested, and in this chapter different methods will be introduced.

The problem of predicting reactivity of very large systems is also of fundamental interest in biology, where the action of enzymes at the molecular level is one of the most important scientific problems. The methods described here could potentially also be used to study

[h] Acoording to the Jaguar manual, implicit solvation approximately doubles the calculation time.

biological reactions. Furthermore, the problem of predicting the three-dimensional structure of proteins directly from their amino acid composition could in principle also be tackled with these methods.

3.12.1 QM/MM

One of the conceptually simplest ways of studying reaction mechanisms is by use of the so-called QM/MM method. This uses a QM calculation for only a very small part of the molecule and standard MM for the remainder of the molecule. However, this approach creates an interface region where a link must be created, allowing the two different theoretical methods to "communicate" *i.e.* perturb each other sterically and electrostatically.[45] The method can be used to allow explicit solvation with a realistic number of solvent molecules,[46] but the method has primarily been used to treat reactions occurring in biological macromolecules as first demonstrated by Warshel and co-workers.[47]

The implementations of QM/MM by Maseras and Morukuma[48] have been used by Maseras and co-workers to predict selectivity in the osmium-catalyzed asymmetric dihydroxylation (chapter 5.2).[49] QM/MM has not been used in the present work - interested readers are referred to literature sources.[50]

3.12.2 Transition State Force Field (TSFF)

A different approach to the description of reactivity with molecular mechanics relies on the development of new parameters capable of representing the TS of the reaction. This so-called "transition state force field" (TSFF) allows for calculation of selectivity with a speed similar to standard MM by directly giving relative energies of the different TS's leading to different enantiomers. This approach has been pioneered by Houk and co-workers,[51] and some of the resulting TSFF's from Houk and other groups have been included in the MM2* force field available with the Macromodel program package.[33] As examples can be mentioned the Diels-Alder cycloaddition,[52] radical cyclization[53], hydride addition to carbonyls,[54] and the boron-mediated aldol reaction.[55]

The procedure for creating the TSFF inverts the curvature of the Hessian in the direction of the reaction coordinate.[56] This artificially introduced curvature is very steep, which effectively freezes the position of the TS along the reaction coordinate. In the resulting force field the TS will be an energy minimum, which allows use of all the standard minimization and conformational searching tools in molecular modelling program packages.

Unfortunately, as a consequence of the inversion of curvature, the TS cannot respond correctly to steric interactions between the two reaction partners. According to the Bell-Evans-

Polyani principle,[30b] increased steric interactions should lead to a TS with a *shorter* distance between the bond-forming atoms, but with a TSFF a *longer* bond is the result. This severely limits the use of the TSFF method since comparisons between TS's with different steric demands should be handled with great caution.

3.12.3 SEAM

What if it was possible to handle complex reactions directly using only molecular mechanics? That would be an extremely fast method – however, a number of problems must be solved first. A major problem is the change in bonding pattern when going from reactants to products. This does not allow a direct comparison between the MM energy on different sides of the TS. This can be solved by adding a constant energy to either reactants or products. This energy difference *must* be calculated using a different method (*e.g.* QM), but since it only involves the isolated reactants and products, the calculation is relatively straight-forward.

In the SEAM procedure, pioneered by F. Jensen,[57] the TS is approximated by the molecular structure, which is equally *disfavoured* with reactant and product force fields, thus having some intermediate structure where the penalties for elongation of bonds is balanced by additional vdW repulsions. This structure is located as the minimum energy structure on the *seam* between the PES for reactants and products. The method does not *a priori* require any new parameters, but the reactant and product force fields should be valid when extrapolated to the TS structure or *equally wrong*, which in principle should give similar results. This will often require a thorough investigation of the terms responsible for the non-bonded interactions and the bond-stretching terms.

3.13 Quotes

Now the basic concepts have been introduced and we are ready to embark on the description of the catalytic asymmetric reactions, which have been the subject of this study. But first I want to convey a couple of opinions on computational chemistry as exemplified by three quotations. I find all three of them interesting – even today, which is quite remarkable considering the first ones were put forward almost two centuries ago!

The first quote is by Auguste Comte (1798-1857), who is definitely not positive towards computational chemistry:

Every attempt to employ mathematical methods in the study of chemical questions must be considered profoundly irrational and contrary to the spirit of chemistry. If mathematical analysis should ever hold a prominent place in chemistry - an aberration which is happily

almost impossible - it would occasion a rapid and widespread degeneration of that science. **Auguste Compte (1830)**

A contemporary scientist was Adolphe Quetelet (1796-1874), who reached the exact opposite conclusion:

The more progress physical sciences make, the more they tend to enter the domain of mathematics, which is a kind of centre to which they all converge. We may even judge the degree of perfection to which a science has arrived by the facility with which it may be submitted to calculation. **Adolphe Quetelet (1828)**

Finally, a very famous quote from P. A. M. Dirac, in which he states that all problems in chemistry can be solved with mathematics:

The underlying physical laws necessary for the mathematical theory of a large part of physics and the whole of chemistry are thus completely known, and the difficulty lies only in the fact that the exact application of these laws leads to equations much too complicated to be soluble. **P. A. M. Dirac (1929)**

4 Palladium-Catalyzed Coupling Reactions

The first of the two reactions in this chapter, the Heck reaction, belongs to the "family" of palladium-catalyzed cross-coupling reactions, which constitutes one of the most important additions to synthetic organic chemistry in the last two-three decades.[58] Many of the important, initial observations regarding the rich chemistry of palladium with organic compounds originated in Japan in the 1960s,[59] but further developments have constantly pushed the limits for palladium catalysis. Many of the reactions discovered with palladium have begun to be transferred to less expensive metals (*e.g.* Ni), which will increase their applicability even further.[60] A general catalytic cycle for the palladium-catalyzed cross coupling reactions is shown in Figure 21, and involves oxidative addition to Pd(0), trans-metalation to give a mixed Pd(II)-complex allowing for a reductive elimination to furnish the coupling product and return the catalytically active Pd(0)-species.

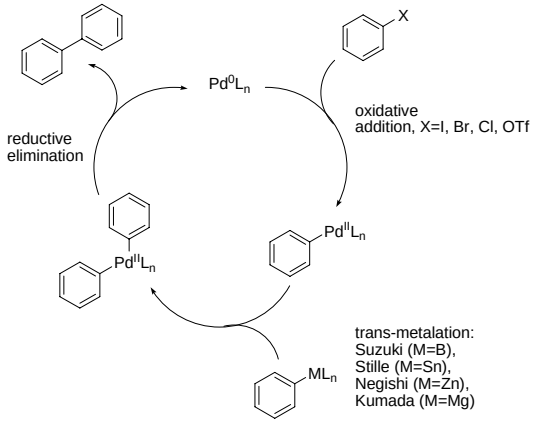

Figure 21 A schematic overview of the catalytic cycle common to many of the palladium-catalyzed cross-coupling reactions.

The first step in the catalytic cycle is the oxidative addition, and in the early catalytic systems X was required to be iodide or bromide. Recent ligand developments have resulted in more reactive forms of palladium(0),[61] and these improved catalysts are capable of adding oxidatively to phenyl bromide at room temperature and phenyl chloride at elevated temperatures. Palladium will also add oxidatively to vinylic halides, which allows the reactions to be performed with vinyl instead of phenyl in many cases.

The name of the palladium-catalyzed coupling reaction is related to the exact nature of the species performing the transfer of the second group to palladium. In most cases this is achieved via transmetalation from a metal, the most frequently used metals being: B,[62] Sn,[63] Zn,[64] and Mg.[65] One of the most popular reactions is the Suzuki reaction,[62] which relies on a boron species to transfer the aryl/alkenyl group to palladium. The Suzuki reaction is very tolerant (*i.e.* allows the presence of functional groups) and can even be performed in the presence of water.. The Sonogashira coupling is characterized by having a terminal acetylene as coupling partner in the second step of the catalytic cycle, but a catalytic amount of copper iodide is usually necessary to achieve the transmetalation.[66] In some cases the alkyl/aryl group can be transferred to palladium by a different mechanism than transmetalation.

The first part of the present chapter will cover one of the earliest examples of this, namely the Heck reaction, where the presence of an alkene allows the aryl group to be transferred via coordination to palladium and subsequent insertion. One of the most recent additions to the "family" is the Buchwald-Hartwig amination,[67] where an amine coordinates to palladium in the second step of the catalytic cycle. The second step of the catalytic cycle is shown in Figure 22 for the Buchwald-Hartwig amination and the Heck reaction.

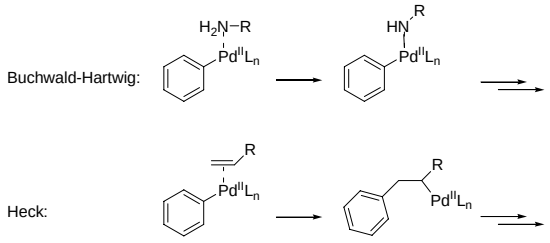

Figure 22 The 2nd step of the catalytic cycle for Buchwald-Hartwig and Heck reactions.

The second part of the present chapter deals with the palladium-catalyzed allylic alkylation (Figure 23), which is traditionally *not* included in the "family" of palladium-catalyzed coupling reactions.

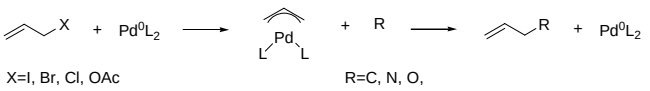

Figure 23 Simplified scheme for the Pd-catalyzed allylic alkylation.

The reaction is characterized by the initial oxidative addition taking place to an alkene with a leaving group in the allylic position, thus forming an η^3-allylpalladium complex. The allylic moiety is now electrophilic and capable of reacting with an incoming nucleophile (a malonate anion as the prototypical example) forming an alkene product.

Although mechanistically distinct from the class of cross-coupling reactions it is still a Pd(0)-Pd(II) couple, which operates in the catalytic cycle.

4.1 Mechanistic Investigations of the Heck Reaction

4.1.1 Discovery

The palladium-catalyzed arylation of olefins (i.e. the Heck reaction) was reported by Mizoroki *et al.* in 1971 (Figure 24),[68] but it was the intensive development of R. F. Heck and co-workers that brought the reaction to the attention of the organic chemistry community in general.[69]

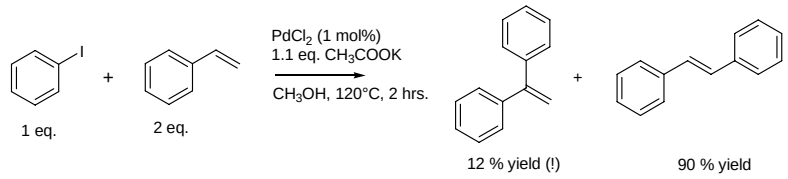

Figure 24 One of the reactions reported by Mizoroki *et. al.* in 1971 which gave birth to the Heck reaction.

The reaction has been reviewed extensively by several authors.[70] Since its discovery the Heck reaction has served as test-bed for many of the new methods in synthetic organic chemistry. For example, in 1984 a new phosphine-free protocol was introduced by Jeffery and co-workers, which relied on the use nBu$_4$Cl as phase-transfer catalyst.[71] The effect of chloride has been ascribed to its ability to coordinate to Pd, thereby increasing the nucleophilicity of Pd(0).[72] Other improvements include immobilized palladium-catalysts,[73] and a range of new catalysts which are much more efficient than "traditional" triphenylphospine-ligated palladium. To this category belongs palladacycles first discovered as catalysts in the Heck reaction by Herrmann and co-workers,[74] Pd-complexes of N-heterocyclic carbenes[75] along with a rapidly increasing number of heterogeneous, so-called "nano-particulate" palladium catalysts.[76] Currently there is an ongoing debate as to whether all these highly active catalysts are merely sources of low-ligated, homogeneous palladium.[77]

4.1.2 Mechanism

As described earlier, the catalytic cycle consists of oxidative addition, coordination to the alkene followed by insertion into the olefin C-C bond, and finally, β-hydride elimination to give the product and a palladium hydride which regenerates the active Pd(0)-catalyst in the presence of a base (Figure 25).

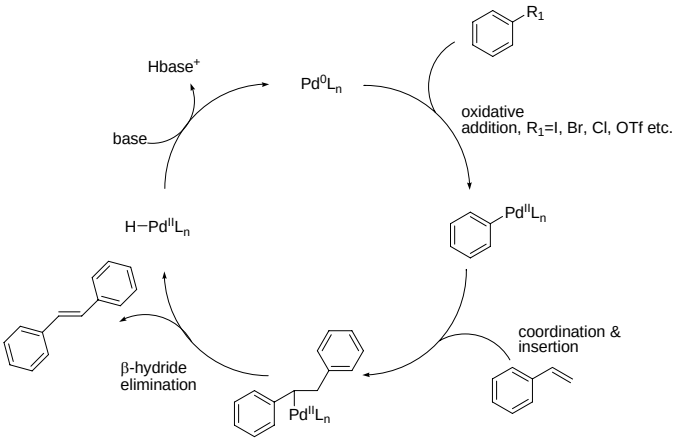

Figure 25 Schematic view of the catalytic cycle for the Heck reaction.

For simplicity only the formation of the thermodynamically favoured (*E*)-product is shown is Figure 25, but in principle all three mono-substitution products can be formed depending on the exact electronic and steric nature of the system. In 1991 Cabri and co-workers noted that the α-substitution product was favoured upon addition of TlOAc.[78] In the beginning of the 1990s the now accepted framework was suggested by Cabri[79] and Hayashi,[80] involving a catalytic cycle with either neutral or cationic intermediates depending on the choice of ligand and leaving group.

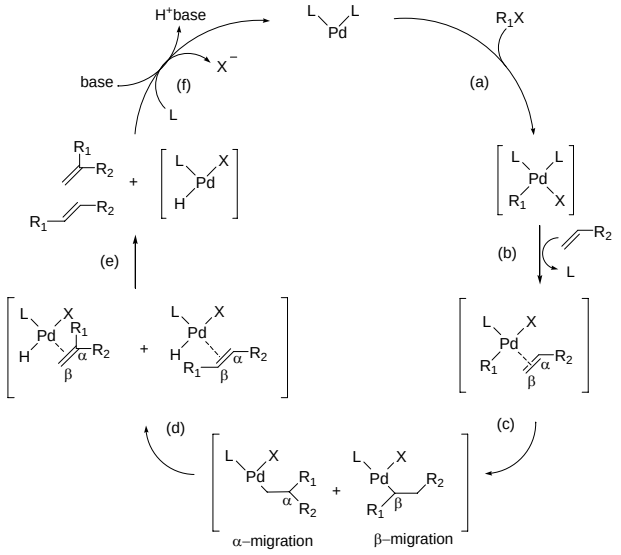

Figure 26 Overview of the neutral version of the catalytic cycle for the Heck reaction.

If a mono-dentate ligand (*e.g.* PPh_3) and a coordinating leaving group (*e.g.* halides) is used a neutral pathway is favoured with palladium ligated by one phosphine and one anion in the crucial, regiodetermining insertion step (Figure 26).

By selecting bidentate ligands (*e.g.* DPPP) and a non-coordinating or only weakly coordinating leaving group (*e.g.* triflate) a cationic pathway can be favoured. Here palladium is ligated by the diphosphine in the regiodetermining insertion step (Figure 27). If a strongly coordinating leaving group is used (*e.g.* iodide), the cationic pathway can still be favoured by addition of a thallium or silver salt.[81]

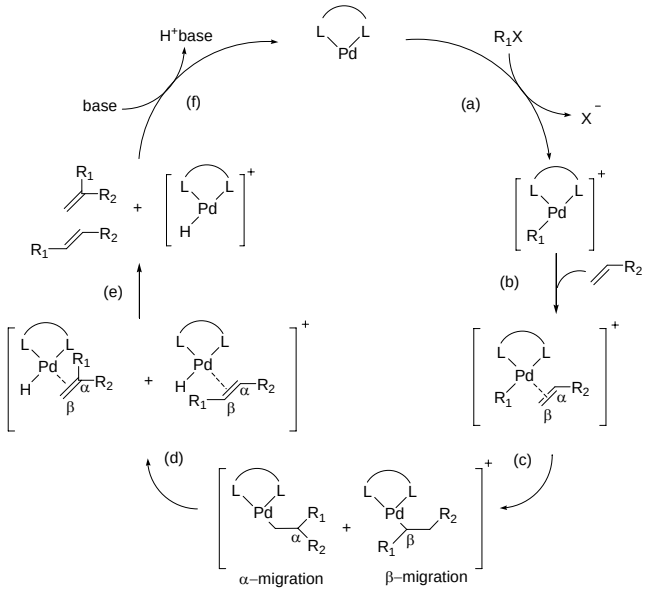

Figure 27 Overview of the cationic version of the catalytic cycle for the Heck reaction.

In a thorough mechanistic study using low-temperature NMR with stoichiometric palladium complexes Ludwig *et al.* have elucidated the influence of solvent polarity and choice of phosphine ligand on the regioselectivity.[82] They did find an effect of the diphosphine ligand on the regioselectivity, which can possibly be related to the bite angle of the ligand. The regioselectivity in the Heck reaction has also been the subject of a recent computational study by Deeth *et al.*, who succeeded in explaining the selectivity for a number of alkene substituents based on the electronic nature of the substituent.[83] These findings could rationalize the regiochemistry for *both* the neutral and the cationic pathway; however, it was found that the electronic effect was pronounced in the cationic pathway.

4.1.3 Asymmetric version

The first examples of asymmetric induction in a Heck reaction were provided almost simultaneously by the groups of Shibasaki[84] and Overman.[85] Although both reactions were intramolecular there are several differences. For example, the reaction reported by Overman and co-workers is actually a tandem reaction allowing the formation of two rings connected in a *spiro*-fashion (Figure 28).

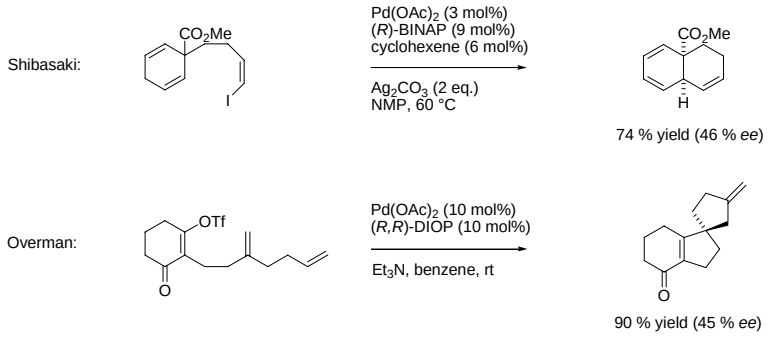

Figure 28 The first examples of asymmetric Heck reactions reported independently in 1989 by the groups of Shibasaki and Overman.

In general, the asymmetric Heck reaction has been must successful with bidentate ligands under conditions favouring the cationic pathway. This indicates that both phosphine atoms of the bidentate ligand should coordinate to palladium for maximum chiral induction. However, Overman and Poon have noted an exception,[86] where the neutral pathway gave superior *ee* (95%, compared to 43% for the cationic version) illustrating that for certain substrates the neutral pathway can be preferred. The development of the asymmetric Heck reaction has been covered in several reviews,[87] including one on the applications of the reaction in natural product synthesis.[88]

4.1.4 Introduction to Hammett Studies

One of the most popular methods for studying the mechanism of an organic reaction is to investigate the influence of electronic factors on the rate of the reaction. The method was developed by L. P. Hammett and originated from considering the acidity constants for a series of benzoic acids with different groups in the *para*- or *meta*-positions (Figure 29),[89] and is now generally referred to as a "Hammett study".[90]

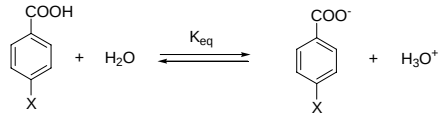

Figure 29 The acid-base equilibrium of *para*-substituted benzoic acids used by Hammett to define σ-values for a range of different substituents, X.

From the equilibrium constant a σ-value was assigned to each substituent allowing for σ(H)=0 per definition, and all other values proportional to log K_{eq} for that particular substituent (K_X, eq. 24). A positive σ-value indicates that the substituent is electron-withdrawing, whereas electron-donating substituents are characterized by having negative σ-values.

$$\sigma_X = \log K_X - \log K_H \tag{24}$$

Hammett was also able to describe the relative *rates* of hydrolysis of the corresponding esters using the same set of σ-values, which established an important connection between equilibrium constants and rate constants. They could be applied to an entire series of related reactions without having to change the σ-values but instead introducing a new parameter (ρ) to account for the different susceptibility of a given reaction to the change in the electronic properties of the substrate (eq. 25).

$$\log\left(\frac{k_X}{k_H}\right) = \sigma_X \rho \tag{25}$$

This new parameter (ρ) is positive when the reaction is accelerated by a decrease electron-density at the reaction centre, and negative when an increase in electron-density leads to rate enhancements. The magnitude of ρ indicates how strongly the rate of the reaction responds to the changes in the electronic properties of the transition state for the rate-determining step, with a typical value of six for a fully developed ion.[91] The method is especially useful when the reaction is taking place at the benzylic position, allowing for direct electronic "communication" with the substituent, X, through the conjugated π-system of the phenyl ring. Since the initial work by Hammett the method has been developed substantially, and a large collection of σ-values are available.[92]

4.1.5 Our Investigaton

As the cationic version of the Heck reaction is most frequently applied in asymmetric synthesis, we decided to perform a Hammett study using this variant of the reaction. To favour the cationic pathway the bidentate DPPP ligand was chosen in combination with phenyl triflate

as the starting material. This allows the use of a series of *para*-substituted styrenes as coupling partners, which probes the electronic effects of the *para* substituent on the overall rate of the catalytic reaction. If a linear Hammett plot is obtained, the slope of the line gives details about the electronic characteristics of the TS for the rate-determining step.[93] To allow determination of reactants and products at different levels of conversion, each individual Heck reaction was performed on a preparative scale to generate the product mixtures containing **2** and **3** as illustrated in Figure 30.

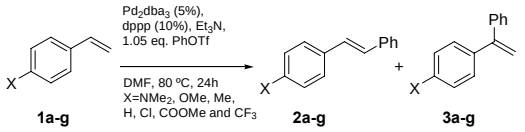

Figure 30 The reactions performed to generate the reference materials **2a-g** and **3a-g**.

In principle the Heck reaction can give three isomers, but in all cases the isolated product was a mixture of the (*E*)-stilbene and 1,1-diphenyl derivatives, whereas the (*Z*)-configured product was never observed. The ratio between the two products was dependent on X, with electron-donating substituents favouring the formation of the 1,1-diphenyl derivative.

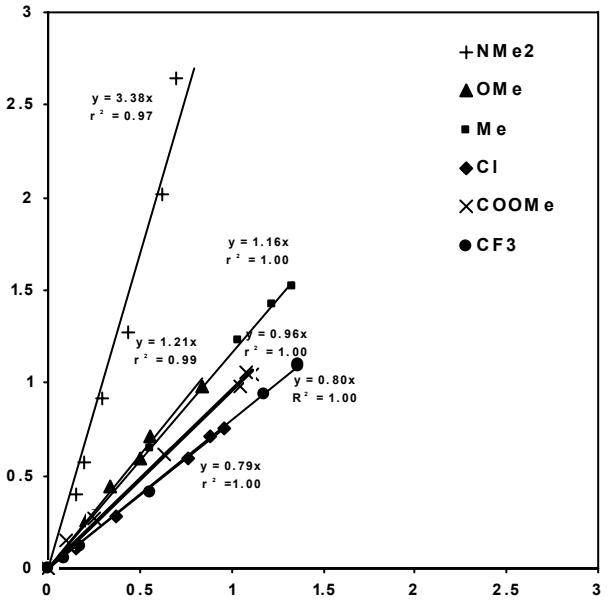

Figure 31 The linear plots obtained from following the disappearance of styrene and *para*-substituted styrenes in a series of competitive reactions.

The observed product ratio was in line with an earlier study on the reaction between styrene and phenyl triflate using DPPP as ligand, which has previously been reported to give a 65/35 mixture of (*E*)-stilbene and 1,1-diphenylethylene in 9:1 DMF:H_2O.[82] The relative reactivities of each *para*-substituted styrene are shown in Table 2 along with the appropriate σ-value.

After some optimizations with the GC program, we were able to identify all reactants and products and to assign retention times (see paper 1 for details). Using the equations introduced in section 3.8 (Molecular Ensembles) linear plots were obtained as shown in Figure 31. The dimethylamino-substituted styrene was clearly the most reactive styrene, with a reactivity more than three times that of styrene. Also the two other electron-donating substituents (OMe and Me) increased the reactivity, although to a lesser extent having a reactivity approximately 20 % higher than styrene. The electron-withdrawing substituents (Cl, COOMe and CF_3) all resulted in a slower reaction than with styrene, by up to 20 %.

Table 2 The selected para-substituted styrenes, associated σ-values and relative reaktivites.92

Compound	**Substituent (X)**	**σ**	**k_{rel}**
1a	NMe_2	-0.87	3.38
1b	OMe	-0.27	1.21
1c	Me	-0.17	1.16
1d	H	0	1
1e	Cl	0.23	0.79
1f	COOMe	0.45	0.96
1g	CF_3	0.54	0.80

With these results in hand a Hammett plot could be constructed for the overall reaction (Figure 32). Interestingly, only the left part of the Hammett plot is linear with a small negative slope (-0.53), indicating that the aryl ring is donating electron density to the reaction centre in the rate determining step. The slope of the line is in agreement with an electrophilic attack of Pd(II) upon the double bond as the rate-determining step. The observed higher reactivity of electron-rich alkenes is in agreement with the observations of Cabri *et al.* (butyl vinyl ether was more reactive than methyl acrylate).[79]

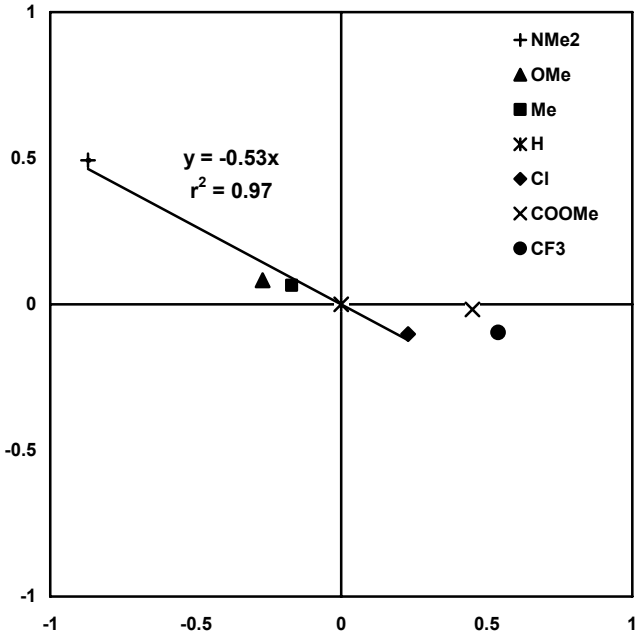

Figure 32 The Hammett plot based on kinetic data and σ-values.

However, the Hammett plot in Figure 32 is not linear over the entire range of investigated σ-values. In the right hand side of the plot (electron-withdrawing substituents) the line flattens out and there is even a slight increase in rate with the COOMe substituent compared to Cl. Such a behaviour usually indicates a shift in the mechanism of the reaction,[94] in this case suggesting two competing mechanisms were operating. One mechanism would be favoured for electron-donating substituents, the other for electron-withdrawing substituents resulting in an overall U-shaped plot although the observed increase in reactivity for COOMe is not particularly significant.[91]

In all cases the observed products were a mixture of two of the three possible regioisomers, namely the ones arising from substitution in the *geminal* or *vicinal* position relative to the phenyl group already present in the starting material. From ^{1}H NMR and GC of the product mixtures it was evident that the ratio (*r*) between the two products depended on the nature of the X substituent; however, this ratio was not constant throughout the reaction. This could be a consequence of a difference in sensitivity of the two products towards the reaction conditions. To remedy this we have chosen to use the initial value of *r* as determined by GC from samples withdrawn from the reaction mixture. The sensitivity of the FID was similar, but not identical, for the two regioisomers and the determined ratio (*r*) were corrected using ^{1}H NMR.

The determined ratios have been collected in Table 3.

Table 3 Overview of the determined ratios between products from geminal- and trans-substitution.

Compound	**Substituent (X)**	***r***
1a	NMe_2	1.27
1b	OMe	0.81
1c	Me	0.89
1d	H	0.78
1e	Cl	0.58
1f	COOMe	0.23
1g	CF_3	0.23

Using this ratio, the determined relative reactivity could be separated into two parts leading to the two observed regioisomeric products, as indicated in eq. 26:

$$k_{rel} = k_{gem} + k_{trans} \tag{26}$$

By some straightforward manipulations (eqs. 27-29) the separated reactivities were obtained, and two new Hammett plots could be constructed, each indicating the electronic effect on the formation of either of the two regioisomers (Figure 33).

$$r = k_{gem} / k_{trans} \tag{27}$$

$$k_{trans} = k_{rel} / (1 + r) \tag{28}$$

$$k_{gem} = r * k_{trans} \tag{29}$$

Interestingly, one of the two Hammett plots now has a linear dependence on σ for all the investigated compounds. The ρ value of -0.76 indicates that a positive charge is built up in the TS of the rate-determining step, which is in line with an electrophilic attack by Pd on the double bond. However, this is only the case for the formation of the *geminal* substitution product, whereas substitution in the *trans*-position does not depend on the electronic polarization of the double bond. For this product only the dimethylamino-substituted styrene is significantly faster than styrene itself and this may very well be due to this substrate acting as a better ligand for palladium.

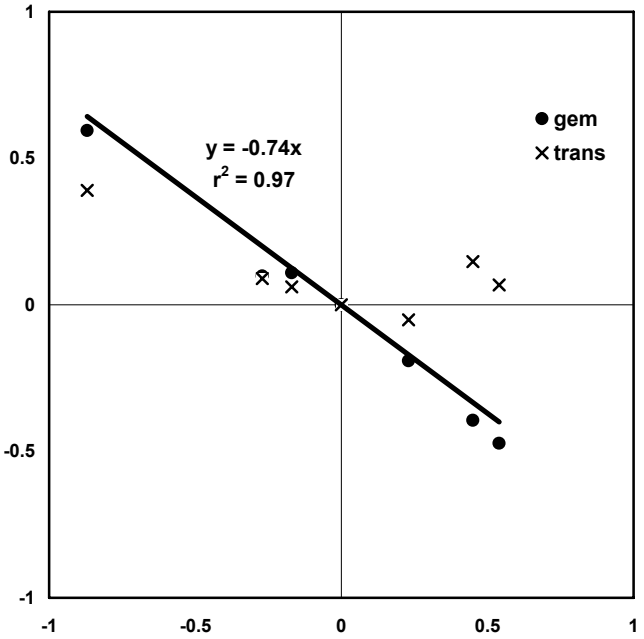

Figure 33 The two new Hammett plots, taking into account the formation of two regioisomeric products **2** and **3**.

The situation can be illustrated by the polarization of the two TS (Figure 34). It is only in the transition state leading to the formation of the α-substitution product (*i.e. geminal)* that the group in the *para*-position can interact with the developing positive charge through resonance.

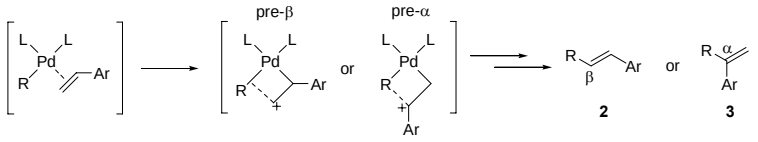

Figure 34 Palladium insertion takes places via two different transition states. Only in the pre-α transition state can the substituent in the *para*-position interact with the developing positive charge.

4.1.6 Conclusions

A Hammett study was performed on the cationic version of the Heck reaction utilizing *para*-substituted styrenes and phenyl triflate as coupling partners. Relative reactivities based on the disappearance of starting material did not give a linear Hammett correlation, although a linear

correlation was observed for the formation of the α-substitution product (also termed *geminal* substitution and giving rise to 1,1-diphenyl derivatives). The formation of this product was accelerated by electron-donating substituents, which is in line with a rate-limiting electrophilic attack by Pd(II) on the double bond, followed by a rapid migratory insertion.

The formation of the β-substitution product (*trans*-substitution, giving rise to (*E*)-stilbene derivatives) did not depend significantly on the electronic character of the substituent in the *para* position of the styrene. The current study has served to characterize the electronic nature of the rate-limiting TS, which could be useful in the development of improved catalytic systems for this reaction.

4.2 Palladium-Catalyzed Allylic Alkylation

The palladium-catalyzed allylic alkylation constitutes one of the major research areas within organic chemistry due to its ability to construct a variety of different bonds (C-C, C-N, C-O etc.) often with excellent enantioselectivity (Figure 35). The reaction has been applied to a large number of natural product total syntheses with good results.[95] Owing to its success, the reaction has been reviewed numerous times,[96] and has also been the subject of several book chapters.[97]

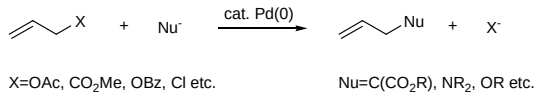

Figure 35 The general transformation performed with Pd-catalyzed allylic alkylation.

As indicated in Figure 35 a variety of leaving groups (X) are tolerated, in addition to the prototypical acetate. Carbonates were introduced by Tsuji,[98] and are particularly useful for sensitive substrates since the liberated base can deprotonate the nucleophile, thus limiting the use of base to catalytic amounts. Another way of achieving this goal is to use the BSA-procedure developed by Trost and Murphy.[99] Chlorides are often too reactive, but has allowed achievement of a relatively high TON (>4000) using only 0.002 mol% of catalyst.[100] For screening of ligands or mechanistic studies a typical of choice of nucleophile is malonates; however, numerous other stabilized carbanions are applicable,[96c] and in addition carboxylates,[101] phenols,[102] and sulphur-based[103] nucleophiles. Many examples of the addition of nitrogen-based nucleophiles (*i.e.* amination) exist.[104] In the following introductory section, the focus will be on the mechanistic features of the reaction with particular focus on regiochemistry. This subject is the "common denominator" for the research described in the following chapters (4.3-4.6).

4.2.1 Discovery

The reaction of a nucleophile with a π-allylpalladium complex was first achieved by Tsuji and co-workers in 1965 with the addition of deprotonated malonate to the π-allylpalladium chloride dimer in DMSO (Figure 36).[105] This particular reaction was stoichiometric in palladium and limited to DMSO as a solvent, presumably due to its coordinating abilities towards palladium.

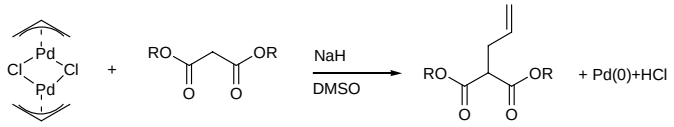

Figure 36 The first example of a reaction between an π-allylpalladium complex with a nucleophile.

However, it was the addition of phosphine ligands (usually PPh_3), which displace chloride, leading to the formation of a cationic allylpalladium complex, that made the reaction synthetically useful.[106] The phosphine ligands could stabilize Pd(0) through back-donation, which allowed the reaction to be run in less coordinating solvents (THF, CH_2Cl_2 etc.) without precipitation of metallic palladium ("palladium black").

4.2.2 Mechanism

The generally accepted mechanism for Pd-catalyzed allylic alkylation involves four discrete steps where regio- and/or stereochemistry can be induced (Figure 37). The catalytic cycle commences with the coordination of a suitably ligated Pd(0)-species to an alkene with a leaving group in the allylic position. This is followed by an ionization (oxidative addition) which generates the π-allylpalladium(II) intermediate. The allyl moiety can be trapped by a nucleophile, which furnishes the final product complexed to Pd(0). A decomplexation releases the product and releases the active Pd(0)-catalyst.

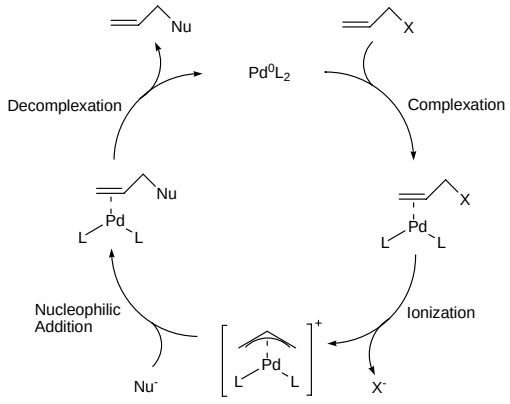

Figure 37 General catalytic cycle for the palladium-catalyzed allylic alkylation.

When one or more substituents are present the allyl intermediate can undergo isomerization prior to nucleophilic attack. A number of different types of isomerization can take place in the

allylpalladium complex including *syn/anti*-isomerization,[107] apparent rotation[108] or exchange of the allyl by S_N2 attack of external Pd(0).[109] In Figure 38 is shown a selection of possible mechanistic pathways but it should be noted that several other proposals exist in the literature. Increased rates of isomerization have been observed upon addition of halides (F^- or Cl^-),[110] or with the use of a more strongly coordinating solvent.[111]

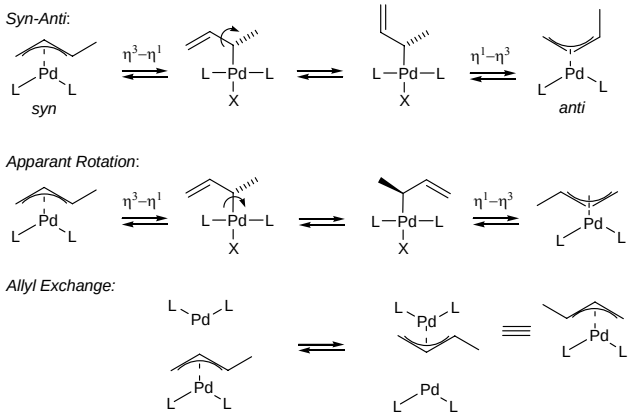

Figure 38 Some of the different types of isomerization processes plausible for allylpalladium complexes.

This is easily rationalized by X=halide/solvent in Figure 38 although a rigorous computational investigation has not yet been reported. In catalytic reactions the concentration of free Pd(0) is very low, and as a result the allyl exchange between different palladium species is very slow.[112]

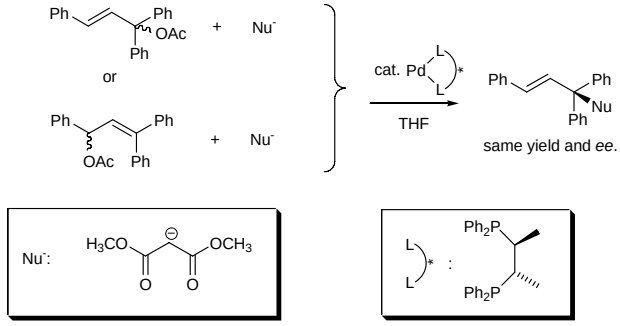

Figure 39 One of the examples of a Pd-catalyzed asymmetric alkylation under thermodynamic control reported by Bosnich and co-workers.

With aromatic substituents isomerization is usually faster than nucleophilic attack as illustrated by Bosnich and co-workers for the asymmetric reaction shown in Figure 39,[113] whereas for alkyl-substituents the rate of isomerization is comparable to the rate of nucleophilic attack.

In principle fine-tuning of the experimental conditions could allow synthesis of either the thermodynamic product (usually arising from the *syn*-allyl complex) or the kinetic product. However, in most applications a chiral ligand is used to control the regio- and enantioselectivity of the nucleophilic addition to an allylpalladium intermediate which has fully equilibrated by *syn-anti* isomerization and apparent rotation processes. In some cases very reactive nucleophiles have been utilized to suppress the isomerization processes completely.[114]

4.2.3 Asymmetric Version

The first example of asymmetric induction in a stoichiometric alkylation was reported by Trost and Dietsche in 1973,[115] however it was the disclosure of a *catalytic* enantioselective allylic alkylation in 1977 which initiated an extensive development of the asymmetric allylic alkylation (AAA), see Figure 40.[116]

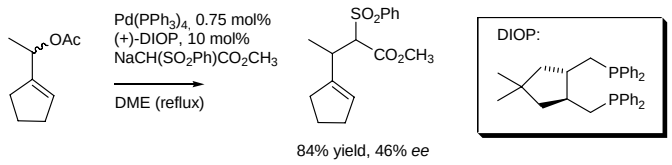

Figure 40 One of the examples of a catalytic asymmetric induction reported by Trost and co-workers in 1997.

Since the bond-forming reaction takes place on the face of the allyl opposite to the metal atom a chiral ligand has difficulties influencing the course of the reaction (*i.e.* to impart enantioselectivity). Two approaches has been taken to overcome this difficulty, the first one being ligands capable of reaching "behind" the allyl as illustrated by the work of Hayashi and co-workers (Figure 41).[117]

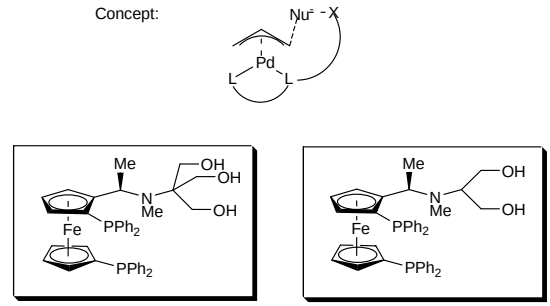

Figure 41 The concept used by Hayashi and co-workers along with two of the chiral ligands.

Although good results were obtained by Hayashi, the majority of later, successful chiral ligands have instead functioned by a distortion of the allyl ligand, thus favouring the formation of the desired enantiomer. The "benchmark" reaction, which has been tested for nearly 100 chiral ligands, is the allylic alkylation of the 1,3-diphenyl-substituted allyl moiety (Figure 42). A summary of 47 ligands which gives enantioselectivities >90% has been collected as part of a recent book chapter.[97]

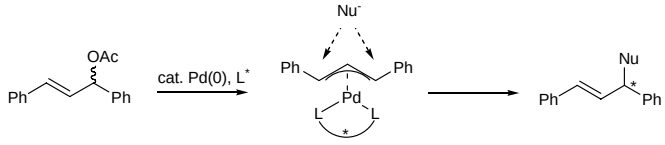

Figure 42 The benchmark reaction used to test the efficiency of new chiral ligands in the Pd-catalyzed asymmetric alkylation.

Unfortunately, when a good ligand has been found by testing it in the benchmark reaction it often does not perform very well on other allylic substrates. In this regard, the benchmark reaction is often considered "easy", whereas the corresponding dimethyl-substituted allyl substrate is considered "difficult". The most successful ligand for allylic substrates with methyl substituents or cyclic substrates has been the so-called "Trost ligand".[118] The ligand has a large bite angle, which allows the phenyl substituents to interact directly with the allyl moiety (Figure 43).

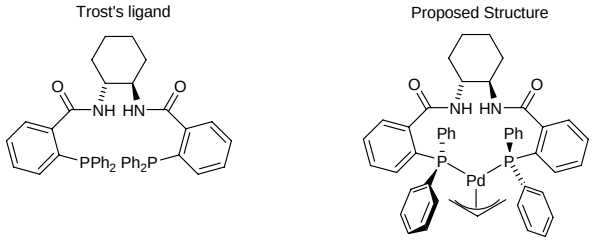

Figure 43 Left: structure of the successful ligand developed by Trost and co-workers. Right: Proposed structure of the π-allylpalladium complex with Trost's ligand.

Large allylic substrates, such as the diphenyl-substituted one in the benchmark reaction is not accommodated very well in the chiral "pocket" and consequently yields relatively poor *ee* (87%). However, this ligand construction has been overwhelmingly effective in the *meso*-desymmetrizations of enantiotopic leaving groups on five-, six, and seven-membered rings (Figure 44).[119]

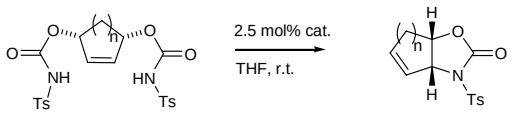

n	*ee*
1	88
2	97
3	95

Figure 44 Examples of *meso*-desymmetrizations performed by Trost and co-workers.

One of the most successful ligand classes are the so-called "PN-ligands" which were developed independently by the groups of Pfaltz,[120] Helmchen[121] and Williams (Figure 45).[122] The enantioselectivity was a result of the combined action of steric and electronic effects. By using two different elements for coordination to palladium an electronic preference for attack at the position *trans* to phosphorus was realized.[123,124,125] Furthermore, a large group (*e.g.* *t*Bu) in proximity of the allyl only allows rotation in one of the two possible directions in the transition from an η^3- to an η^2-coordination mode (Figure 45, right).

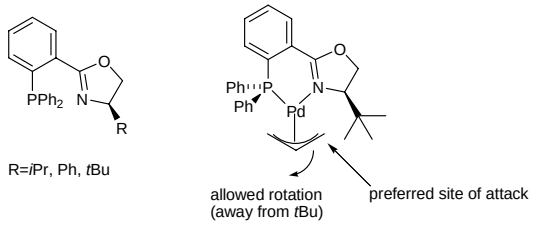

Figure 45 The general structure for some of the successful P,N-ligands along with a simple illustration of the regio- and enantio-determining elements.

Since their discovery, the P,N-ligands have proven useful in several other Pd-catalyzed reactions,[126] and as such they constitute an important addition to the "traditional" P,P- or N,N-ligands.

4.2.4 Metals other than palladium

Finally, it should be mentioned that the allylic alkylation has been extended to several other transition metals with tungsten,[127] molybdenum and iridium[128] yielding the most promising results. Trost and Hachiya have reported excellent yields and enantioselectivities using a Mo-catalyst in the allylic alkylation of the "difficult" substrates bearing only a small alkyl substituent.[129]

In the following chapter a computational study of nitrogen-based ligands in the Pd-catalyzed allylic alkylation will be presented. The short Pd-N bond should allow positioning of chiral control elements very close to the metal centre, but the inability of nitrogen-based ligands to stabilize palladium(0) often results in precipitation of palladium black during the reaction. The good ligation of palladium(II) has allowed the isolation and characterization of the allylpalladium complexes, and in the following chapter the obtained results using two phenanthroline-type ligands will be compared to computational results.

4.3 Phenanthroline-type Ligands

4.3.1 Introduction

The aim of this computational study is to investigate the selectivity-determining features of Pd-catalyzed allylic alkylation using nitrogen-based ligands. The applications of these ligands in asymmetric synthesis have recently been reviewed.[130] Nitrogen-based ligands of the phenanthroline-type have some advantages in mechanistic studies where it has been possible to isolate the *syn*- and *anti*-crotylpalladium complexes, characterize them, and study their reactivity towards nucleophiles.[131,132] This gives access to a large body of experimental data, which is not easily obtainable for the more popular P,P- or P,N-based ligands. A previous computational study on the allylic amination by Blöchl and Togni[123c] employed a neutral NH_3 as nucleophile. With this nucleophile, transition states can be found in gas phase, whereas for C-C bond formation this is not possible.[133] Here, the reaction between the cationic allylpalladium complex and the negatively charged nucleophile occurs without a barrier. Previously, it has been shown that a solvation model is necessary to stabilize the reactants, thus leading to the existence of a transition state also in the computational description of the reaction.[133] In the current study we employ a Poisson-Boltzmann self-consistent reaction field polarized continuum solvation model, which has been found to give good results at a relatively low computational cost.

4.3.2 Experimental Results

This study is directed towards explaining the differences in selectivity observed experimentally with phenanthroline or neocuproine (1,10-dimethylphenanthroline) as ligands, while using sodium malonates as nucleophiles. The first part of the experimental results concerning the *syn-anti* equilibrium was reported in 1992 (Figure 46).[131,134]

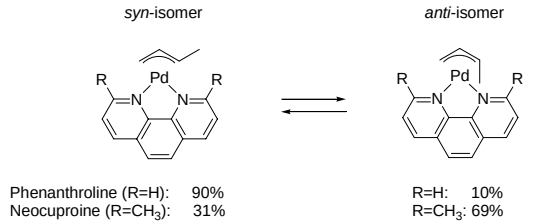

Figure 46 The equilibrium distributions between the *syn* and *anti* isomer of the allylpalladium complex are shown for the two ligands included in this study.

By reacting the isolated *syn*- and *anti*-(η^3-2-butenyl)palladium complexes independently with either dimethyl malonate or diethyl methylmalonate the following isomeric distributions were obtained (Figure 47).

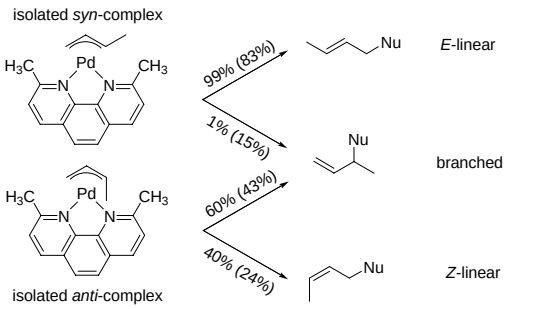

Nucleophiles: First numbers: $CMe(CO_2Et)_2$, in parenthesis: $CH(CO_2Me_2)_2$

Figure 47 Overview of the selectivities obtained by Sjögren *et. al.* when using the isolated *syn*- and *anti*-allylpalladium complexes with diethyl methylmalonate as nucleophile.

On the *syn*-isomer, attack at the terminal position is favoured giving rise to formation of the *E*-linear product. With diethyl methylmalonate the selectivity is absolute (99%), whereas for the less sterically demanding dimethyl malonate there is also formation of minor amounts of the branched isomer (15%) as a result of attack in the internal position. With the *anti*-isomer, attack at the internal position is slightly favoured regardless of which nucleophile is used. With the diethyl methylmalonate the ratio is 60:40 in favour of internal attack, whereas for dimethyl malonate as nucleophile there seems to have been some degree of isomerization leading to 33% of the *E*-linear product, from terminal attack on the *syn*-isomer and also an elevated level of branched isomer from internal attack on either the *syn* or the *anti*-isomer.

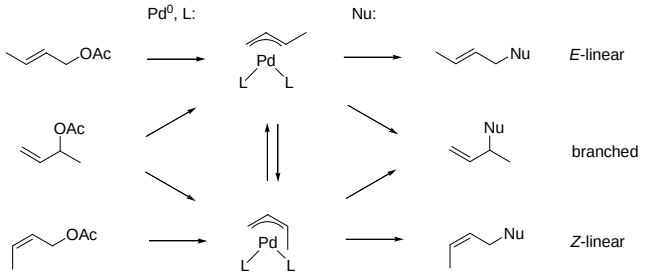

Figure 48 Overview of the possible reactions between regiochemical isomers during the course of the reaction.

The observed results could be rationalized by the reactions and equilibria depicted in Figure 48. The difference in the propensity for isomerization of *E*- and *Z*-stereoisomer has allowed the development of a *stereoconvergent* procedure (Figure 49),[135] where both enantiomers of a starting material are turned into the same enantiomer, an approach which has recently proved useful in total synthesis of two natural products.[136]

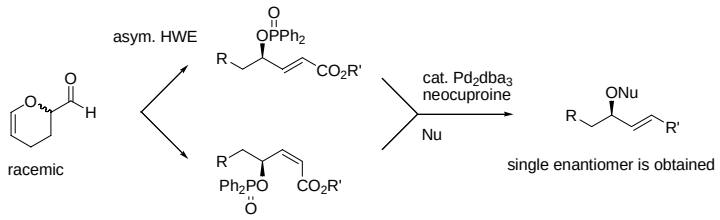

Figure 49 Example of the *stereoconvergent* procedure which has recently been used in natural products synthesis by Rein and co-workers.[136]

4.3.3 Computational Methods

All calculations were performed using Jaguar version 4.2 (release 77)[137] at the B3LYP level of theory.[39] The basis set used was LACVP*, which corresponds to a 6-31G* basis set for non-metal atoms and an effective core potential (ECP) and basis set for palladium developed by Hay and Wadt.[138]

Initial calculations were performed *in vacuo* using ammonia as nucleophile, where a full vibrational analysis of transition state structures were possible, followed by reoptimization of the transition state in solvent using the Poisson-Boltzmann self consistent reaction field[42] (PB-SCRF) with parameters for CH_2Cl_2 (ε=9.08, M_w=84.93 and ρ=1.3266 resulting in a probe radius of 2.332). With the anionic malonate nucleophile, transition states could only be obtained using the solvation model.

4.3.4 Results

Examining the experimental system in detail one immediately realizes that the size of the system is relatively large for a thorough quantum chemical investigation. Rather than to use a mixed QM/MM approach, we have decided to investigate the two selectivity-determining factors, namely the ligand-allyl interactions and the allyl-nucleophile interactions, separately. This simplification requires that the ligand and nucleophile does not interact directly, and for the systems employed here this is a valid assumption, with the large palladium-atom acting as a

"spacer". The philosophy and the model systems employed in the current work are illustrated in Figure 50.

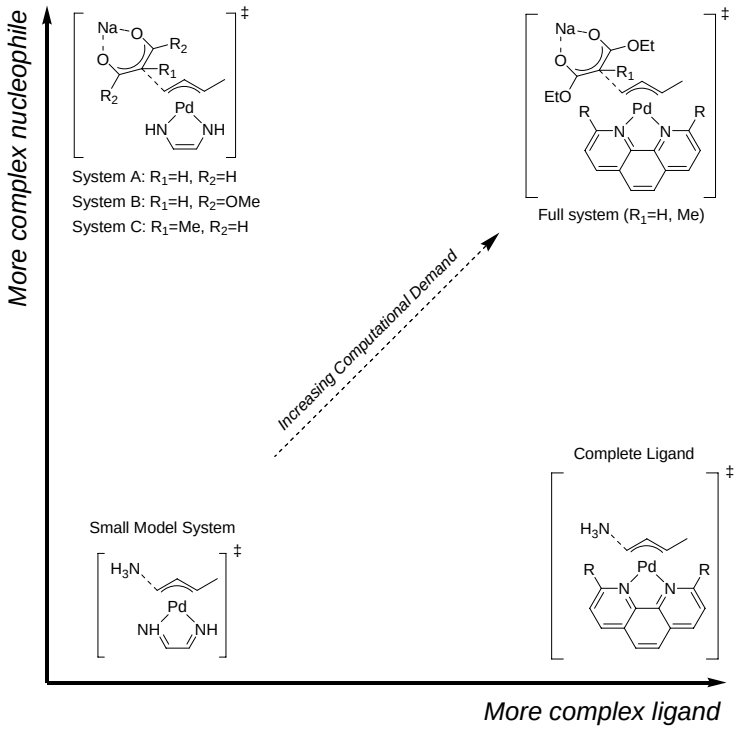

Figure 50 Illustration of the model systems used in the current study. With the complete ligand either phenanthroline (R=H) or neocuproine is used (R=Me).

4.3.4.1 Small Model System

Calculations on the isolated *syn*- and *anti*-allyl complexes revealed a preference for the *syn*-isomer (8.7 kJ/mol) and this difference is also reflected in the relative energies of the transition states, where the transition states from the *syn*-isomer have the lowest energies. In gas phase the lowest energy transition state was obtained for attack of NH_3 in the internal position (C-N distance 2.02 Å). Attack in the terminal position on the *syn*-allyl was disfavoured by 3 kJ/mol (C-N distance 1.93 Å); however, this preference for internal attack is not present when a solvation model is employed. Also for the *anti*-allyl species attack in the internal position was the preferred regioisomer of the transition state (7.2 kJ/mol higher than *syn*, internal and C-N

distance 2.03Å). Finally, the least favoured mode of attack was in the terminal position on the *anti*-allyl.

When a solvation model (CH_2Cl_2) was used the C-N distance in the TS was elongated by approximately 0.2 Å. Furthermore, the relative energies changed so the overall most favourable isomer is now terminal attack on the *syn*-allyl, with internal attack on the *syn*-allyl disfavoured by less than 1 kJ/mol. Both of the *anti*-configured transition states have an approximately 7 kJ/mol higher energy than the lowest energy TS. All energies and C-N distances for the discussed TS structures have been collected in Table 4.

Table 4 Relative energies for the 8 transition states obtained with the α,α-diimine model system using ammonia as nucleophile.

Pd-allyl	Position	gas phase		with solvation	
		C-C dist. (Å)	TS Energy (kJ/mol)	C-C dist. (Å)	TS Energy (kJ/mol)
anti	internal	2.03	7.2	2.26	7.1
anti	terminal	1.94	9.5	2.19	7.0
syn	internal	2.02	0.0	2.24	0.6
syn	terminal	1.93	3.0	2.18	0.0

4.3.4.2 Model system A

With the transition states for the simple ammonia nucleophile in hand we turned our attention to the more realistic stabilized carbanions. The first and simplest model consisted of the malonic dialdehyde anion (model system A) while keeping the α,α-diimine ligand as model for phenanthroline/neocuproine (Figure 50, top, left). With a non-symmetrical nucleophile as the malonate-type there are three possible isomeric transition states corresponding to the three rotamers with respect to the forming C-C single bond. Throughout this work they have been identified by which portion of the allyl the chelating sodium cation is proximal to, *i.e.* the allyl moiety, a methyl group (only possible when the attack is internal) and a hydrogen atom in either *syn*- or *anti*-position (Figure 51, right).

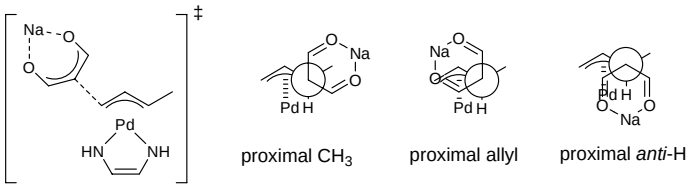

Figure 51 The model system A used to investigate the "inherent" reactivity and selectivity with the minimalist α,α-diimine as ligand and malonic dialdehyde as nucleophile.

Using model system A and a solvation model for CH_2Cl_2 the 12 different transition states were located. The relative energies and the length of the forming C-C bond are shown in Table 5 for the twelve possible TS. All three rotational isomers for each possible TS were located. Shown in bold are the lowest relative energies obtained for each of the TS leading to the four possible regioisomers, which are also the structures depicted in Figure 52.

Table 5 Relative energies for the 12 transition states obtained with the α,α-diimine model system using malonic dialdehyde as nucleophile. Bold indicates the lowest TS for each isomer.

Pd-allyl	**Position**	**prox. CH_3**		**prox. Allyl**		**prox. *syn*-H**		**prox. *anti*-H**	
		C-C dist. (Å)	TS Energy (kJ/mol)	C-C dist. (Å)	TS Energy (kJ/mol)	C-C dist. (Å)	TS Energy (kJ/mol)	C-C dist. (Å)	TS Energy (kJ/mol)
anti	internal	2.18	**6.1**	2.19	7.6	2.21	10.4		
anti	terminal			2.14	**5.2**	2.17	7.0	2.16	8.0
syn	internal	2.19	**0.0**	2.16	1.7			2.21	6.4
syn	terminal			2.14	1.4	2.17	**0.8**	2.18	1.8

For the *anti*-isomer terminal attack is favoured slightly (~1kJ/mol), whereas for the *syn*-isomer internal attack is favoured by approximately the same amount of energy. In general, the length of the forming C-C bond was 2.14-2.21 Å in the transition state (Figure 52).

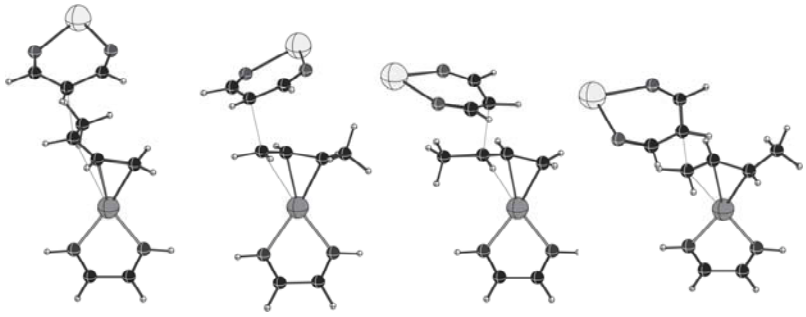

Figure 52 The lowest energy transition states determined for each regioisomer, obtained for attack of the malonic dialdehyde on either the *anti*-allyl (two on the left) or on the *syn*-allyl (two on the right). For each orientation of the allyl attack on the internal position is shown to the left of the terminal position.

4.3.4.3 Influence of ester groups (model system B)

Using the α,α-diimine model ligand as before, the methyl ester groups were now added to the nucleophile (Figure 50, system B). This results in a more sterically hindered nucleophile, which should behave similarly to the ethyl ester used in the experimental work. Figure 53 depicts the transition states with lowest energy, one for each of the four possible isomers.

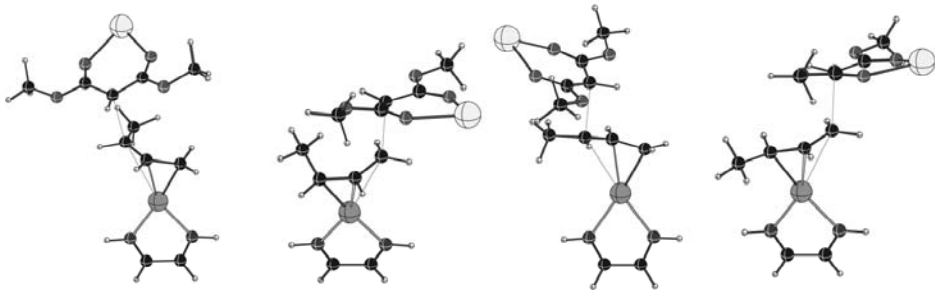

Figure 53 The four lowest energy transition states with methoxy groups added to the nucleophile.

In Table 6 the energy of the different isomers relative to the most favourable isomer is shown along with the length of the forming C-C bond in the transition state.

Table 6 Relative energies for the 12 transition states obtained with the α,α-diimine model system using dimethyl malonate as nucleophile. Bold indicates the lowest TS for each isomer.

Pd-allyl	**Position**	**prox. CH_3**		**prox. Allyl**		**prox. *syn*-H**		**prox. *anti*-H**	
		C-C dist. (Å)	TS Energy (kJ/mol)	C-C dist. (Å)	TS Energy (kJ/mol)	C-C dist. (Å)	TS Energy (kJ/mol)	C-C dist. (Å)	TS Energy (kJ/mol)
anti	internal	2.40	**8.3**	2.38	12.6	2.37	10.1		
anti	terminal			2.29	10.1	2.31	**8.3**	2.31	8.7
syn	internal	2.36	**1.5**	2.39	11.8			2.38	6.5
syn	terminal			2.30	5.7	2.32	**0.0**	2.32	2.3

Enlargement of the malonate nucleophile also including two methyl ester moieties have lead to the expected lowering of energy for approaches where the steric interactions between the incoming nucleophile and the allyl are minimized. When comparing to the TS obtained with the smaller malonic dialdehyde, the approach termed "prox. allyl" has increased by about 4 kJ/mol in energy when compared to the approaches proximal to the hydrogen situated on the allyl (*syn* or *anti*). The approach over the methyl substituent has also increased in energy although to much lesser extent (ca. 1-2 kJ/mol). Interestingly, addition to the *anti*-allyl is expected to take place with 50:50 distributions between the internal and the terminal position, which is in good agreement with the experimental results. For the *syn*-allyl attack in the terminal position is now the most favoured transition state of the 12 isomers, although the internal attack is only disfavoured by 1.5 kJ/mol.

4.3.4.4 Influence of a methyl group (model system C)

With the more sterically demanding methylmalonate nucleophile, attack at the less hindered terminal position on the *syn*-allyl accounts for all of the isolated product. This was investigated using the α,α-diimine model ligand and methyl malonic dialdehyde as nucleophile (Figure 50, system C). Relative energies and length of the forming C-C bond for the 12 obtained TS have been collected in Table 7. The increased steric demand of the nucleophile has lead to the expected discrimination between internal and terminal attack on the *syn*-allylpalladium complex, the latter now being favoured by >6 kJ/mol. This is in good agreement with the experimental observation that only linear product is formed from this isomer. Also for the *anti*-allyl palladium complex attack in the terminal position is now the favoured reaction path, although the

difference is smaller (4-5 kJ/mol). This is in contrast to the experimental observations where almost equal amounts of linear and branched products were obtained, but the difference could very well be ascribed to the influence of the ligand, which will be investigated in the following section.

Table 7 Relative energies for the 12 transition states obtained with the α,α-diimine model system using methylmalonic dialdehyde as nucleophile. Bold indicates the lowest TS for each isomer.

Pd-allyl	Position	prox. CH_3		prox. Allyl		prox. *syn*-H		prox. *anti*-H	
		C-C dist. (Å)	TS Energy (kJ/mol)	C-C dist. (Å)	TS Energy (kJ/mol)	C-C dist. (Å)	TS Energy (kJ/mol)	C-C dist. (Å)	TS Energy (kJ/mol)
anti	internal	2.18	12.9	2.18	15.2	2.19	**12.2**		
anti	terminal			2.18	**7.4**	2.16	8.7	2.17	8.6
syn	internal	2.18	**7.5**	2.16	10.8			2.20	9.2
syn	terminal			2.13	3.6	2.17	**0.0**	2.18	3.5

4.3.4.5 Calculations with large ligands

Initial calculations were performed on the ground-state allyl complexes using the "complete"[i] ligands phenanthroline and neocuproine (Figure 54).

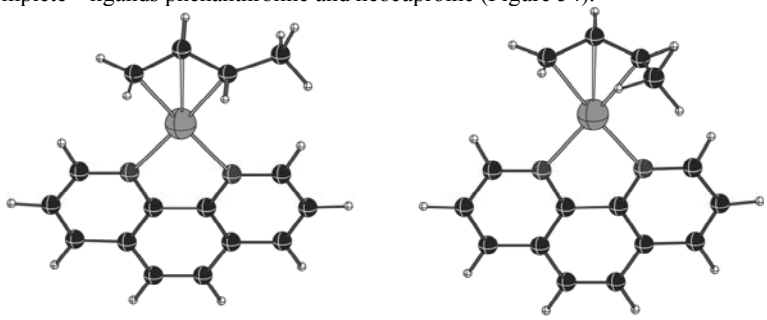

Figure 54 The structures of the *syn* (left) and *anti* (right) allylpalladium complexes with phenanthroline as ligand.

[i] In this respect "complete" indicates that the ligands are identical to those used experimentally.

With phenanthroline the *syn* isomer of the palladium allyl complex is favoured by 7.1 kJ/mol compared to the *anti* isomer. At ambient temperature this corresponds to a *syn*:*anti* ratio of 95:5, which compares relatively well to the experimentally determined *syn*:*anti* ratio of 90:10.[139]

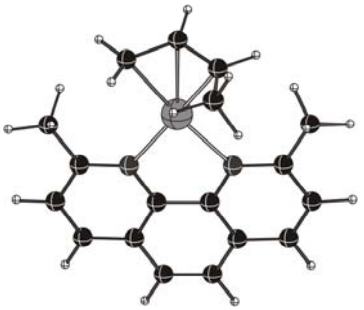

Figure 55 The *anti*-allyl palladium complex with neocuproine as ligand. Notice how the bent *anti*-allyl fits nicely between the two methyl substituents on the ligand.

Similar calculations were performed with the neocuproine ligand, where the two additional methyl groups are positioned very close to the allyl moiety, thus favouring the bent *anti*-isomer over the extended *syn*-isomer (Figure 55). The exclusion of the *syn*-isomer from the "pocket" between the two methyl groups leads to two different *syn*-isomers with the allyl moiety positioned on opposite sides with respect to plane of the ligand (Figure 56).

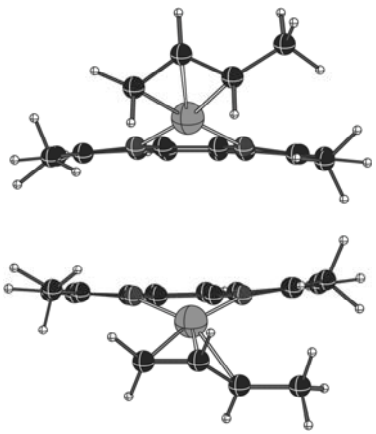

Figure 56 The two different *syn*-allyl complexes found with the neocuproine ligand. Note the steric congestion which forces palladium out of the plane of the ligand and also causes the ligand to bend away from the allyl moiety.

The strained nature of the two *syn*-allylpalladium complexes when neocuproine is used as ligand has important consequences for the regioselectivity of nucleophilic attack. As mentioned previously, the addition of a nucleophile results in a change in hapticity (η^3-allyl → η^2-olefin) and as a consequence a rotation of the entire group takes place while the nucleophile is approaching.[140] Depending on the steric influence exerted by the ligand on the allyl moiety this can either favour or disfavour a particular reaction pathway (Figure 57).

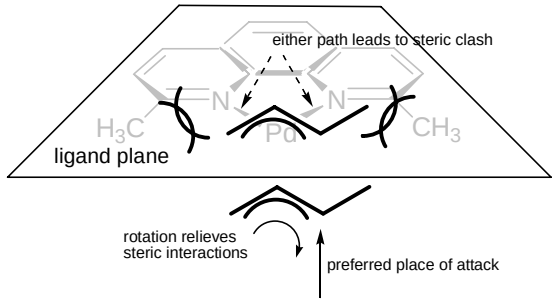

Figure 57 With neocuproine as ligand the *syn*-allylpalladium complex is pre-determined to react in the internal position due to a relieve of steric strain via rotation to the η^2-olefin complex.

Using NH_3 as a model nucleophile this phenomenon was investigated quantitatively by location of the relevant transition states in gas phase (Table 8). Determination of the transition states with a solvation model gave energies in agreement with the determined gas phase energies within 1-2 kJ/mol.

Table 8 Data for the eight transition states obtained with the phenanthroline or neocuproine as ligands and ammonia as nucleophile (gas phase). Only the lowest energy TS is reported for each conformer.

Pd-allyl	Position	phenanthroline		neocuproine	
		C-C dist. (Å)	TS Energy (kJ/mol)	C-C dist. (Å)	TS Energy (kJ/mol)
anti	internal	1.93	7.4	1.94	1.1
anti	terminal	1.86	10.6	1.88	8.8
syn	internal	1.91	0.0	1.95	0.0
syn	terminal	1.85	4.3	1.89	3.2

As illustrated in Figure 57 the *syn*-allyl isomer situated below the plane of the ligand is set up for nucleophilic attack in the internal position. This is clearly seen in the structures and energies using a simple NH_3 model, where this isomer is favoured by 3 kJ/mol compared to nucleophilic attack in either of the allylic carbon atoms on the isomer situated above the plane of the ligand.

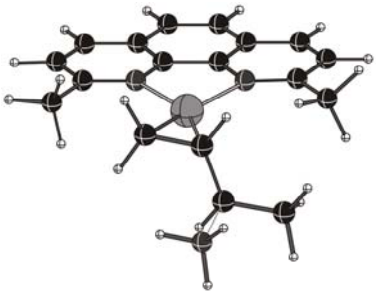

Figure 58 The favoured internal attack on the *syn*-allyl. In this case the rotation of the allyl is "sterically allowed" and brings the forming double bond into the correct square-planar orientation.

Terminal attack on the allyl moiety situated below the plane of the ligand leads to a steric clash between the methyl substituents on the allyl and on the ligand, respectively. This clearly unfavoured transition state could not be located.

The reactivity of the *anti*-isomer was also probed by a NH_3 model nucleophile, and here internal attack was favoured by 7 kJ/mol compared to terminal attack (Figure 58). This can be attributed to steric interactions between the allyl moiety and the methyl substituents on the neocuproine ligand, since for the small model system (with α,α-diimine as ligand) the two paths are isoenergetic. Experimentally, the two reaction paths were observed to give a mixture of branched and linear product indicating that the two competing TSs are almost equal in energy. With the methyl-substituted nucleophile (model system C) we noted a preference for attack in the terminal position (4-5 kJ/mol); however, when the effect of the full ligand is included this difference in energy is reduced to 1-2 kJ/mol, which is in good agreement with the experimental observations.

4.3.5 Conclusions

The palladium-catalyzed nucleophilic allylic substitution was investigated at the B3LYP level of theory. This initial study started with a rather simple model system, which was extended to larger systems involving realistic ligands and nucleophiles. The present study has illustrated

that the overall selectivity in this reaction can be derived from a sum of ligand-allyl and allyl-nucleophile contributions, which significantly reduces the computational demand.

The calculated selectivities were in reasonable agreement with values derived from experimental studies, which holds great promise for further developments with computational predictions of selectivity in this reaction.

4.4 Memory Effects – experimental approach

4.4.1 Introduction

The term "memory effect" has been used to describe products or product distributions resulting from Pd-catalyzed allylic alkylations which depend on the regiochemistry or enantiopurity of the starting materials. The first examples were reported by Fiaud and Malleron,[141] who discovered that enantiomerically enriched cyclohexenyl acetate retained some of the optical activity upon alkylation – even when using *achiral* ligands. These results were immediately disputed by Trost and Schmuff – although these authors regrettably argued on the basis of results obtained with a different combination of substrate and catalyst.[142]

In 1990 Hayashi and co-workers observed a different *ee* of the chiral product in an allylic amination of an η^3-butenylpalladium complex using a chiral ligand of the "Trost family". The linear crotyl acetate afforded the chiral product in 84% *ee*, whereas use of the branched 3-acetoxy-1-butene resulted in only 64% *ee* (Figure 59).[143]

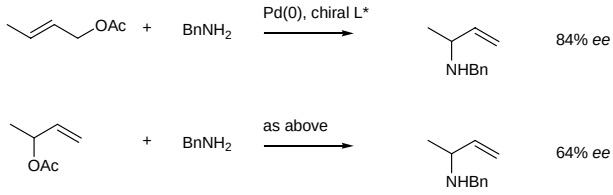

Figure 59 The memory effects observed by Hayashi and co-workers.

In a later study Hayashi and co-workers discovered that the addition of LiI lead to the exclusive formation of the linear product (Figure 60), and were able to show that the observed regiochemistries could be reproduced by stoichiometric reaction of the isolated allylpalladium complexes (Figure 61).

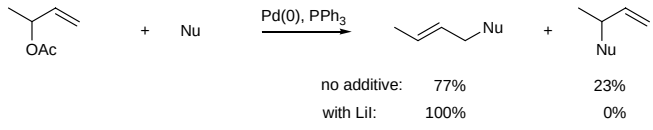

Figure 60 The dramatic effect of LiI on the regiochemistry of the Pd-catalyzed allylic alkylation.

However, one should notice that the straightforward inclusion of the neutral, mixed η^3-allylpalladium complexes as reactive intermediates in the catalytic reaction implies that nucleophilic addition takes place *trans* to the halide. Usually, the larger *trans*-effect of phosphorus is used to argue for a more facile ionization and nucleophilic addition *trans* to phosphorus.

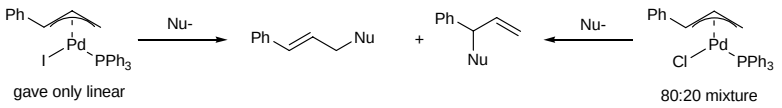

Figure 61 The stoichiometric reactions used by Hayashi and co-workers to justify the involvement of a mixed, neutral η^3-allylpalladium complex in the catalytic reaction.

In a comparison of PPh_3 and PCy_3 Williams and co-workers noted a strong influence of the ligand on the regiochemistry of the products arising from allylation of 3-acetoxy-1-butene (Figure 62).[144] These results imply that isomerization takes place with a rate comparable to nucleophilic addition.

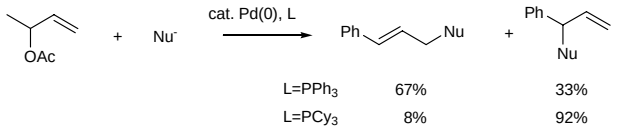

Figure 62 The dramatic influence of the phosphine ligand on the regiochemistry of the Pd-catalyzed allylic alkylation reported by Williams and co-workers.

However, it was the impressive "tour de force" by Lloyd-Jones and co-workers which really brought the memory effects to the attention of researchers in the field.[145] In an isotopic desymmetrization, Trost and Bunt had noticed that the *ee* of the product when using enantiomerically enriched substrate was dependent on the absolute configuration of the chiral ligand.[146] This memory effect implies that a fully symmetric η-allylpalladium complex as intermediate is *not* the only mechanism operating. By using "isotopic desymmetrization" Lloyd-Jones and co-workers could measure the *ee* of the each part of the product arising from the two enantiomers of a racemic substrate *independently* (Figure 63).

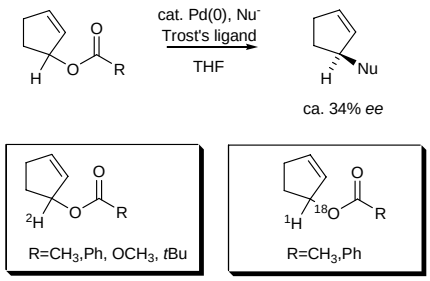

Figure 63 Above: The reaction studied by Lloyd-Jones and co-workers. Below: The isotopically marked ("desymmetrized") substrates used to unveil the reason for the observed memory effects.

This interesting study concluded that ion-pairing between the leaving group and the nucleophile, as suggested by Trost and Bunt, was not responsible for the observed memory effects. In contrast, Lloyd-Jones and co-workers suggested the observed memory effects to be related to the ability of Trost's ligand to change hapticity during the catalytic reaction.[147]

4.4.2 Our Approach

The remaining parts of chapter 4.4 can be considered as a short résumé of paper 2. In the current study[j] we wished to investigate the dynamics of the η^3-butenylpalladium complexes also employed by Hayashi and Williams. However, by also including the *Z*-configured linear acetate the degree of isomerization of the intermediate allylpalladium complexes could be estimated. The three isomeric starting materials (*E, Z,* and branched) can lead to two isomeric (η^3-allyl)Pd moieties (*syn* and *anti*), which can equilibrate and in turn produce three isomeric products upon nucleophilic addition (Figure 64).

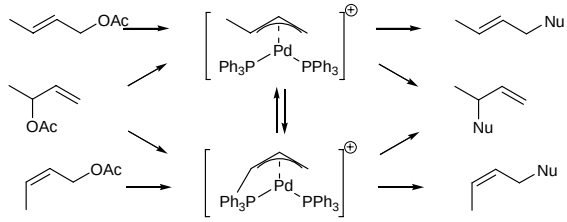

Figure 64 The possible reactions and equilibria in the Pd-catalyzed allylic alkylation of isomeric butenyl substrates.

[j] The described experimental work was performed by Thomas Jensen and Jacob Hoppe.

As indicated in Figure 64 the *E*-linear substrate ionizes exclusively to the *syn*-allylpalladium complex, whereas the *Z*-linear substrate ionizes to give the *anti*-allylpalladium complex. Nucleophilic addition can take place at either end of the allyl complex; however, previous experiments have indicated a strong preference for the formation of linear product from the *syn*-allyl intermediate. This is not the case for the *anti*-allyl intermediate, which has been observed to give almost equal amounts of the branched and the *Z*-linear product.[132] Notice that "cross-over" from *E*-substrate to *Z*-product, or vice versa, is only possible via isomerization of the intermediate allylpalladium complex. With simple PPh_3 ligands the *syn*-allylpalladium complex is thermodynamically more stable than the *anti*-allyl complex.

The branched substrate should give a result intermediate between that of *E*- and *Z*-substrates, entirely dependent on the initial ionization preference (*anti*/*syn*). A slow isomerization between the *syn*- and *anti*-allylpalladium complexes can give rise to memory effects; however, if no other mechanisms other than those depicted in Figure 64 are operating, the product distribution obtained from the branched substrate must be a linear combination of the distributions obtained using *E*- and *Z*-substrates. By investigation of the product distribution from each of the three isomeric substrates in Figure 64, it is possible to elucidate the degree of isomerization of the intermediate and the ionization preference of the branched substrate, as well as to detect memory effects not included in Figure 64 by deviations from the linear relationship between the three product distributions.

Experimentally, this is detected by comparing the distribution of linear products from *E*- and *Z*-linear substrates respectively (any branched product can be ignored in this analysis). If the *E*- and *Z*-substrates yield identical linear product distributions, there are no memory effects as the intermediate allylpalladium complex has fully equilibrated prior to nucleophilic addition. Conversely, if there is no crossover, that is, if only *E*-linear product is obtained from *E*-substrate and *Z*-linear product is obtained from *Z*-substrate, there is no equilibration (isomerization) of the intermediate allylpalladium complexes. The product distributions from Pd-catalyzed allylic alkylation of the three isomeric acetates have been collected in Table 9.

Table 9 Obtained product distributions from allylic alkylation of isomeric butenyl acetates.

Entry	Substrates	*E*-product	Branched	*Z*-product
1	*E*-linear	77%	16%	7%
2	branched	59%	26%	14%
3	*Z*-linear	15%	38%	47%

If nucleophilic attack is slow compared to the isomerization of the intermediate, the same product distribution should be expected from all three substrates. This is obviously not the case; *E*-acetate yields mostly *E*-product from terminal attack on the *syn*-intermediate, whereas *Z*-acetate yields almost equal amounts of branched and *Z*-products. A more detailed analysis of the product distribution from *E*- and *Z*-linear substrates shows that under the current reaction conditions, only 12% of the *syn*-complex (from *E*-acetate) and 17% of the *anti*-complex (from *Z*-acetate) isomerizes before reaction with nucleophile, and that the ratio of terminal:internal attack is 88:12 for *syn,* and 57:43 for *anti*. Thus, for both substrates, there is more than 80% of the product resulting from reaction of the nucleophile with the initially formed isomeric form of the allylpalladium complex. Using the above ratios in analyzing the product distribution from branched acetate, we can conclude that the initial ionization yields approximately 70% *syn*-complex. However, we also see a slight excess of internal product compared to what would be expected from the observed amounts of *E*- and *Z*-product (observed: 26%, predicted: 19%).

To study the "halide effect",[148] the allylic alkylation of the butenyl acetates was also performed with the addition of small amounts of allyl chloride (10% relative to Pd). In the presence of Pd(0) the very reactive allyl chloride will immediately liberate a controlled amount of chloride ions to the reaction mixture. We expected the main effect of the chloride ions to be an acceleration of the *syn/anti*-isomerization.[110] With this in mind, the product distributions from the three isomeric acetates should become more similar upon chloride addition. The results are shown in Table 10.

Table 10 Obtained product distributions from allylic alkylation of isomeric butenyl acetates in the presence of 0.5 mol% chloride.

Entry	Substrates	*E*-product	Branched	*Z*-product
4	*E*-linear	76%	16%	8%
5	branched	36%	51%	13%
6	*Z*-linear	45%	21%	34%

When looking at the observed product distributions, the initial expectation (i.e. faster *syn/anti*-isomerization) is clearly fulfilled, as shown by the higher amount of *E*-product from *Z*-substrate. However, the most drastic effect is observed in the alkylation of the branched acetate. The results from the *E*- and *Z*-substrates show the two extremes of initial ionization, to pure *syn*- and *anti*-complex, respectively. If only the mechanism in Figure 64 was operating, the product distribution should be a linear interpolation between these two extremes, but the results with

branched acetate show almost twice as much branched product as from either of the linear substrates. This is a strong indication that the intermediate in this case is not the symmetrically ligated (η^3-allyl)Pd complex shown in Figure 64.

Somehow, the chloride ion must interact with palladium to yield a less symmetric intermediate. A search for an explanation for this "chloride effect" will be part of the computational study on the Pd-catalyzed allylic alkylation in presence of phosphines and chloride presented in chapter 4.5.

4.5 Memory Effects – a Computational Study

4.5.1 Introduction

In this chapter a computational study of the palladium-catalyzed allylic alkylation is reported. The study is directed towards explaining the "memory effect" observed upon addition of catalytic amounts of chloride to the "traditional" catalytic system employing PPh_3 as ligands for palladium. A general catalytic cycle was shown earlier (Figure 37); however, this cycle is incapable of explaining the effect of chloride discussed in the previous chapter.

As with several other important transition metal-catalyzed reactions, thorough experimental investigations by Amatore, Jutand and co-workers have led to changes in the "generally accepted" catalytic cycle.[149] For example, when an allylic leaving group can coordinate to palladium (*e.g.* acetate, carbonate) the formation of a neutral η^1-allylpalladium species after the initial oxidative addition by the active Pd(0)-species is proposed - albeit still in equilibrium with the traditional cationic η^3-allylpalladium species. However, since many of these findings were based on observations performed with stoichiometric allylpalladium complexes their relevance to the catalytic reactions is still not fully resolved. A discrepancy between observable intermediates and reactive intermediates present only under catalytic conditions is not an unfamiliar phenomenon, with the most prominent example being the induction of stereoselectivity in asymmetric hydrogenation, which was unveiled by Halpern and co-workers.[24,150]

Herein we wish to study the reactivity of some of the proposed intermediates in the catalytic cycle for palladium-catalyzed allylic alkylation in the presence of chloride anions, and thus attempt to achieve an overall understanding of the catalytic reaction. Computational chemistry is applied in order to facilitate the inclusion of reactive intermediates, which are usually not detectable during a catalytic process.

Examples of halide effects are abundant within the area of transition metal-catalyzed organic transformations and the subject has recently been reviewed thoroughly.[148] For example halides can be used as additives to accelerate oxidative addition in cross-coupling reactions.[151] The phenomenon "memory effect" has been observed independently by several research groups,[141,143,144,145] and has been observed to appear in the presence of chloride anions – either added as Bu_4NCl or originating from the precursor metal complex when using for example the $[Pd(\eta^3\text{-}C_3H_5)(\mu\text{-}Cl)]_2$ dimer along with added triphenylphosphine as catalyst.

Several different explanations of the memory effect have been put forward, including η^1-allyl complexes with palladium ligated by one chloride and two phosphines,[149] ion-pairing between leaving group (often acetate) and nucleophile[146] and *trans*-effect directing nucleophilic

attack to the allylic position *trans* to phosphorus in a η^3-allyl complex with palladium ligated by one chloride and one phosphine.[108a,111,123]

The anionic chloride-ligated Pd(0) complexes of the general formula $[PdL_2Cl]^-$ (L=PR_3, R=H, Me, vinyl and Ph) have previously been the subject of a thorough computational investigation,[152] and here we wish to take this investigation one step further and include an allyl group in the coordination sphere of palladium. In particular, the stability of the proposed of η^1-coordinated allyl group is investigated and compared to the η^3-coordination mode. Furthermore, the reactivity of these structures towards nucleophiles is addressed, followed by a summary of implications for the overall catalytic cycle and general understanding of palladium-catalyzed allylic alkylations.

4.5.2 Computational Methods

All structures were optimized using density functional theory (DFT) with the hybrid density functional, B3LYP. The calculations were performed in Jaguar v. 4.2 build 77 program package[137] using the LACVP* basis set. The LACVP* basis set uses the Hay-Wadt small-core ECP and basis set for palladium, and 6-31G* for all light atoms.[138] All calculations were carried out using the PB-SCRF solvation model[42] with parameters suitable for dichloromethane (dielectric constant 9.08 and probe radius 2.33237Å). When the η^3-allyl complexes are compared to TS, the energy of the η^3-allyl complexes were calculated for a pre-reactive complex with the nucleophile situated 3.0Å from the allylic carbon atom as shown in Figure 65. This gave an energy below that of the TS, which is not the case for the isolated η^3-allyl complex due to lack of electrostatic interactions.

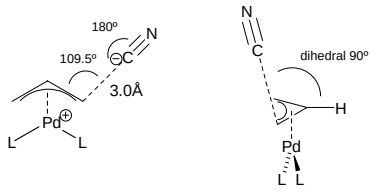

Figure 65 The location of the nucleophile used for the calculation of single-point energies for the pre-reactive complex of the η^3-allylpalladium complexes.

4.5.3 Results

Selection of an appropriate model system is always a challenging task in computational chemistry, and one often has to make compromises between system size and level of theory.

Without a solvent model the reaction between a cationic η^3-allylpalladium complex and a carbanion occurs without a barrier, as shown previously.[133] Transition states can only be located *in vacuo* when using neutral nucleophiles (*e.g.* ammonia), but from a chemist's point of view the use of a carbanion and a solvent model seems more appropriate. The choice of substituents on phosphorus has a great influence on the size of the systems under investigation, and will be investigated thoroughly since this is of relevance to computational investigations of transition metal-catalyzed reactions in general.

A very simple PH_3 moiety is used to do the initial transition state searching. PMe_3 is also included since this is a very popular choice in computational organometallic chemistry as a model for PPh_3, despite the fact that it has different electronic characteristics (PMe_3 is substantially more electron-donating than PPh_3). Vinyl groups have recently been shown to behave similarly to the larger phenyl substituents in a computational study on the viability of anionic, chloride-ligated Pd(0) complexes.[152] Finally, we have used the experimentally relevant PPh_3 ligands to achieve the correct steric and electronic effects on the systems under study and consequently be able to compare directly to experimental observations. Since the most popular nucleophiles used experimentally are stabilized carbanions (*e.g.* malonate-type nucleophiles), this was modelled by the use of the computationally less demanding cyanide anion.

4.5.4 Pd(II)-Allyl complexes

The first complexes considered were the classical, cationic η^3-allylpalladium complexes, in which palladium is ligated by two phosphine ligands (Figure 66, centre).

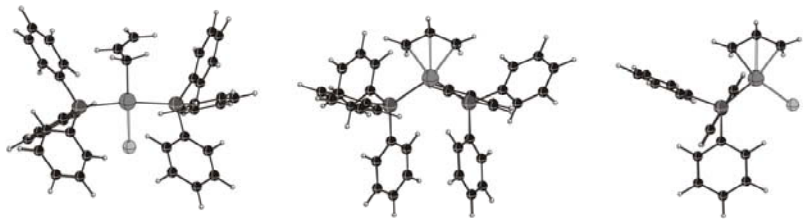

Figure 66 Structures of the optimized ground-state allyl complexes with PPh_3 as ligand. Left: The σ-allyl complex with two phosphine ligands and one chloride. Centre: The cationic π-allyl complex with two phosphines. Right: The neutral π-allyl complex with one phosphine and one chloride as ligands.

In the presence of chloride anions there is a possibility for direct coordination to palladium, while displacing one of the allylic termini yielding neutral $Pd(PR_3)_2Cl(\eta^1\text{-}C_3H_5)$ complexes (Figure 66, left). As mentioned previously these complexes have been proposed as possible

intermediates in the palladium-catalyzed allylic alkylation in the presence of chloride ions. A mechanism involving two consecutive S_N2' attacks can then explain the observed memory effects.[149] Furthermore, a neutral η^3-allylpalladium complex ligated by one chloride and one phosphine, *i.e.* having the formula $Pd(PPh_3)Cl(\eta^3\text{-}C_3H_5)$ and possibly originating from reaction between $[Pd(PPh_3)Cl]^-$ and the allylic precursor has been considered (Figure 66, right). The difference in *trans*-effect of the two ligands introduces electronic and geometrical differentiation of the two termini on the η^3-ligated allyl.[108a,111,123]

Figure 67 shows all the considered allylpalladium complexes with relative energies. We have chosen to use the neutral $Pd(PR_3)_2Cl(\eta^1\text{-}C_3H_5)$ complexes as energetic reference compounds (*i.e.* with an energy of 0 kJ/mol) within each series of different phosphine ligands.

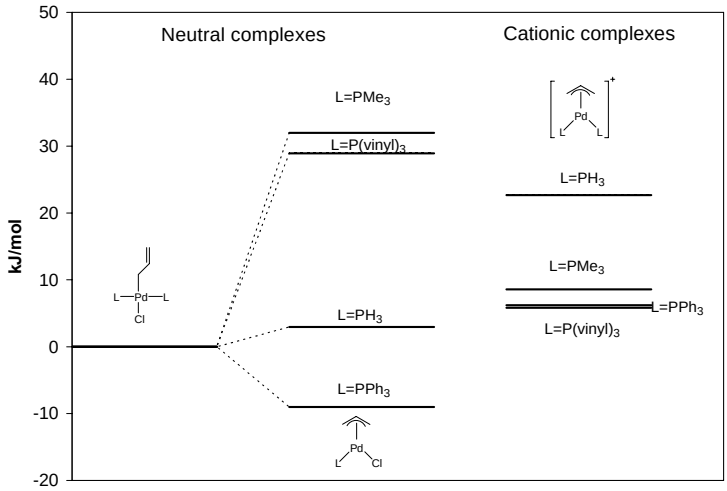

Figure 67 Relative energies of the possible ground-state allyl complexes with three different model phosphine ligands. All energies are relative to the neutral $Pd(PR_3)_2Cl(\eta^1\text{-}C_3H_5)$ complex.

The assessment of equilibria with more than a single component on either side can sometimes be a difficult task in computational chemistry. This is even more so if the comparison involves charged molecules, in which case an accurate method of accounting for solvation is absolutely crucial.

At first, we will focus on differences between the model phosphine ligands where such inaccuracies are minimized through cancelling of errors. With the smallest phosphine, PH_3, the cationic η^3-allylpalladium complex is destabilized by 23 kJ/mol and the neutral, mixed

$Pd(PH_3)Cl(\eta^3\text{-}C_3H_5)$ complex by 3 kJ/mol. When the substituents on the phosphine are either methyl or vinyl the picture changes quite drastically. Now the cationic η^3-allylpalladium complexes are only destabilized by 6 kJ/mol for PMe_3 and 9 kJ/mol for $P(vinyl)_3$.The corresponding mixed η^3-allylpalladium complexes are now destabilized by 29 kJ/mol and 32 kJ/mol, respectively. When the large PPh_3 is introduced the stability of the mixed $Pd(PPh_3)Cl(\eta^3\text{-}C_3H_5)$ is significantly enhanced, now being even more stable than the $Pd(PPh_3)_2Cl(\eta^1\text{-}C_3H_5)$ complex. Since this comparison is between two neutral molecules (actually three since the last component, the PPh_3 ligand is also neutral) a good accuracy should be expected. Besides the difference in potential energy the η^3-allylpalladium complex is also favoured entropically.[153] This effect is not considered in this work, but work on similar systems has revealed contributions from entropy corresponding to ~40-60 kJ/mol at ambient temperatures.[154]

The comparison between complexes of different charge is usually regarded as being associated with a high degree of uncertainty, in particular when the charge density is high. Previously, in an investigation of the free energy of solvation of small anions the error was found to be 25 kJ/mol for solvation of chloride in THF,[155] which is comparable to the observed energy differences in the current work. However, the computed free energy of solvation was always larger than the experimental values, which in the comparison above favours the cationic η^3-allylpalladium complexes (Figure 67), but in spite of this the cationic complex ($L=PPh_3$) has a higher energy than either of the neutral complexes.

Previous work within the group has identified mono-ligated palladium (both neutral and anionic) as being significantly more reactive towards aryl iodide than their bis-ligated counterparts.[156] Although there are significant mechanistic differences between the activation of an allylic leaving group in an S_N2 fashion and the oxidative addition to an aryl halide, which has been reported to proceed by an S_NAr-like mechanism,[157] we have chosen to investigate allylpalladium complexes with only one additional ligand. The optimized structures had the expected square-planar geometry with an open quadrant regardless of the ligand (PR_3 or chloride) but the energy in solution was >100 kJ/mol higher than the corresponding $Pd(PPh_3)_2Cl(\eta^1\text{-}C_3H_5)$ complex. Including one explicit CH_2Cl_2 and positioning it in the free coordination site with a chloride pointing towards palladium lowered the energy by approximately 20 kJ/mol, but the complexes are still considered energetically inaccessible compared to the traditional square-planar Pd(II) complexes.

4.5.5 Pd(0)- Olefin complexes

In the initial coordination of the olefin to a diphosphine-ligated Pd^0-species there is a remarkable difference between the large PPh_3 and the smaller model phosphines. With the model phosphines PH_3, PMe_3 and $P(vinyl)_3$ coordination to PdL_2 is favoured by 42, 35, and 40 kJ/mol, respectively, whereas with the larger PPh_3 ligands on palladium coordination of the olefin is now sterically unfavoured, leading to a *increase* in potential energy of 5 kJ/mol. This was a strong indication that none of the model systems could give relevant results for the experimental systems with PPh_3 ligands. Two conclusions to be drawn: i) The selection of a physically relevant model system is very difficult and should be carried out with great caution. ii) With the ever increasing computational capability in mind, one should perhaps more often attempt to perform the computational investigation using largest possible system – preferably the full system.

The obtained results are in agreement with a recent experimental and theoretical investigation on coordination of olefins to Pd(0) by Popp *et. al.*,[158] where bonding is considered to occur between a electron-rich, nucleophilic Pd(0) and an electron-accepting olefin. Besides the obvious decrease in steric congestion around palladium, a chloride ligand can also increase the electron density on the metal centre making it a better donor towards olefins.

4.5.6 Transition States

When approaching a cyanide anion to one of the allylic termini of η^3-allylpalladium complexes transition states could be located. The TS resulting from attack of CN^- on the two different π-allylpalladium complexes in Figure 66 are shown in Figure 68.

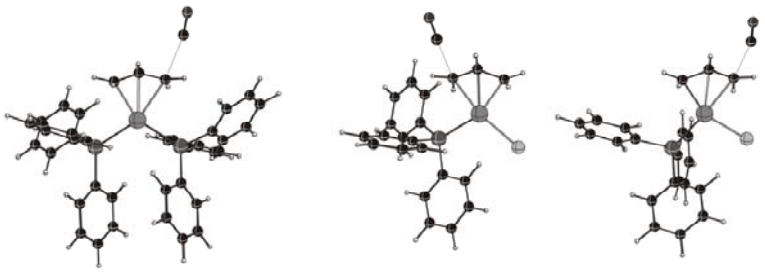

Figure 68 Transition state structures obtained when approaching the cyanide model nucleophile to the η^3-allylpalladium complexes. For the unsymmetrical allyl complex the two transition states from attack *trans* to chloride (centre) and *trans* to phosphorus (right) are shown.

The transition states obtained in this fashion are all early (reactant-like), which indicates that the non-stabilized cyanide anion is very reactive. In Figure 69 the reaction profile for all four different phosphine ligands are shown and we note distinct differences related to the nature of the phosphine ligand. For instance, the barrier is 18 kJ/mol for the full PPh_3 whereas the smaller phosphines have lower barriers in the range of 5-10 kJ/mol. In all cases the reaction is highly exothermic, yielding an olefin-complex with 120-150 kJ/mol lower energy than the allyl complexes. In principle, the cyanide anion can also be viewed as a model leaving group, allowing for conclusions to be drawn for the entire catalytic cycle.

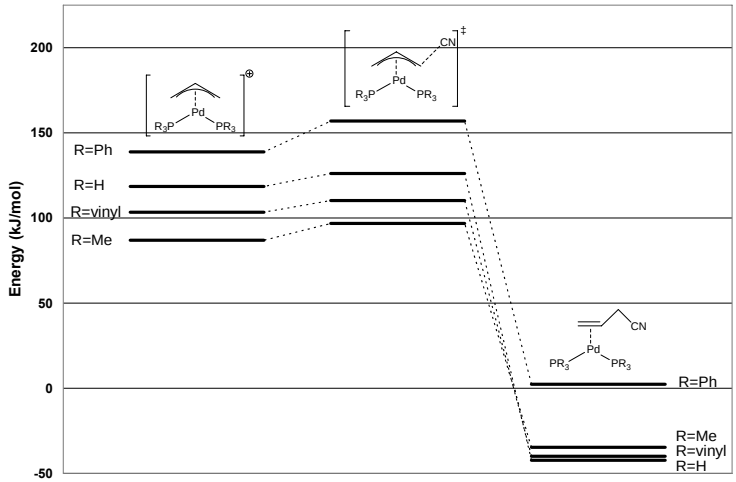

Figure 69 Reaction profiles for a symmetrical, diphosphine-ligated palladium species. All energies are relative to the isolated $Pd^0(PR_3)_2$ species with the relevant model phosphine.

To compare the energies of the relevant transition states the unsymmetrical η^3-allylpalladium complexes PdLCl(η^3-allyl) were examined. These complexes are structurally quite similar to the usual cationic η^3-allylpalladium complexes ligated by two phosphines (or one diphosphine), but when one phosphine is replaced by a chloride, this induces electronic differentiation of the two allylic termini.[124,125] This difference is observable even in the ground-state of the η^3-allylpalladium complexes (Figure 66, right), and in the transition state this effect leads to a difference in energy for the two reaction pathways.

For all four phosphine ligands the preferred reaction path is attack *trans* to phosphorus, with an energy difference between the two transition states of 1, 3, 3 and 4 kJ/mol for the ligands

PH_3, PMe_3, $P(vinyl)_3$ and PPh_3, respectively. For clarity only the pathway *trans* to phosphorus is shown in Figure 70. When comparing to PPh_3, the most suitable model phosphines are PH_3 and $P(vinyl)_3$ with the electron-donating methyl groups in PMe_3 resulting in differences of ca 50 kJ/mol – the difference being more pronounced for Pd(II) than for Pd(0). All energies are relative to the isolated $[Pd^0(PR_3)Cl]^-$ species and olefin with the relevant model phosphine.

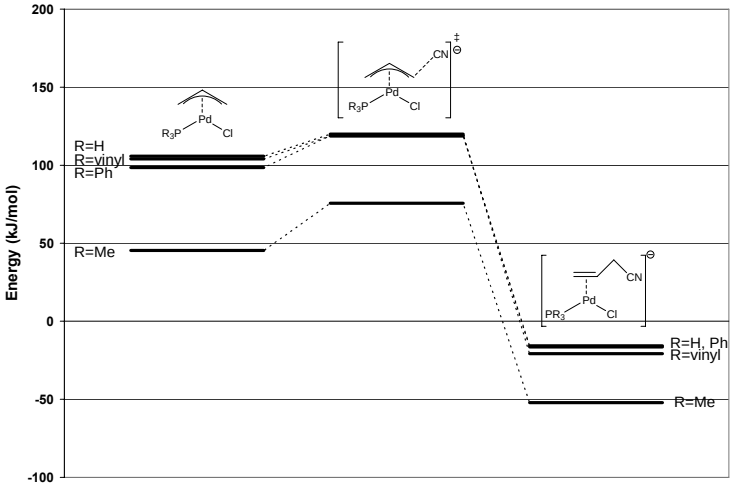

Figure 70 Reaction profiles for the nucleophilic attack on an unsymmetrical allylpalladium species ligated by one phosphine and one chloride. PH_3 and $P(vinyl)_3$ are close to PPh_3, whereas the reaction profile with PMe_3 is significantly different.

Despite several attempts we were not able to obtain transition states resulting from nucleophilic attack on the η^1-allylpalladium complexes without dissociation of ligands from the coordination sphere of the metal. However, this lack of reactivity towards nucleophiles is in good agreement with experimental work by Szabo and co-workers in which η^1-allylpalladium complexes were found to behave as nucleophiles themselves.[159]

4.5.7 Discussion - Cationic or Neutral?

When compared to the cationic diphosphine-ligated pathway (Figure 69) the major difference when chloride is present lies in the coordination of the olefin prior to oxidative addition. With only one phosphine and a small chloride even the large PPh_3 can easily accommodate the olefin as ligand, leading to a significant decrease in energy upon coordination

to Pd(0), see Figure 71. From this point the two reaction profiles are quite similar: i) Oxidative addition to yield a reactive η^3-allylpalladium intermediate requires ca. 150 kJ/mol, ii) Nucleophilic attack with a barrier of ca. 20 kJ/mol finally gives a stable olefin complex.

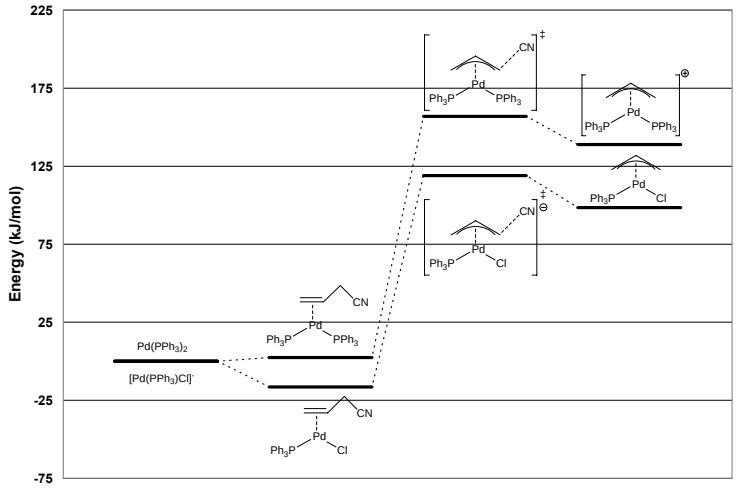

Figure 71 Comparison of the "traditional" diphosphine-ligated pathway originating from the neutral $Pd(PPh_3)_2$ and proceeding through a symmetrical, cationic allylpalladium intermediate and the chloride-induced pathway, with a negatively charged $Pd(PPh_3)Cl$ as starting point.

Since the oxidative addition is the first step in the catalytic cycle, the acceleration of this step in the presence of chloride has important consequences for the overall selectivity under catalytic conditions. During a catalytic reaction the neutral η^1-allyl complexes will not be present in significant amounts; however, without a nucleophile present they could be the resting state of palladium(0). When there is no chloride present the reaction proceeds through the cationic η^3-coordinated allylpalladium complex (with two PPh_3 moieties as ligands), but in the presence of chloride through the neutral η^3-coordinated allylpalladium complex instead (one PPh_3 and one chloride as ligands).

But how can the "memory effect" be rationalized? Most synthetic reactions are carried out with only catalytic amounts of palladium and phosphine (usually two PPh_3 per Pd), which is formed *in situ* either from $Pd(dba)_2$ + 2 PPh_3 or from $[Pd(\eta^3\text{-}C_3H_5)(\mu\text{-}Cl)]_2$ + 4 PPh_3. When chloride ions are present in the reaction mixture, the higher reactivity of the anionic $[Pd(PPh_3)Cl]^-$ in the initial oxidative addition compared to the neutral $Pd(PPh_3)_2$ will lead to

preferential formation of the neutral, unsymmetrical η^3-allylpalladium complex. This should be followed by a fast nucleophilic attack (significantly faster than ligand exchange), which regenerates the reactive, anionic Pd(0)-catalyst. As a consequence the major part of the product will arise from nucleophilic addition to the unsymmetrical [$Pd(PPh_3)Cl(\eta^3$-allyl)]. The electronic difference between the phosphine ligand and chloride in the unsymmetrical η^3-allylpalladium complex can rationalize the observed "memory effects".

This scenario is outlined in Figure 72. The usual cationic η^3-allylpalladium complex on the left, whereas the neutral, unsymmetrical η^3-allylpalladium with one chloride and one phosphine ligand is shown on the right. Under catalytic reaction conditions there is a large excess of allyl acetate and the initial oxidative addition will be the rate-limiting step in the catalytic cycle. If this step is accelerated when chloride is ligating palladium, the major part of the formed product will arise from the pathway shown on the right hand side. Notice how the position of the carbon atom bearing the leaving group (OAc, marked with # in Figure 72) is kept *trans* to phosphorus and this is also the favoured place of attack by the nucleophile. In the cationic path all "memory" is lost in the symmetrical η^3-allylpalladium complex.

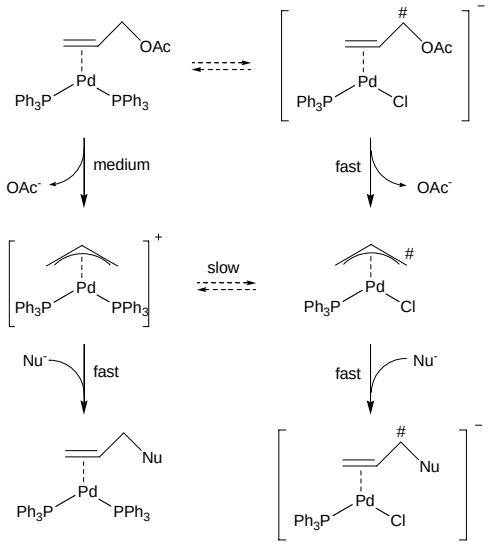

Figure 72 The two pathways involving η^3-allylpalladium complexes in Pd-catalyzed allylic alkylation. The overall selectivity-determining step under catalytic conditions is coordination of the olefin and subsequent oxidative addition, which is significantly faster when chloride is coordinating to palladium. (# indicates that the carbon atom bearing the leaving group is the one attacked by the nucleophile).

4.5.8 Conclusions

The palladium-catalyzed allylic alkylation was investigated using DFT/B3LYP for a series of different phosphine ligands. To our surprise, none of the smaller phosphine ligands were found to give good agreement with PPh_3, which could affect the conclusions of numerous other computational studies performed with PH_3 or PMe_3 as ligands.

The relative energies of the intermediate allyl complexes were determined, along with the reactivity towards a model cyanide nucleophile. When chloride is present the increased reactivity of the anionic $[Pd^0(Cl)PPh_3]^-$ towards oxidative addition readily explains the "memory effects" observed in experiments as arising from nucleophilic addition *trans* to phosphorus in an neutral, unsymmetrical η^3-allylpalladium complex.

4.6 Intramolecular Allylic Alkylations

4.6.1 Introduction

This project is part of an ongoing collaboration with the group of Prof. Poli in Paris. The experimental part of the project has been carried out by Poli and co-workers at Université Pierre et Marie Curie (Jussieu), whereas the computational calculations have been performed at Department of Chemistry, DTU. The results have been published as paper 3.

Prof. Poli uses the Pd-catalyzed allylic alkylation to construct nitrogen-containing heterocycles via a regio- and stereoselective intramolecular reaction (Figure 73).[160]

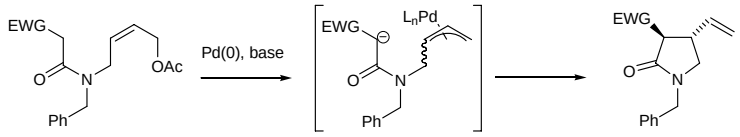

EWG=CO_2Me, CN, COMe, $PO(OEt)_2$, $PhSO_2$

Figure 73 General overview of the reaction developed by Poli and co-workers.

Before I was involved in the project, a computational study had already been performed aimed at calculating the preference for formation of either a 5- or a 7-membered ring.[161] This study showed a clear preference for formation of the 5-membered ring with nitrogen or oxygen as tethering atoms, whereas substrates with a carbon-tether lead to the formation of product mixtures containing 5- and 7- membered rings.

4.6.2 Results & Discussion

Due to the strained nature of the formed rings the reaction must be heated to 90ºC (DMF) or to reflux (THF and CH_2Cl_2). However, it was discovered that the use of 0.1 eq nBu$_4$NBr as a phase-transfer catalyst enabled the reaction to proceed at room temperature.[162] We speculated that the rate increase could be due to the absence of the chelating Na^+ counterion, and this was indeed confirmed by DFT/B3LYP calculations of the possible transition states (Table 11). Without Na^+ the enolate moiety could also assume the *E*-configuration, which in all cases gave TSs 13-18 kJ/mol lower in energy than the *Z*-isomer.

Table 11 Relative Energies and Length of the Forming Bond for the Eight Possible TS's.

entry	*syn/anti* allyl	*endo / exo*	*E / Z*	E_{rel} (kJ/mol)	C-C bond length (Å)
1	*syn*	*exo*	*E*	0.0	2.62
2	*syn*	*exo*	*Z*	12.5	2.69
3	*syn*	*endo*	*E*	81.9	2.79
4	*syn*	*endo*	*Z*	100.0	2.78
5	*anti*	*exo*	*E*	5.1	2.63
6	*anti*	*exo*	*Z*	20.9	2.71
7	*anti*	*endo*	*E*	53.6	2.58
8	*anti*	*endo*	*Z*	65.9	2.60

The two most favourable transition states (entries 1 and 5, Table 11) have been shown in Figure 74. The length of the forming bond is approximately 0.2 Å longer than when the enolate exists as a Na^+-chelate,[161] which also indicates that the free anion is more reactive.

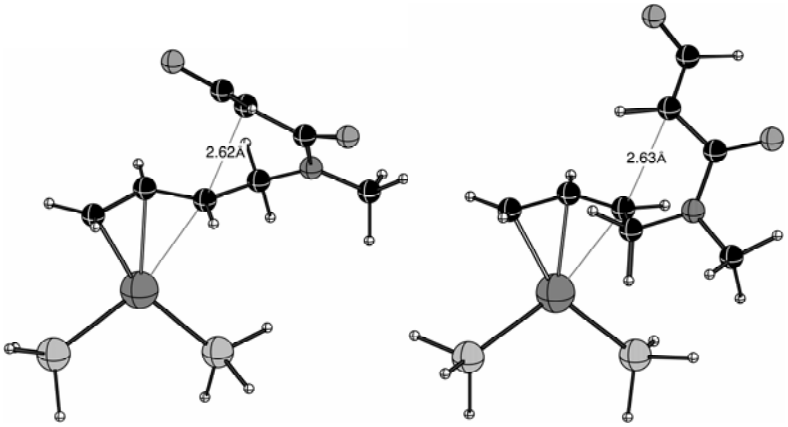

Figure 74 The two energetically most favourable of the eight TS's. Left: *syn*, *exo*, *E* (Table 11, entry 1), Right: *anti*, *exo*, *E* (Table 11, entry 5).

4.6.3 Conclusions

The present study is a good example of the level that computational chemistry has reached today, where the physical explanation for the initial experimental observations was obtained quickly. The computational study provides a sound explanation for the experimental observations, that phase-transfer catalysis could permit the reaction to be performed at room temperature, was quickly explained to be a direct result of the absence of Na^+ ions.

The computational prediction that *any* means of removing Na^+ ions would be equally effective was verified by new experiments, documenting that a simple crown-ether to complex Na^+ was satisfactory, and it was even possible to develop an improved experimental protocol using only catalytic NaH (0.1 eq) and 15-crown-5 (0.2 eq) albeit with slightly lower yields (68% compared to 93% with *n*-Bu_4NHSO_4).

This study stands out by the ability of the computational tools to truly *predict* the course of chemical reactions.

5 Catalytic Asymmetric Oxidations

This part of the thesis concerns catalytic asymmetric oxidations, which was one of the first areas where catalytic asymmetric reactions "matured", with the Sharpless Ti-catalyzed epoxidation of allylic alcohols as a good example (Figure 75).[28]

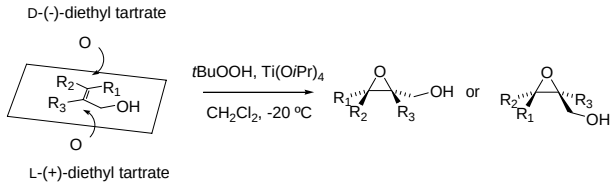

Figure 75 The Sharpless epoxidation reaction including a mnemonic device for prediction of the major enantiomer depending on the choice of chiral ligand.

The products of the reaction are epoxides (three-membered ring containing two carbons and an oxygen), which are useful intermediates in organic synthesis due to their ability to undergo ring-opening reactions with a large variety of nucleophiles, as exemplified by the work of Caron and Sharpless (Figure 76).[163] In this study excellent selectivities were obtained for the ring-opening at C-3 ranging from 6.4:1 (PhSH) to 100:1 (*i*PrOH) using $Ti(OiPr)_4$ as catalyst in a series of reactions which did not occur uncatalyzed.

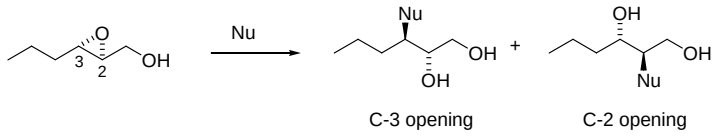

Figure 76 Regioselective ringopening of epoxide by use of $Ti(OiPr)_4$ catalyst.

The epoxide ring also constitutes an important pharmacophore in many natural products, making them important synthetic targets. However, in the 1980s there were no good methods for achieving asymmetric induction in the epoxidation of *unfunctionalized* alkenes. In the following chapter the Jacobsen-Katsuki Mn(salen)-catalyzed epoxidation is introduced, which constitutes the first practical approach to the asymmetric epoxidation of unfunctionalized alkenes (Figure 77).

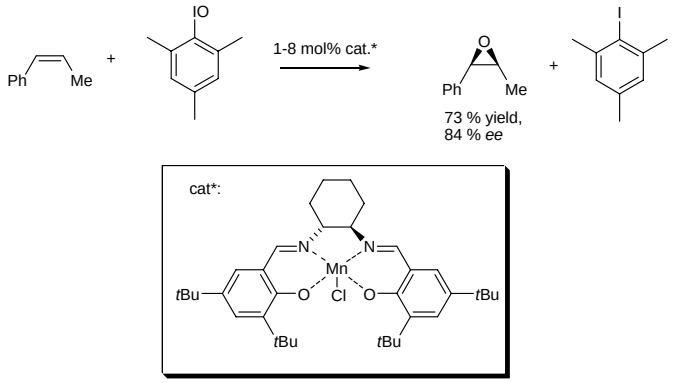

Figure 77 One of the examples of asymmetric, Mn(salen)-catalyzed epoxidation of alkenes reported by Jacobsen and co-workers.[29a]

Owing to its success in synthetic organic chemistry, the mechanism of the reaction has been subject to considerable debate and the features responsible for chiral induction have been discussed. In the present work a kinetic study of all possible methyl-substituted styrenes is performed in order to elucidate the features responsible for chiral induction.

The second chapter in this part of the thesis concerns the Osmium-catalyzed asymmetric dihydroxylation (chapter 5.2), a reaction which was also pioneered by Sharpless and co-workers (Figure 78).

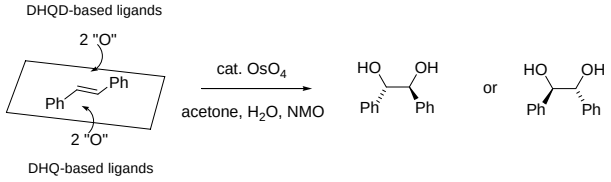

Figure 78 The Sharpless asymmetric dihydroxylation catalyzed by osmium. The enantiomer of the diol can be predicted from the choice of chiral ligands for osmium.

The selectivity-determining features of this reaction are probed by a series of twelve alkenes with different substitution patterns. The experimental reactivities and selectivities are compared to results obtained using a tailored molecular mechanics method.

5.1 The Mn(Salen)-catalyzed asymmetric epoxidation

5.1.1 Introduction

The disclosure of the Sharpless asymmetric epoxidation reaction in 1980,[28] prompted a search for a reaction capable of introducing similar, high levels of enantioselectivity without the strict requirement of a neighbouring alcohol functionality capable of coordinating to the active catalyst. This search was inspired by nature, where asymmetric epoxidation is carried out by the P450 enzyme, in which the active site consists of a Fe-porphyrin ring system (Figure 79). This enzyme is used abundantly in nature to perform a variety of different oxidations, often with excellent regio- and enantioselectivity.[164]

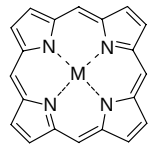

Figure 79 The porphyrin ring system, which is fully conjugated. M denotes a divalent metal cation, such as Fe(II), Mg(II) or Zn(II).

Model systems based on the Fe-porphyrin ring system, but with added groups (often chiral) to alter reactivity and selectivity, have been very important for the understanding of the biological systems. A large difference in reactivity between *cis*- and *trans*-alkenes lead Groves and Nemo to propose a side-on approach of the olefin to the metal-oxo complex (Figure 80).[165]

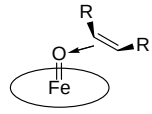

Figure 80 Illustration of the side-on approach suggested by Groves *et al.* The circle represents the porphyrin ring system.

This approach vector rationalizes two important experimental observations, namely i) higher reactivity of *cis*-alkenes than *trans*-alkenes; ii) asymmetric induction due to non-bonded interactions between the incoming olefin and the plane of the porphyrin. They also noted that this angle of approach gives maximum overlap between the filled π-orbitals on the olefin and the vacant π*-orbitals on the iron-oxo moiety.

The formation of minor amounts of *trans*-epoxides from *cis*-alkenes was a strong indication of a step-wise reaction mechanism via an reactive intermediate such as a metallaoxetane, a carbocation or a radical (Figure 81).

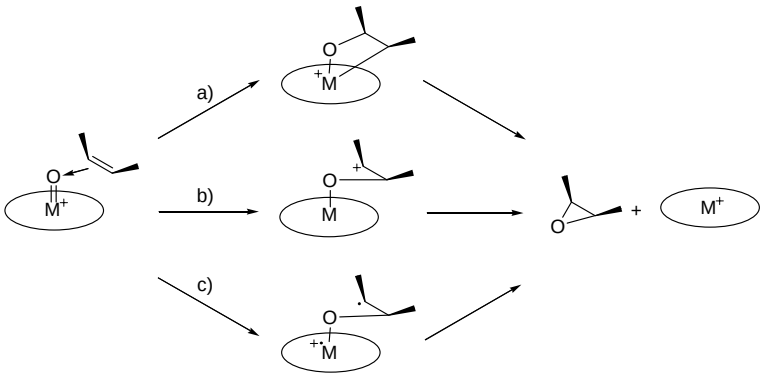

Figure 81 Three different proposals for the proposed intermediate in the Fe-porphyrin catalyzed epoxidation; a) metallaoxetane, b) cationic intermediate and c) radical intermediate.

5.1.2 Salen-based epoxidation catalysts

The first salen-based epoxidation system was based on Cr and developed by Kochi and co-workers in 1985 (Figure 82).[166]

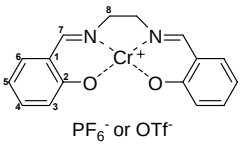

Synthesized Catalysts:
a unsubstituted
b 8,8,8',8'-CH_3
c 5,5'-Cl
d 7,7'-CH_3
e, 7,7'-C_6H_5
f, 5,5'-Cl, 8,8,8',8'-CH_3
g, 5,5'-OMe, 8,8,8',8'-CH_3
h, 4,4',6,6'-OMe, 8,8,8',8'-CH_3

Figure 82 The selection of Cr-salen catalysts investigated by Kochi and co-workers. Prime denotes mirror positions on the right hand side of the molecule.

Kochi was also able to obtain crystals suitable for X-ray crystallography of the cationic oxochromium(V) complex as well as for the adduct with pyridine N-oxide (Figure 83). In the five-coordinate oxochromium(V) complex the chromium atom is displaced ~0.5Å above the mean plane of the salen ligand.

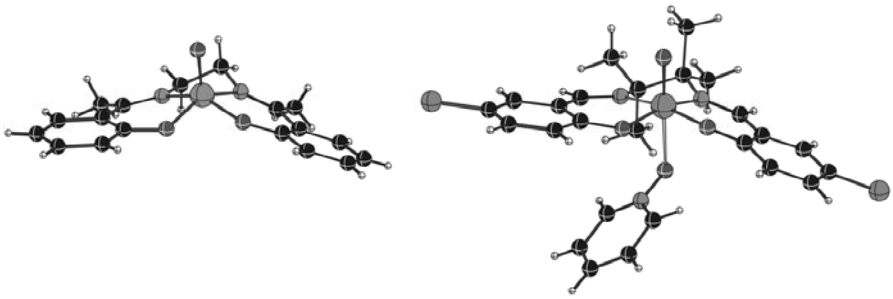

Figure 83 The two of the crystal structures reported by Srinivasan and Kochi.[167] Left: The cationic oxochromium(V) complex. Right: Pyridine *N*-oxide as axial ligand changes the conformation of the salen ligand.

When a sixth ligand (pyridine *N*-oxide) is coordinated from below, the chromium atom is pulled back towards the plane of the salen ligand reducing the distance to 0.26Å. In the crystal structures one also sees the lack of planarity of the salen ligand induced by the existence of two sp^3-hybridized carbon atoms (8 and 8' respectively).

Following their work on Cr-salen complexes Kochi and co-workers in 1986 developed the Mn(salen)-catalyzed epoxidation using the complexes shown in Figure 84 with iodosylbenzene as stoichiometric co-oxidant.[168]

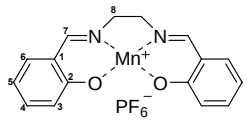

Synthesized Catalysts:
a unsubstituted
b 3,3'-OCH_3
c 5,5'-OCH_3
d 7,7'-C_6H_5
e 5,5'-Cl
f 5,5'-NO_2
g 5,5'-NO_2, 8,8,8',8'-CH_3
h 3,3',5,5'-NO_2

Figure 84 The achiral Mn(salen) catalysts investigated by Kochi and co-workers.

The reaction was investigated using a range of olefins including styrene, 4-methylstyrene, 4-methoxystyrene, 4-chlorostyrene, (*Z*)-β-methylstyrene, (*E*)-β-methylstyrene, *(Z)*-stilbene and *(E)*-stilbene, and the reaction proceeded in consistently good yields (compared to the Cr-salen catalysts investigated earlier) and with high stereoselectivity. Furthermore, the span of reactivity was rather narrow and the reaction was also useful with unreactive alkenes, such as 1-octene. For the 4-substituted styrenes, Kochi noted that the reactivity followed a Hammett correlation with a ρ value of -0.3.

For the transfer of oxygen to the alkenes was put forward a mechanism similar to the one proposed by Groves and co-workers in the context of metal(porphyrin)-catalyzed oxidations (Figure 85).[169]

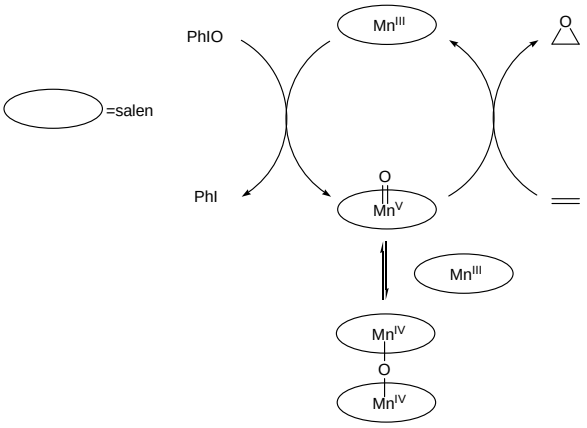

Figure 85 The mechanism proposed by Kochi and co-workers for the transfer of oxygen from the co-oxidant (iodysylbenzene) to the Mn^{III}(salen) complex. The Mn^{V}-oxo species is considered to be the active species delivering the oxygen atom to the alkene.

The reactive intermediate is considered to be the Mn^{V}-oxo species, but due to the reactivity of this species it could not be detected directly. The main species in solution was proposed to be a μ-oxo-Mn^{IV}(salen) dimer, which was detected by UV spectroscopy. The rate of epoxidation of this species towards alkenes measured stoichiometrically was slower than the overall rate of the catalytic reaction, which effectively excluded the μ-oxo-Mn^{IV}(salen) dimer as active oxygen-transferring species under catalytic conditions. Recently, in a study using electrospray tandem MS it has been possible to detect the elusive Mn^{V}-oxo species directly.[170]

5.1.3 Asymmetric version

In 1990 there was a breakthrough when the groups of Katsuki and Jacobsen simultaneously developed asymmetric versions of the Mn(salen)-catalyzed epoxidation reaction.[29,171]

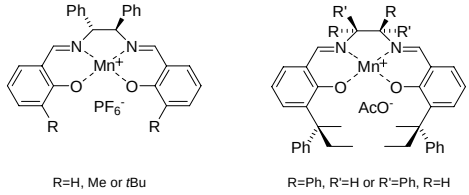

Figure 86 Some of the first chiral Mn(salen) catalysts for epoxidation. On the left examples from Jacobsen and co-workers, whereas examples from Katsuki *et al.* are shown on the right.

The two groups both incorporated chirality at the 8- and 8'-positions and Katsuki and co-workers also added chiral groups to the 3- and 3'-positions. A selection of the first catalysts for asymmetric epoxidation is shown in Figure 86.

Later improvements lead to the synthesis of the so-called "Jacobsen's catalyst" in 1991 (Figure 87),[172] which has been made commercially available in both enantiomeric forms. This compound was elected "Reagent of the year 1994".[173]

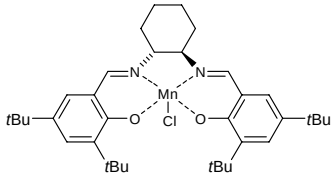

Figure 87 The very successful catalyst, which is commercially available and is known as "Jacobsen's catalyst".

The beneficial effect of additives (e.g. pyridine or pyridine *N*-oxide) on the yield of epoxide was recognized in the initial investigations by Kochi and co-workers,[168] and later shown by Skarzewski *et al.* to arise from direct coordination the Mn atom.[174] This coordination was suggested to break up the μ-oxo-Mn^{IV}(salen) dimer thereby increasing the concentration of the active, monomeric Mn^{V}-oxo species.

This coordination was strongly supported by the synthesis of the catalyst shown in Figure 88 by Jacobsen and co-workers,[175] where the X-ray structure clearly showed the coordination of pyridine *N*-oxide to manganese. When used in catalytic epoxidation this complex did not show any dependence on additional added pyridine *N*-oxides, strongly indicating that the effect of the pyridine *N*-oxides was indeed due to coordination to the metal centre.

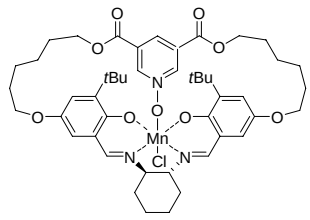

Figure 88 The complex with a "built-in" pyridine *N*-oxide synthesized by Jacobsen and co-workers. This complex was active in asymmetric epoxidation but was not affected by additional added *N*-oxides.

In 1999 Miura and Katsuki reported a very interesting reaction, which illustrates some of the fundamental features of the Mn(salen)-catalyzed epoxidation. Using a achiral Mn(salen)-catalyst together with a chiral additive the authors were able to obtain an impressive 83% *ee* in the epoxidation of 2,2-dimethylchromene.[176] The result was rationalized by a suggested equilibrium between two enantiomeric forms of the achiral catalyst. By coordination to the free axial position the chiral additive makes the two complexes diastereomeric, promoting an excess of one diastereomer over the other resulting in a net induction of chirality in the reaction. The optimal reaction conditions for this transformation are shown in Figure 89.

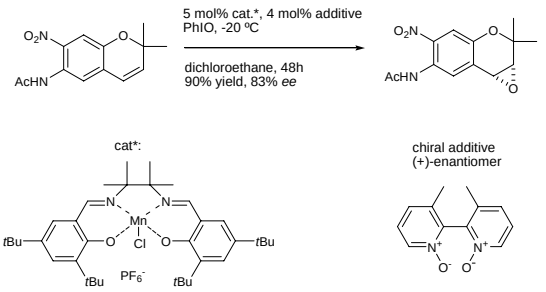

Figure 89 An example of asymmetric epoxidation with an achiral catalyst performed by Miura and Katsuki.

This example shows that the conformation of the salen ligand backbone can be influenced dramatically by the coordination of a chiral additive. In the usual, chiral Mn(salen)-catalysts this is achieved by having a fixed stereochemical configuration at the two carbon atoms adjacent to the nitrogen atoms.

5.1.4 Mechanistic Considerations

The three mechanisms proposed for the Fe(porphyrin)-catalyzed epoxidation (Figure 81) have also been proposed for the Mn(salen)-catalyzed asymmetric epoxidation. The existence of a non-concerted pathway was realized early on, and was prompted by the observed formation of *trans*-epoxides from *cis*-alkenes.[168] Interestingly, Jacobsen and co-workers discovered that addition of a chiral quaternary ammonium salt prolonged the lifetime of the intermediate radical allowing for synthesis of *trans*-epoxides with high enantiomeric excess starting from *cis*-alkenes (Figure 90).[177]

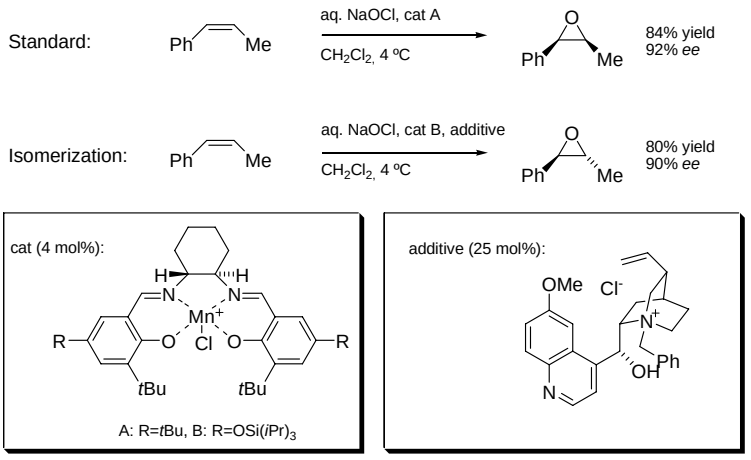

Figure 90 Illustration of the enormous change in diastereoselectivity observed upon addition of a quaternary ammonium salt.

Although a *chiral* quaternary ammonium salt was used, there was no change in either the sense, or the magnitude of the chiral induction upon addition of the salt.

Manganaoxetanes have also been proposed as intermediates in this reaction,[178] as has been the case for other transition metal-catalyzed oxidations,[179] and the area was reviewed early.[180] Initially, this proposal received strong support from the observation of a non-linear relationship between enantioselectivity and the reaction temperature.[181] Furthermore, experiments involving a radical probe were also interpreted in favour of a reversible formation of manganaoxetane.[182] The breakdown of the intermediate manganaoxetane can form the epoxide in a concerted manner or go via a radical intermediate, which complicates the interpretation of the results; however, today the manganaoxetane pathway has been ruled out.

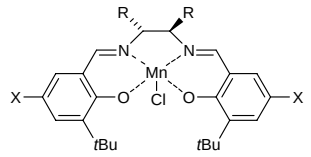

Figure 91 The catalysts employed in the Hammett study by Jacobsen and co-workers, where EWG or EDG groups were incorporated in the 5- and 5'-positions.

Using the catalysts depicted in Figure 91, Jacobsen and co-workers performed a Hammett study by varying the electronic character of the substituents in the 5- and 5'-position.[183] For three different substrates (2,2-dimethylchromene, *cis*-β-methylstyrene and *(Z)*-2,2-dimethyl-3-hexene) the enantioselectivity of the product was found to vary in a linear fashion with the Hammett σ-value. In all three cases the correlation coefficient was excellent and the slope was negative (from -0.10 to -1.37 depending on substrate), which indicates that an electron-donating substituent on the salen ring stabilizes the Mn(V) oxo intermediate. This decreases the reactivity of the catalyst towards alkenes, which in turn leads to a later transition state according to the Hammond Postulate.[184] Jacobsen and co-workers explain the beneficial effect of a late transition by a "higher degree of stereochemical communication" between the two reaction partners.[183]

This impressive experimental study prompted L. Cavallo and H. Jacobsen to perform a complementary computational study to elucidate the influence of the electronic effects.[185] Using the model system depicted in Figure 92 the calculations did indeed show a correlation between the distance of the evolving C-O bond in the transition state ($d_{C\text{-}O}$) and the electronic character of the catalyst used. The distances varied from 1.98 Å for the methoxy substituent to 2.04 Å when a nitro group was employed and the correlation was linear when using σ^{+}_{para} values.[185]

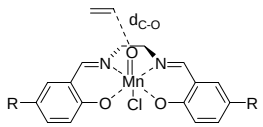

R=H, NO_2, OMe, *t*Bu, Cl and Me

Figure 92 The model system used by Cavallo and Jacobsen in the computational investigation of the electronic effects in the Mn(salen)-catalyzed epoxidation.

The spin state of the active species in the Mn(salen)-catalyzed epoxidation has been the subject of a vivid debate over the years and recently the concept of "two-state reactivity" have been introduced.[186] This opens up the possibility of a change in the spin-state of the metal somewhere along the minimum energy path from reactants to products, which in principle could explain the observed product ratios.

It is generally accepted that radical intermediates are involved in this reaction,[187] whereas a parallel concerted mechanism has been shown also to be operative.[182,188] The following kinetic study aims at explaining the selectivity-determining features of the reaction, which in principle does not have to differ depending on the exact mechanism.

5.1.5 Our project

The mechanism of the Mn(Salen)-catalyzed epoxidation reaction has been studied intensively; however, most studies have been performed using different catalysts, substrates and/or reaction conditions. Furthermore, in the majority of the examples from the chemical literature only yield and *ee* have been reported. In most cases the absolute configuration is given by analogy to similar substrates, and a full, rigorous assignment is rare to find. The Mn(Salen)-catalyzed asymmetric epoxidation is well-known for its ability to induce chirality in *cis*-disubstituted alkenes, whereas *trans*-disubstituted alkenes give rise to poor enantioselectivity. A prominent example is the β-methylsubstituted styrenes where the *ee*'s were measured to 84% and 20% for the *cis*-disubstituted and *trans*-disubstituted alkenes, respectively.[29a] To investigate this in more detail, we chose the group of methyl-substituted styrenes (Figure 93) and envisaged to perform a thorough investigation of (i) reactivity relative to that of styrene itself in competition experiments, (ii) enantioselectivity and absolute configuration, (iii) diastereoselectivity in cases for which the epoxidation could give rise to a combination of *cis*- and *trans*-configured products (paper 4).

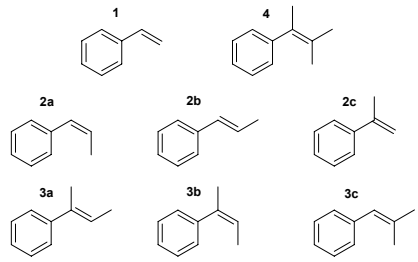

Figure 93 The structures of all possible methyl-substituted styrenes investigated here.

5.1.6 Results and Discussion

All the alkenes **1-4** could be separated using GC, allowing determination of the relative concentrations at various levels of conversion in competition experiments. With the concentrations of styrene and the relevant mono- or dimethyl-substituted styrene in hand, the relative reactivity of the two substrates could be determined, assuming a first order reaction in each styrene and identical reaction orders in other reactants (eq. 18).

Using a chiral column made it possible to determine yield, *ee* and even diastereoselectivity in samples withdrawn from the reaction mixture. The major enantiomers of each epoxide have been shown in Figure 94, with the absolute configuration determined as follows.

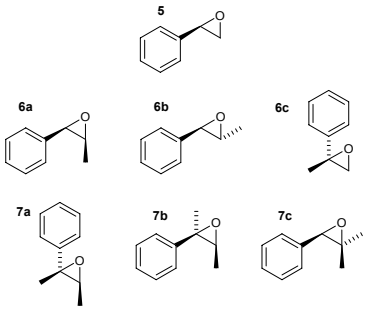

Figure 94 The seven epoxides detected as the expected major products from the epoxidation reaction of alkenes **1-3**. Trimethylstyrene did not yield significant amounts of epoxide under these reaction conditions.

For **5**, absolute configuration was assigned by comparison with a commercially available sample (Sigma-Aldrich) while **6a** could be assigned by comparison with literature data (see ref. 29a). For **6b**, **6c**, and **7b** we relied on chemical correlation with epoxides derived from chiral 1,2-diols which were themselves the products of Sharpless asymmetric dihydroxylation of alkenes **2b**, **2c**, and **3a,** respectively (Figure 95). The epoxides were generated either with inversion (tosylation, ringclosure) or retention of configuration using trimethyl orthoacetate and trimethylsilyl chloride.[189]

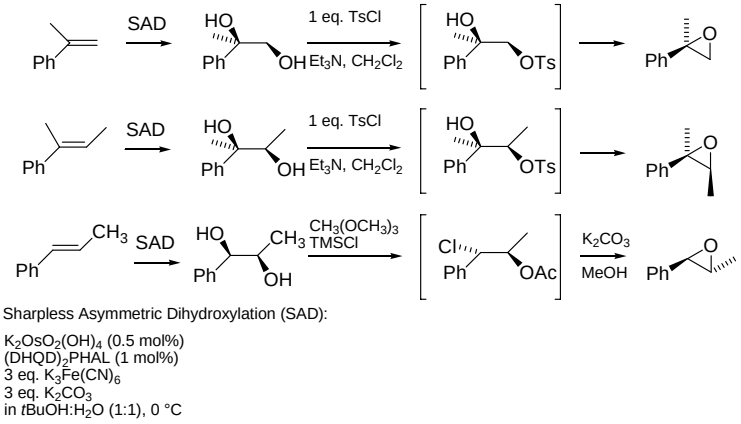

Figure 95 The methods of chemical correlation using stereochemically well-defined reactions to generate reference material of high enantiomeric purity.

Finally, the absolute configurations of **7a** and **7c** were assigned by comparison with the products of Shi asymmetric epoxidation of alkenes **3a** and **3c**, respectively.[190] The Shi epoxidation is an organo-catalytic epoxidation reaction, which relies on the *in situ* formation of a reactive dioxirane from a fructose derivative (Figure 96).

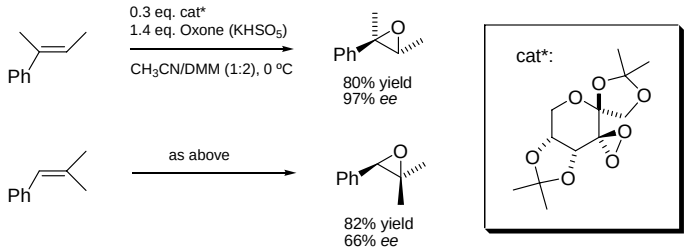

Figure 96 The Shi epoxidation used to generate reference material allowing assignment of the absolute configuration of epoxides **7a** and **7c**.

Of the eight alkenes investigated in the Jacobsen-Katsuki epoxidation, styrene was the fastest reacting alkene and the relative reactivity for styrene was set to equal to 1. This first set of competition experiments gave satisfactory results for all three methylsubstituted alkenes **2a-c** and one of the dimethylsubstituted alkenes (**3a**).

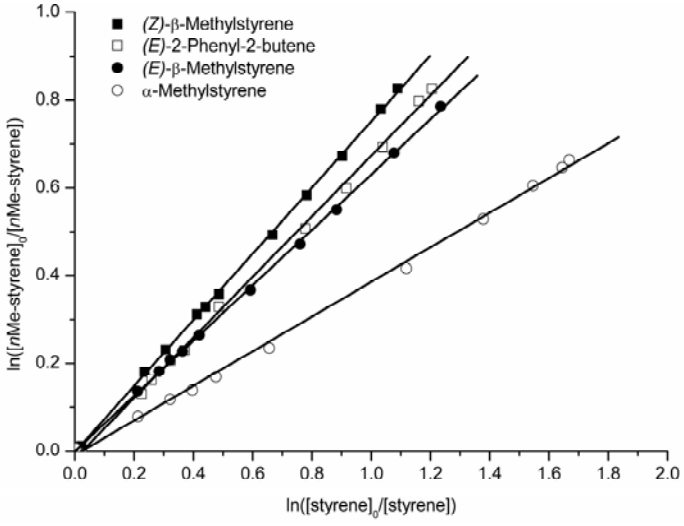

Figure 97 The results from the epoxidations of **2a-c** and **3a** in competition with styrene.

The data from the kinetic experiments involving **2a-c** and **3a** were plotted according to the equations discussed in chapter 3.8, yielding a straight line for each competition experiment, as expected (Figure 97). The obtained relative reactivities, enantio- and diasteroselectivities, and absolute configuration of the major enantiomer have been collected in Table 12.

As shown in Table 12 (entries 2 - 4) the relative reactivities of **2a-c** were 0.75, 0.39 and 0.63, respectively, and in all three cases the correlation was excellent, with $r^2 > 0.999$. Interestingly, the dimethyl-substituted **3a** was the third-fastest reacting alkene (relative reactivity 0.67, r^2=0.997) of all the substrates tested (Table 12, entry 5).

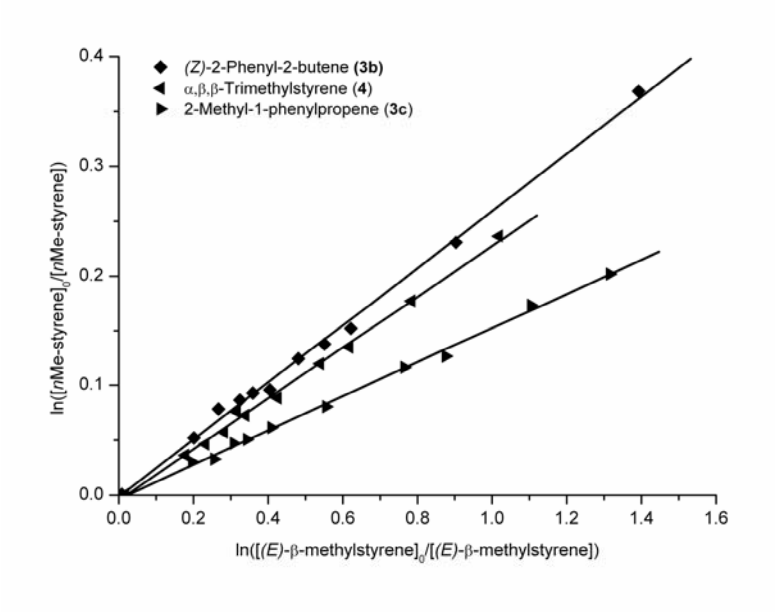

Figure 98 The results from the epoxidations of **3b-c** and **4** in competition with *E*-β-methylstyrene.

The two remaining dimethyl-substituted styrenes **3b** and **3c** were subjected to identical competition experiments with styrene and the initial results obtained within 30 min indicated relative reactivities of 0.10 and 0.06, respectively. However, the plot was not linear during the entire run and both compounds were therefore subjected to new competition experiments involving **2b**. The measured reactivities were 0.26 and 0.15 and, correcting for the reactivity of **2b** itself, one again obtains relative reactivities of 0.10 and 0.06 for **3b** and **3c**, respectively, but now with increased accuracy (Table 12, entries 6 and 7; r^2=0.997 and 0.996, respectively).

Tetrasubstituted alkene **4** was very unreactive in the standard preparative asymmetric epoxidation procedure (only 24% conversion after 3 hr) and only minor amounts of the epoxide

could be isolated, due to degradation of the reactant and product under the reaction conditions. In the competition experiment, **4** was epoxidized together with **2b** and the reactivity of **4** relative to styrene was calculated to 0.09 with r^2=0.995 (Table 12, entry 8) but again only minor amounts of the epoxide could be detected. The plot for epoxidation of alkenes **3b**, **3c**, and **4** in competition with **2b** is shown in Figure 98.

Table 12 Relative kinetics in the Jacobsen epoxidation for the eight alkenes under investigation along with measured enantio- and diastereoselectivities.

Entry	Alkene	Major Product	Relative reactivity[a]	*ee* epoxide	Absolute configuration[b]	Diastereo-meric ratio *(dr)*
1	**1**	**5**	1.00	53%	*(R)*	-
2	**2a**	**6a**	0.75	89%	*(R)*	10.3[c]
3	**2b**	**6b**	0.39	25%	*(R)*	72.2[d]
4	**2c**	**6c**	0.63	54%	*(S)*	-
5	**3a**	**7a**	0.67	73%	*(S)*	~ 500[e]
6	**3b**	**7b**	0.10	71%	*(R)*	5.3[f]
7	**3c**	**7c**	0.059	61%	*(R)*	-
8	**4**	**8**	0.079	< 5%	-	-

a) The correlation coefficient was larger than 0.995 in all cases.

b) The presence or absence of a methyl group in the α-position does not change the sequence in the Cahn-Ingold-Prelog system, so *(R)* indicates the same sense of chirality throughout.

c) The *ee* of the diastereomeric epoxide **6b** was 73% and the configuration was *(S)*.

d) The high *dr* resulted in very small amounts of the diastereomeric epoxide and the *ee* could not be determined accurately.

e) Only the major enantiomer of the diastereomeric epoxide was detected.

f) The *ee* of the diastereomeric epoxide **7a** was 31% and the configuration was *(S)*.

At this point we were pleased that our approach had succeeded in producing a reasonable amount of information, which had been obtained using identical reaction conditions in all the kinetic experiments. However, even with reactivity and selectivity for all seven reactive methylsubstituted styrenes at hand the interpretation of the results were far from straightforward. Our first attempt was a plot of selectivity (%*ee*) as a function of relative reactivity (Figure 99), inspired by the overall good correlation observed for the osmium-catalyzed asymmetric dihydroxylation.[191]

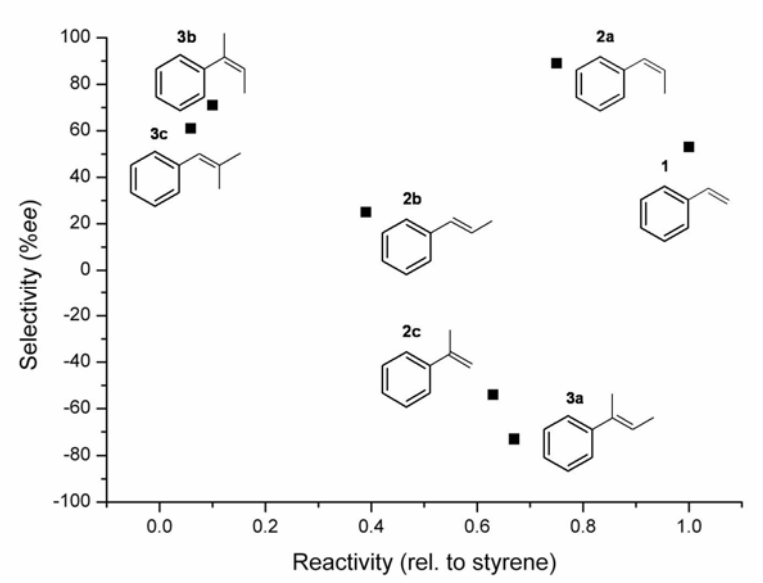

Figure 99 Selectivity (measured as %*ee*) plotted against the relative reactivity (measured in competition with styrene). Positive *ee* values denotes the formation of the *(R)*-enantiomer at the benzylic position as major product, negative *ee* values the *(S)*-enantiomer.

Initially, we had been troubled by the high reactivity of the trisubstituted alkene **3a**; however, the discovery that the major enantiomer had the (*S*)-configuration at the benzylic position was very encouraging. This was the first indication that this substrate reacted by a different path than the "traditional one", as exemplified by the observed (*R*)-configuration of epoxide **6a** arising from epoxidation of *cis*-β-methylstyrene.

The next step was an isolation of the reactivity to each of the two enantiomeric products using the following equations (*ee* in %, $-100 \leq ee \leq 100$):

$$r_{tot} = r_R + r_S \tag{30}$$

$$r_R = \frac{r_{tot}(100 + ee)}{200} \tag{31}$$

$$r_S = r_{tot} - r_R \tag{32}$$

In Table 13 we have listed the isolated reactivities of both enantiomers for each substrate, relative to the total reactivity for styrene.

Table 13 Isolated reactivities leading to either (*R*)- or (*S*)-configuration at the benzylic position.

Entry	Structure	Rate to *(R)*-enantiomer	Entry	Structure	Rate to *(S)*-enantiomer
1	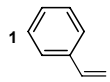	0.77	8	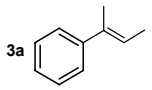	0.58
2	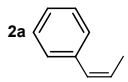	0.71	9	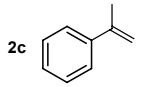	0.30
3	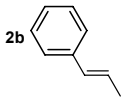	0.39	10	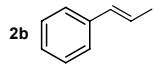	0.24
4	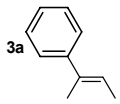	0.09	11	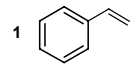	0.24
5	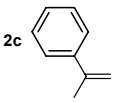	0.09	12	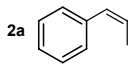	0.04
6	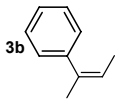	0.09	13	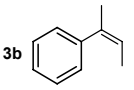	0.01
7	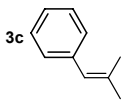	0.05	14	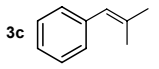	0.01

Based on the results in Table 13 we propose two different reaction paths, with opposite enantiomeric preference at the benzylic position and with different orientations of the styrene

derivative with respect to the Mn(Salen)-catalyst. The reaction path leading to the (*R*)-configured epoxides (left column, Table 13) has reactivities which are in accordance with an approach with the phenyl pointing away ("distal") from the salen ligand. For unsubstituted (Table 13, entry 1) or *cis*-disubstituted (Table 13, entry 2) styrenes this path is very fast and selective, whereas methyl-substitution in the β-position reduces the reactivity by 50 % (Table 13, entry 3). This path is almost completely blocked for substrates with a methyl in the α-position (Table 13, entries 4-6).

Concerted, electrophilic reactions of styrene derivatives will have strongly asynchronous TS,[188] due to the large difference in the stability of partial positive charge in the α–position (benzylic) compared to the β-position. This is probably the main reason for the observed low reactivity of substrate **3c**, where the two methyl substituents interact sterically with the Mn(Salen)-ligand due to the asynchronicity of the TS (Figure 100).

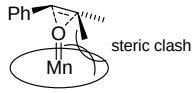

Figure 100 Illustration of the steric interactions between the two methyl substituents in the β-position of **3c** and the salen ligand.

When examining the structures of the substrates with a high reactivity towards the epoxide with a (*S*)-configuration (right column, Table 13) they all lack a substituent *cis* to the phenyl group. This is in line with an approach with the phenyl pointing towards the salen ligand ("proximal"), which is almost completely blocked by a substituent *cis* to the phenyl (Table 13, entries 12-14). Methyl substitution in the α-position gives a rate increase (Table 13, entries 8 and 9) which can be attributed to the more electron-rich double bond due to the weakly electron-donating methyl substituent. Methyl substitution in the β-position does not affect the rate to the (*S*)-enantiomer (Table 13, entries 10 and 11).

The proposal of two different approach vectors with opposite enantiomeric preference is able to rationalize the low selectivity observed with styrene and *trans*-β-methylstyrene by the simple fact that for these substrates both approaches are possible. Using the results from styrene itself, the reactivity of the distal pathway is approximately three times as high as for the proximal pathway. At this point we want to note that both Katsuki[192] and Jacobsen[193] have observed opposite enantiomeric preference for related tri-substituted alkenes; however, the current study uniquely serves to *quantify* the reactivity of the two pathways.

By also following the formation of the different regioisomers in the epoxidation of substrates **2a-b**, **3a-b** we were able to monitor the isomerization preference of the intermediate radical. In

the case of **2a-b** both styrenes were quite reactive; with the higher thermodynamic stability of the *trans*-configured product influencing the isomerization – giving diastereomeric ratios of 10 and 72 for the formation of *cis*- and *trans*-epoxides, respectively. For the substrates **3a-b** the difference in thermodynamic stability of the products is negligible and cannot rationalize the huge difference in diastereomeric ratios (5.3 vs. ~500). Only one of the substrates (**3a**) had a high reactivity (via the proximal pathway), but when the diastereomeric intermediate had formed, a facile isomerization was possible, resulting in a very low diastereomeric ratio of 5.3. The long life-time of the intermediate also had a detrimental effect on the enantioselectivity of the epoxide formed via isomerization. We measured an *ee* of 31% of **6a** formed from **3b**, compared to 73% *ee* measured in the reaction where **3a** was used to generate **6a** in a stereospecific reaction.

In conclusion, we postulate two modes of approach of the alkene, the "distal phenyl" path and the "proximal phenyl" path as illustrated in Figure 101.

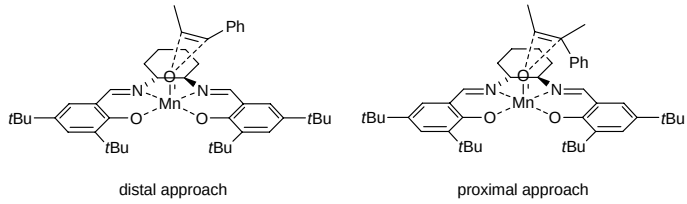

Figure 101 Simple illustrations of the two proposed approach vectors. Left: The "traditional" distal approach illustrated with **2a**. Right: The proximal approach vector suggested to be operating for the trisubstituted alkene **3a**.

Further experimental and theoretical studies are necessary to expand this mechanistic rationale to different substrates and ligands, but the current study has served to clarify some of the ambiguities observed for the simple methylsubstituted styrene substrates.

5.1.7 Conclusions

A kinetic study with eight methylsubstituted styrenes has been carried out using Jacobsen's catalyst, while simultaneously measuring the diastereo- and enantioselectivity. This has allowed an identification of two separated reaction pathways operating in parallel and furnishing the epoxide product with opposite configurations at the benzylic position. One path with the phenyl group pointed away from the salen ligand (distal) was found to be highly enantioselective for *cis*-β-methylstyrene (89% *ee*). The other path (proximal) was found to be enantioselective for the epoxidation of (*E*)-2,2-dimethylstyrene (73% *ee*).

This distinction between two different approach vectors allows a rationalization for the low enantioselectivity observed for substrates which are capable of reacting in both orientations, *e.g.* styrene (53% *ee*) and *trans*-β-methylstyrene (25% *ee*).

This set of reactivity and selectivity for a number of structurally similar substrates constitutes an excellent testing ground for the development and bench-marking of new theoretical methods.

5.2 Osmium-Catalyzed Dihydroxylation

This part of the thesis is based on papers 5 and 6. The synthesis and kinetic studies of alkenes **1** and **3** have been reported in paper 5, whereas the synthesis and kinetic studies of alkenes **2** and **4** are reported in paper 6. The chapter commences with an introduction to the osmium-catalyzed asymmetric dihydroxylation, followed by a description of the work performed.

5.2.1 Introduction

The stoichiometric reaction of OsO_4 with alkenes has been known for more than 100 years,[194] and the reaction was performed catalytically by Hofmann using chlorate as co-oxidant as early as 1912.[195] A characteristic feature of the reaction was the exclusive formation of *cis*-diols after cleavage (*i.e.* stereospecificity). This observation lead Criegee to propose an intermediate osmium(VI) monoglycolate ester as shown in Figure 102.

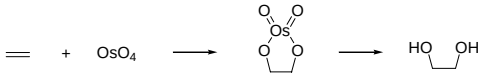

Figure 102 The mechanism suggested by Criegee involving an intermediate, cyclic osmate ester.

In later work, Criegee discovered that the reaction was strongly accelerated in the presence of pyridines,[196] which inspired the development of an asymmetric version of this reaction by Hentges and Sharpless in 1980 based on chiral nitrogen-containing ligands (Figure 103).[197]

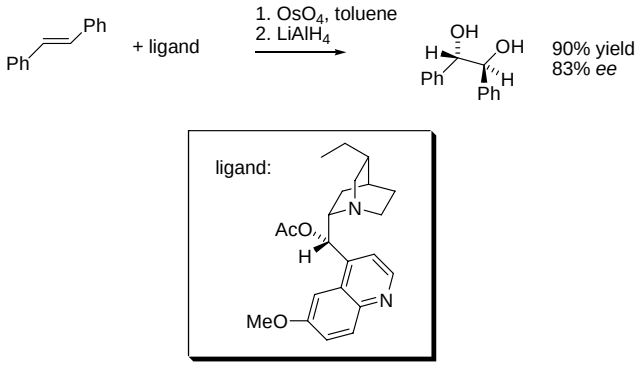

Figure 103 One of the first examples of asymmetric induction in the reaction of OsO_4 with alkenes reported by Hentges and Sharpless.[197]

Later it was shown that the resulting enantioselectivity was even higher than originally suggested (83% *ee*), with ~95% *ee* now being the accepted selectivity for the dihydroxylation of *trans*-stilbene.[198] Through the 1980s development of the reaction proceeded mainly along two paths. One was the synthesis and testing of new chiral ligands, allowing for the achievement of higher enantioselectivity for some of the "simple" substrates as for example styrene and *trans*-stilbene, but also representatives from some of the other alkene classes.[189] Some of the most efficient chiral ligands have been collected in Figure 104 and all consists of two identical cinchona alkaloid-bases chiral units tethered by an aromatic linker.

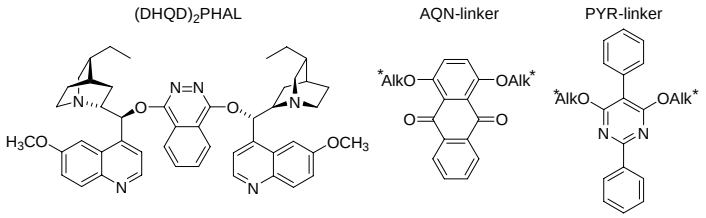

Figure 104 Three of the most popular ligands for asymmetric dihydroxylation. The full alkaloids (Alk) have only been included in the ligand shown on the left-hand side.

The phthalazine linker (PHAL) is advantageous for aromatic substrates,[199] whereas the diphenylpyrimidine linker (PYR) gives higher enantioselectivity for aliphatic substrates.[200] Recently, the antraquinone (AQN) moeity has been introduced,[201] which is the ligand of choice for terminal alkenes in general, including the synthetically important vinylic and allylic compounds.[202]

The other main thrust in the laboratories of Prof. K. B. Sharpless was the development of a catalytic asymmetric protocol, since the toxicity and cost of osmium made this development an absolute necessity. This first step was taken with an asymmetric version of the so-called "Upjohn procedure" using *N*-morpholine-*N*-oxide as reoxidant in 1988,[203] which relied on a modification of a catalytic system developed in the 1970s.[204] Only a couple of years later the superior two-phase system (*t*BuOH:H_2O) using potassium hexacyanoferrate as reoxidant was invented (Figure 105).[205] The separation of the dihydroxylation and reoxidation in organic (*t*BuOH) and aqueous phases, respectively, removed the deleterious influence of the so-called "second-cycle" on the observed asymmetric induction in the Upjohn system.[206]

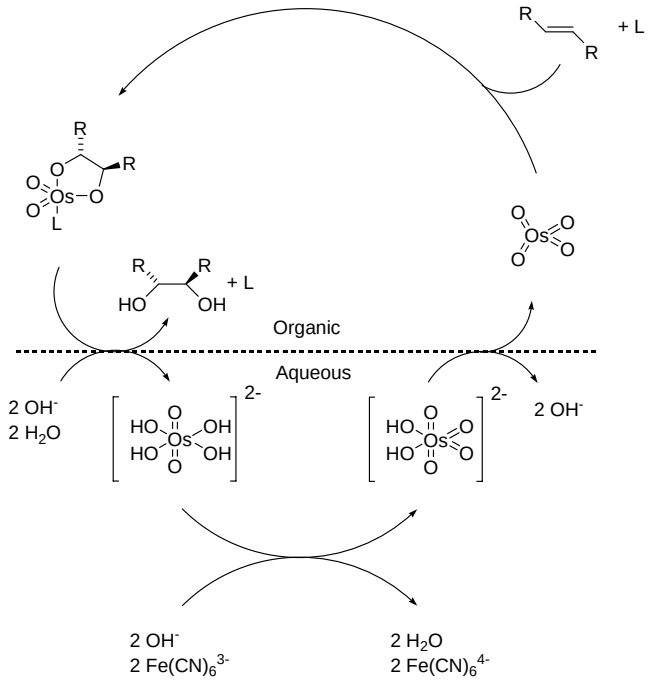

Figure 105 Proposed catalytic cycles for dihydroxylation in the organic phase (upper) and re-oxidation of Os(VI) to Os(VIII) in the aqueous phase (lower).

5.2.2 Mechanistic considerations

Two mechanisms have been advanced for the formation of the cyclic osmate ester from OsO_4 and alkene. A concerted [3+2] mechanism, in parallel to the well-known cycloaddition reactions (*e.g.* Diels-Alder) was the first mechanistic proposal, put forward in 1922 by Böseken.[207] A stepwise mechanism with initial formation of a metallooxetane (through a [2+2] cycloaddition) was proposed by Sharpless in 1977 in parallel to that suggested for similar oxidations with chromyl chloride.[179] Both mechanisms have been outlined in Figure 106, and through the years several investigations have been performed by two of the strongest advocates for each of them: E. J. Corey (3+2) and K. B. Sharpless (2+2).

As discussed previously (3.7.2 TS Optimization) the enantioselectivity usually rises with decreasing temperature; however, in 1993 Sharpless and co-workers illustrated that asymmetric dihydroxylation has maximum enantioselectivity at 0°C.[208]

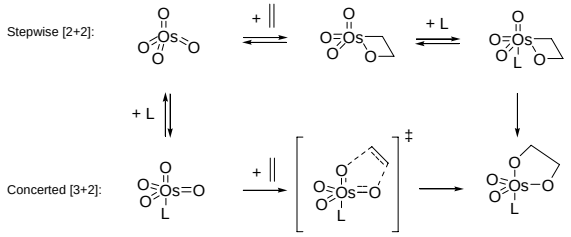

Figure 106 Overview of the two different mechanistic proposals for the dihydroxylation of alkenes using OsO_4.

This behaviour indicates that the reaction consists of multiple steps, something which is in accordance with a step-wise [2+2] mechanism. Corey explains this result by the reversible formation of a reactive complex prior to the actual [3+2] cycloaddition reaction.[209]

In 1995 Corey and co-workers published a thorough mechanistic study, which concluded that the asymmetric dihydroxylation follows the well-known Michaelis-Menten kinetics.[210] However, the observation of a ceiling rate constant for the reaction could also be due to a limited rate of re-oxidation in the two-phased *t*BuOH:H_2O catalytic system. Earlier kinetic studies in one-phased toluene solutions by Sharpless and co-workers had not given any indications of a ceiling rate constant.[211]

In 1997 the mechanism was determined to be the concerted [3+2] cycloaddition by Corey and co-workers using kinetic isotope effects.[212] Later the method was used again by Sharpless and co-workers on a range of different substrates and again the results were in accordance with a [3+2] mechanism.[213]

The two mechanisms have also been subject to extensive theoretical studies. The methods used have included pure quantum mechanical studies[214,215,216] as well as QM/MM studies.[49a] All of these studies agree on the [3+2] mechanism as being the most likely mechanism of oxygen transfer in the osmium-catalyzed dihydroxylation.

In 1999 Norrby *et. al.* published a paper where the selectivity (measured as %*ee*) for the dihydroxylation of a number of structurally different olefins was calculated computationally and compared to experimental values.[217] These calculations successfully described the selectivity using a transitions state force field based on quantum mechanical calculations for the concerted [3+2] mechanism. The correct prediction of the selectivity based on the [3+2] mechanism gives further support to this pathway.

5.2.3 Prediction of absolute configuration

One of the salient features of the osmium-catalyzed asymmetric dihydroxylation was the straightforward prediction of absolute configuration of the major enantiomer as consequence of

the choice of chiral ligand. This so-called "mnemonic device" was first proposed by Sharpless and co-workers in 1991 (Figure 107), and could successfully predict the absolute configuration of mono- and *trans*-disubstituted olefins.[218]

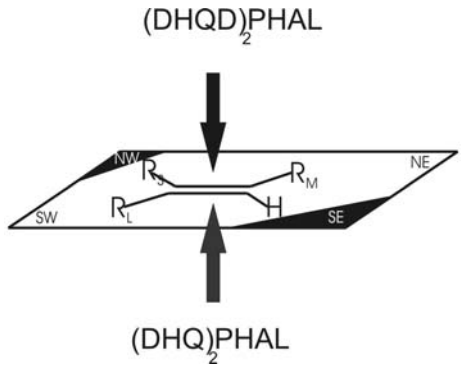

Figure 107 The original mnemonic device published by Sharpless and co-workers.

The indices L, M and S denotes large, medium, and small groups, respectively, but the mnemonic device was highly reliable for mono- and *trans*-disubstituted alkenes. These two alkene classes both orient themselves having the same prochiral face of the olefin up, irrespective of which of the two "allowed" orientations of the alkene is active.

A few years later an attractive area was included in the SW corner of the mnemonic device to account for the measured rate increase when the size of the "large" group was increased (Figure 108).[211] The success of the AD reaction is largely dependent on the acceleration of the osmylation when the chiral ligand coordinates to osmium. This phenomenon is known as Ligand Accelerated Catalysis (LAC), and the osmium-catalyzed asymmetric dihydroxylation constitutes one of the most clear-cut examples.[219]

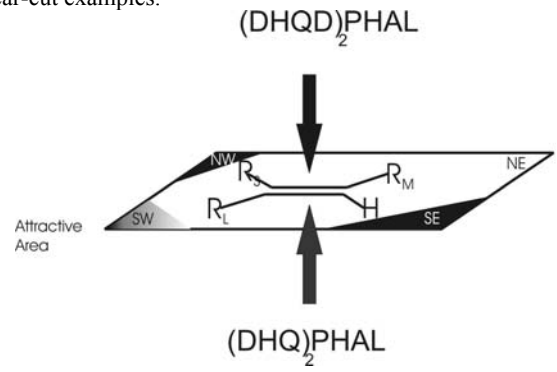

Figure 108 The mnemonic device published by Sharpless and co-workers in 1994, which includes an attractive area in the SW corner.

As a test of the efficiency a dihydroxylation was carried out with 20 times more OsO_4 than chiral ligand (0.2 and 0.01 mol%, respectively), but in spite of this the measured enantioselectivity was still 96% yielding a rate difference of 480 between the reactions with OsO_4 and OsO_4·L.[202]

5.2.4 Mapping of Mnemonic Device

Some features of the mnemonic device could readily be explained by comparison to an X-ray structure of the product complex (Figure 109).[220] The complex was obtained with one of the earlier chiral ligands, but the results can be extrapolated to the new generation of more efficient ligands. The steric hindrance due to the presence of the carbonyl oxygen in the benzoate can be held responsible for the steric hindrance in the SE corner. With the introduction of the phthalazine linker this feature was enhanced, not allowing substituents larger than a simple hydrogen to occupy this position. The increase in rate when large, aromatic substituents could orient themselves towards the SW corner was explained by Sharpless and co-workers as attractive π-π interactions between the substrate and the phthalazine linker.

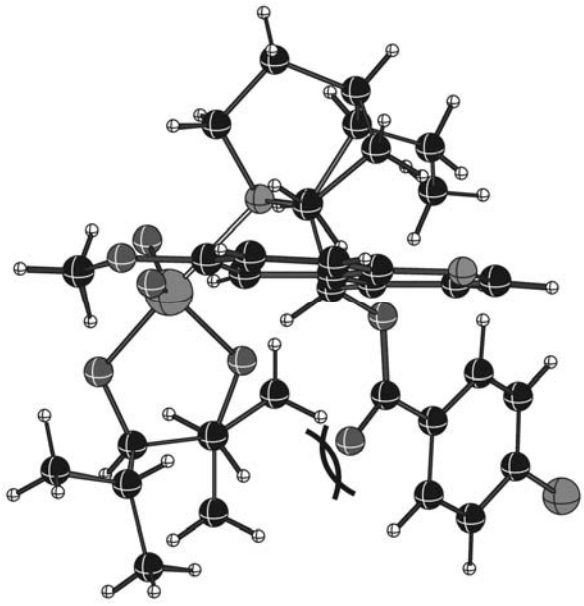

Figure 109 The crystal structure of the osmylate ester obtained using one of the early chiral ligands with a *para*-chlorobenzoate moiety. The carbonyl oxygen is responsible for the steric hindrance in the SE corner of the mnemonic device.

However, the moderate steric hindrance in the NW corner could not readily be explained using a molecular structure of the osmium-ligand complex.

Based on the [3+2] mechanism Corey and co-workers also identified an area of the active catalyst as being responsible for the observed rate increase with aromatic substrates. They focused on a chiral pocket created between the two quinoline moieties.[221] Interestingly, the superposition of a 3D-structure of the active catalyst on top of the mnemonic device reveals the attractive interactions suggested by Sharpless to be present in the SW corner is actually located in what corresponds to the NE corner of the mnemonic device. In a similar manner the accelerating features described by Corey can be identified in the "actual" SW corner of the mnemonic device.

5.2.5 Our Project

To further improve the understanding of the controlling features in the AD reaction we have devised a group of test substrates consisting of twelve tri-substituted alkenes (Figure 110).

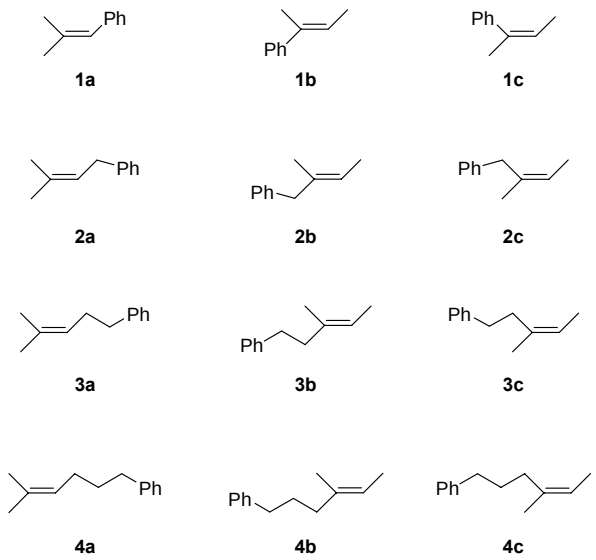

Figure 110 The four groups of alkenes used to investigate the selectivity-controlling features in the AD-reaction.

Recognition of the massive steric hindrance in the SE corner of the mnemonic device as a result of the presence of the PHAL linker allows basically only one orientation of a tri-substituted alkene in the chiral pocket. By utilizing the three different substation patterns (*gem*-

dimethyl, *cis*-dimethyl and *trans*-dimethyl), the large group is "directed" towards one of the three remaining corners of the mnemonic device. In Figure 110 the alkenes have been oriented in accordance with a mnemonic device, which allows one to appreciate that the **a** alkenes will probe the influence of the large group in the NE corner of the mnemonic device. In a similar manner the alkenes denoted **b** and **c** probes the influence of the large group in the SW and NE corners, respectively.

The present study focuses on the interaction of the active catalyst with a phenyl moiety, but the present approach could be also extended to other functional groups. The choice of a phenyl is motivated by the observation of superior selectivities with this structural motif – probably due to favourable interactions with the aromatic moeities already present in the catalyst.

A competitive dihydroxylation between **a** and **b** alkenes within a group allows a quantification of the importance of the stabilizing interactions suggested by Sharpless (NE corner, **a** series),[211,222] and the interactions proposed by Corey and co-workers (SW corner, **b** series).[209,210] The **c** alkenes probes whether the NW corner indeed contains minor steric hindrance as suggested in the mnemonic devices reported by Sharpless,[211,218] or merely an absence of stabilizing interactions as suggested by the 3D structure of the active catalyst (Figure 109).

By comparison of alkenes within a series the distance-dependence of the stabilizing interactions can be revealed, although the difference in flexibility also must be taken into account.

5.2.6 Kinetic Study

The relative rates of reactivity within each class of alkenes are determined by pair-wise competition experiments, where the rate of disappearance of the alkenes is followed by GC, as described in chapter 3.8. The plots obtained for all four groups of alkenes reacted with stoichiometric OsO_4 in toluene are shown in Figure 111 to Figure 114. Within each group of isomeric alkenes, one was selected as reference compound either since it had a reactivity in between that of the other two alkenes or simply due to ease of separation (GC).

For the first two groups of alkenes the differences in reactivity within the group was rather large. This called for the use of the alkene with an intermediate reactivity to be used a reference compound (i.e. alkene **1b** in group **1** and alkene **2b** in group **2**). Within groups **3** and **4** the alkenes could not all be separated on GC, which made it necessary to use the alkenes **3c** and **4a** as reference compounds. Within these groups the differences in reactivity were rather small, so the accuracy in the determination of relative reactivity was unaffected by the choice of reference compound.

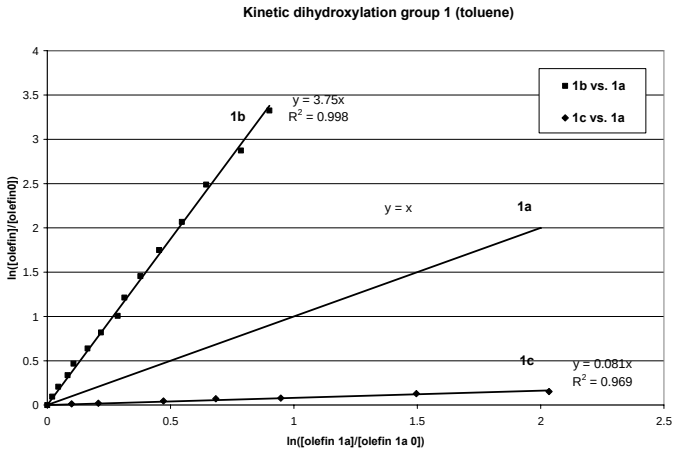

Figure 111 Relative rates of reaction within group 1. **1b** and **1c** were both measured against **1a** and for this reason **1a** has the relative rate 1 (y=x).

In group 1, compound **1b** is clearly the fastest reacting alkene, documenting the importance of the stabilizing interactions in the SW corner of the Sharpless mnemonic (Figure 108). Substrate **1a** is the second fastest reacting alkene, approximately four times slower than **1b**. The fact that it is more than 10 times faster than the slowest reacting alkene (**1c**) shows the NE corner also interacts favourably with the phenyl group. The slowest reacting alkene (**1c**) points the phenyl group towards the NW corner of the Sharpless mnemonic, which does not afford stabilization and without the use of molecular modelling could be interpreted as a slight steric hindrance. The results from group **1** reveal a difference in reaction rate of more than a factor of 40 between the slowest and the fastest alkene. The large difference can be attributed to the fact that the phenyl group is connected directly to the double bond, and the conjugation does not allow the phenyl group to rotate freely to relieve strain or steric repulsion inside the pocket created by the ligand. The results from group **1** are in accordance with the Sharpless mnemonic (Figure 108), which singles out the SW corner as especially attractive towards aromatic groups.

The group **2** alkenes were investigated in a similar manner and the results are shown in Figure 112. Within this group **2a** is by far the fastest reacting alkene. Clearly this means that the NE corner is far better in stabilizing a benzyl group than any other corner. Alkene **2b** reacts about 40% faster than **2c**, which shows that the SW corner is only marginally better in stabilizing a benzyl group than the NW corner.

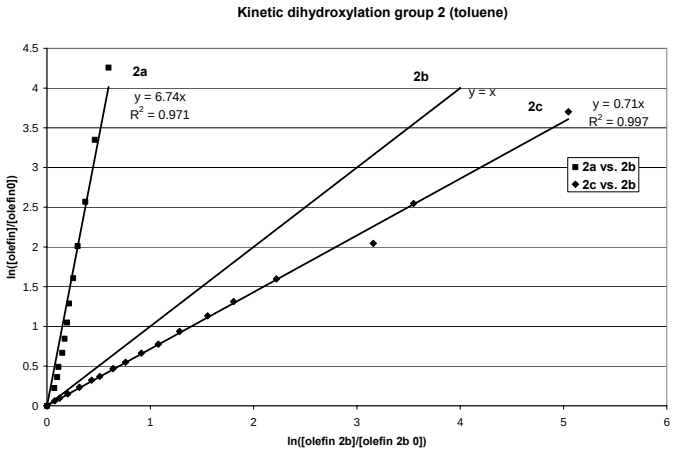

Figure 112 The relative rates of reaction within group 2.

These results are in sharp contrast to the predictions from the Sharpless revised mnemonic (Figure 108) which predicts the SW corner to be more favourable than NE.

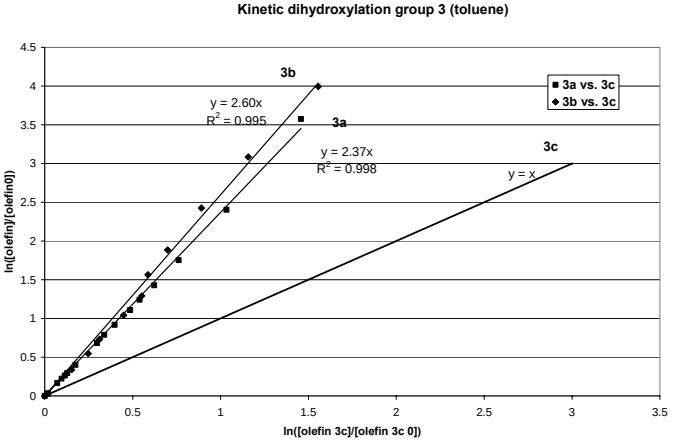

Figure 113 The results of the kinetic dihydroxylations with the alkenes **3**.

The results for the alkenes **3** are shown in Figure 113. In this case two parts of the osmium-ligand complex, corresponding to the NE and SW corners of the mnemonic device, are equally good in stabilizing the aromatic part of the alkene. Again, this is in contrast to the revised mnemonic device suggested by Sharpless (Figure 108). The difference in reactivity is much smaller for this substrate group than for the previous groups. This can be attributed to the fact

that the phenyl groups in alkenes **3** and **4** are connected to the double bond with a flexible tether, allowing it to reach through space towards any stabilizing interactions available, with less dependence on the position of the origin of the tether.

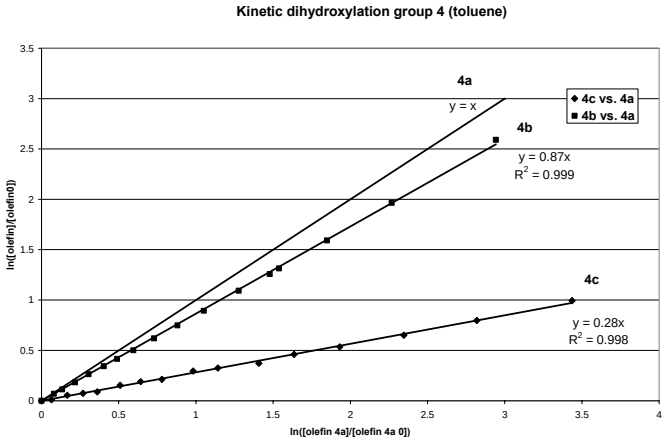

Figure 114 The results of the kinetic dihydroxylation of the alkenes **4**.

The results for the kinetic dihydroxylation of alkenes **4** are shown in Figure 114. The same explanations as the ones advanced for group 3 can also be applied here. Substrates **4a** and **4b** show very similar reactivity. The slowest reacting alkene is **4c**, which has the large group in the NW corner. This alkene can obtain stabilizing interactions only by "wrapping" around to the other areas of the ligand.

Having established the relative rates of reactivity for the one-phase system in toluene, we turned our attention to the more synthetically useful two-phase *t*BuOH:H_2O solvent system.[k] Our initial results using alkenes from group 1 were unsuccessful due to too large differences in reactivity between the substrates. When the difference in reactivity approaches a factor of 10 the changes in the concentration of the slowest reacting alkene becomes very small, thus leading to large uncertainties in the determination. Instead, we chose to select competing pairs from the entire set of 12 alkenes, based solely upon relative reactivity. Using alkene **2a** as reference compound the relative reactivities of **1a**, **1b** and **3a** could be established (Figure 115).

[k] The kinetic study in *t*BuOH:H_2O was performed by Gitte Holm Jensen and Marie Louise Nygaard Andersen.

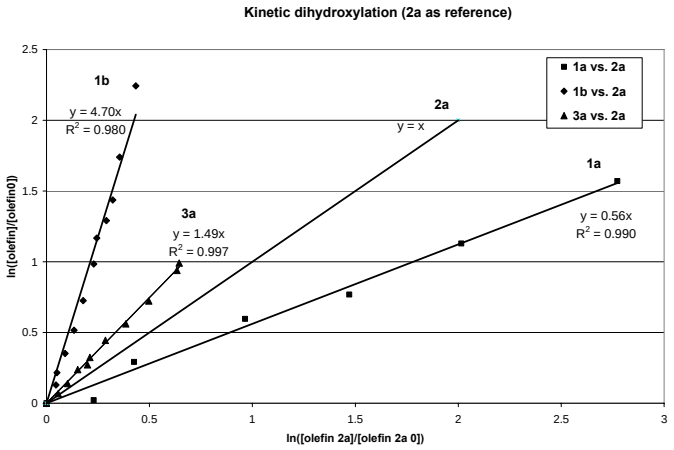

Figure 115 Kinetic plots for alkenes **1a**, **1b** and **3a**, which were all determined relative to alkene **2a**.

The reactivity of the substantially slower-reacting **c** alkenes from groups 1-3 were determined relative to alkene **2c**, and it was also possible to determine the relative reactivity of alkene **2b** in the same group (Figure 116).

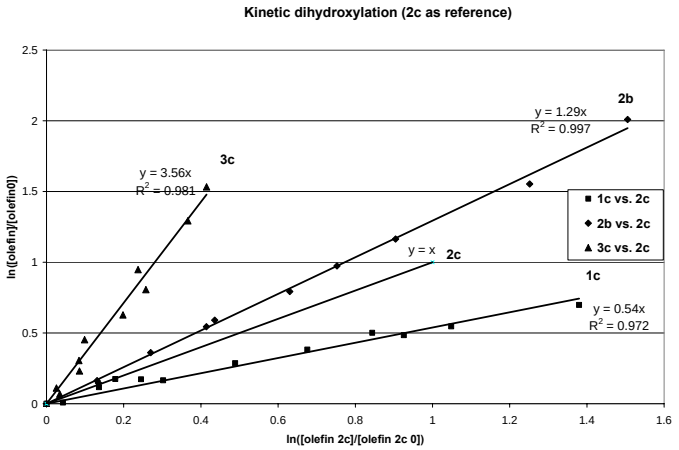

Figure 116 Kinetic plots for alkenes **1c**, **2b** and **3c**, which were all determined relative to alkene **2c**.

For the alkenes **3** it was possible to determine the relative reactivity of all three alkenes within the group, and in addition alkene **4b** could also be related to **3b** (Figure 117).

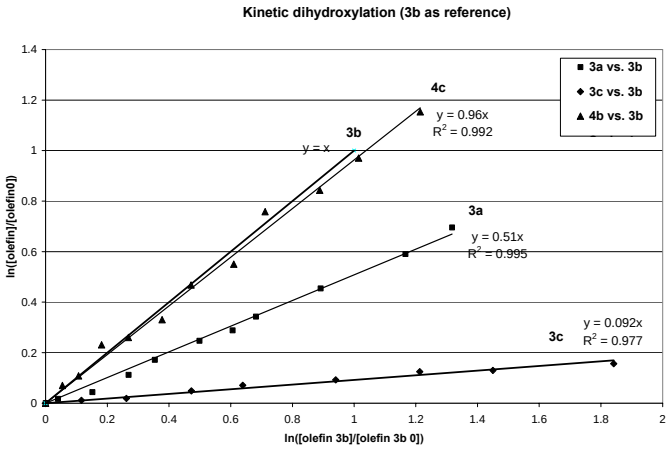

Figure 117 Kinetic plots for alkenes **3a**, **3c** and **4c**, which were all determined relative to alkene **3b**.

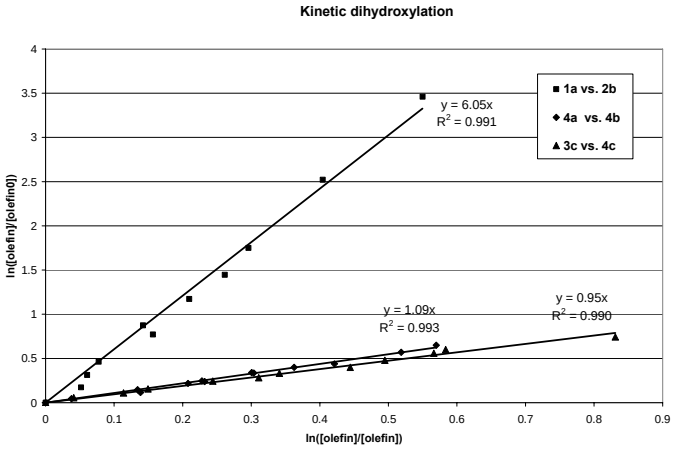

Figure 118 The remaining kinetic dihydroxylations, which enable us to determine the relative reactivity of all 12 alkenes. Note that the competitive dihydroxylations collected in this plot have been performed using different reference compounds. Thus, the relative reactivity of the compounds within this plot cannot be assessed directly.

The remaining determinations of relative reactivities have been collected in Figure 118. The results of the kinetic dihydroxylations are summarized in Figure 119. A dotted arrow indicates the difference in reactivity was too large to be determined. A full line arrow indicates the difference in reactivity could be determined. The reactivity of each alkene compared to the slowest reacting alkene **1c** is shown in a square next to each alkene, whereas the experimentally

determined relative reactivity from each successful pair-wise competition is shown in an ellipse on the corresponding arrow.

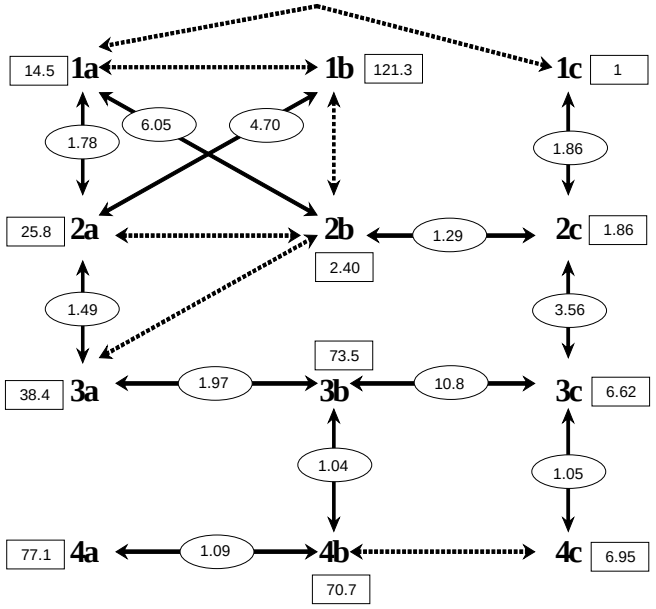

Figure 119 Overview of the experimentally determined relative reactivities in the two-phase *t*BuOH:H_2O system. A dotted arrow indicates the difference in reactivity was too large to be determined. A full arrow indicates a successful determination, with the relative reactivity shown in an ellipse.

Along with the kinetic dihydroxylations the resulting diols were synthesized using catalytic amounts of osmium in *t*BuOH:H_2O and the resulting *ee* was measured by chiral GC. Table 14 summarizes experimental reactivities determined in toluene along with reactivity and selectivity (%*ee*) in the two-phase *t*BuOH:H_2O. Although only one orientation should be preferred for trisubstituted alkenes the experimental selectivity is low in some cases. This is true for all the **c** alkenes, indicating that the NW corner does not provide much stabilization for a phenyl moiety. With a benzyl substituent the SW corner does not provide stabilization – something which spurred our interest, and we will return to later.

In all cases the absolute configuration was assumed to arise from the "allowed" orientation with the vinylic hydrogen positioned close to the PHAL linker. In principle the diols with low *ee* could arise from an alternate orientation, but for the present comparison with theoretical calculations the absolute configuration of these substrates are not essential.

Table 14 Experimentally determined reactivities and enantioselectivities for the dihydroxylation of all twelve alkenes.

Alkene	k_{rel} (experimental)[a]		*ee* (%)
	toluene	*t*BuOH:H_2O	exp
1a	12.1	14.4	96.4
1b	45.3	119.5	99.8
1c	*1*	*1*	72.6
2a	9.3	13.8	97.6
2b	1.40	1.29	28.0
2c	*1*	*1*	21.3
3a	2.37	5.8	95.6
3b	2.58	11.3	89.0
3c	*1*	*1*	49.4
4a	3.53	11.3	96.7
4b	3.06	10.4	94.2
4c	*1*	*1*	46.4

(a) Reactivities (k_{rel}) relative to alkene **c** in each group of isomers.

5.2.7 Computational Methods

To achieve a better understanding of the reactivity- and selectivity-determining features of the asymmetric dihydroxylation of the twelve alkene probes we decided to perform a computational study. The transition states were modelled using a Q2MM force field (see 3.12.2 Transition State Force Field (TSFF)) in the program MacroModel v. 8.0.[33]

Conformational searches were performed to account for all possible isomers of each TS, with separate searches being performed for each of the four different orientations of each alkene. In the following discussion each orientation will be described by which corner of the mnemonic device the "probing" phenyl moiety points toward. As mentioned previously, we *a priori* expect

the isomer with the vinylic hydrogen close to the PHAL linker as the most favoured orientation for the tri-substituted alkenes employed in this study.

The conformational search consisted of a systematic Monte Carlo search[223] with inclusion of the torsional degrees of freedom in the substrates (one less than the group number) and the torsions responsible for the overall conformation of the ligand. In this initial search torsions of ethyl and methoxy groups were excluded. The generated ensemble of conformations were re-optimized using a tight energy cutoff (20 kJ/mol) and the resulting ensemble of conformations were used as input for the following mixed Monte-Carlo[224]/Low Mode[225] search which was performed for 100000 steps. In the Monte Carlo part of the search the full set of torsions was now included. Finally, another reoptimization was performed either *in vacuo* or with the built-in solvation model for H_2O. These two sets of calculations represent two extremes. The experimental results were expected to lie in between these two sets, with the toluene results closer to gas phase, and the bi-phasic results (where the reaction probably occurs in the *t*BuOH-phase) closer to the results obtained with the continuum model for water.

The free alkenes were subjected to systematic Monte Carlo searches only, since these have few enough degrees of freedom so that it is possible to guarantee a complete coverage of the conformational space using a systematic search.

Ensemble energies for each conformational search are obtained by Boltzmann summation over all conformations according to eq. 33, and thus include conformational entropy, but not vibrational or solvation contributions, unless included explicitly in each individual conformational energy. Note that eq. 33 can also be used to combine several different ensembles (like those for all alkene orientations) into one global ensemble.

$$E = -RT \ln\left(\sum_i e^{-E_i/RT} \right) \tag{33}$$

Enantioselectivities are calculated by combining all paths contributing to one enantiomer into one ensemble using eq. 33, and are reported as relative activation barriers. The enantiomeric ratio (*er*) and *ee* can then be calculated using eqs. 34-35 . The calculation of *ee* is defined to yield a positive number if the major enantiomer is obtained from the expected orientation of the alkene with the vinylic hydrogen close to the PHAL linker, whereas a negative number indicates a preference for the opposite enantiomer.

$$er = e^{(E_{SW+NE} - E_{SE+NW})/RT} \tag{34}$$

$$ee = \frac{er - 1}{er + 1} \tag{35}$$

In molecular mechanics the obtained energy is with reference to a hypothetical strain-free molecule, which does not allow a direct comparison between molecules with different bonding schemes. To allow such a comparison we invoke an isodesmic equilibrium, where the competition between two alkenes for the active catalyst is seen as a pseudo-equilibrium where the alkene in one TS exchanges with free alkene to form an alternative TS. The difference in activation energy ($\Delta\Delta E^{\ddagger}$) can then be obtained from eq. 36, where E in all cases corresponds to total ensemble energies obtained from all contributing conformations for one type of TS or alkene. We define the reference alkene as alkene 1, so that eq. 36 always yields a positive number for any alkene that reacts faster than the reference (alkene **c** in each group (toluene), or **1c** globally (*t*BuOH:H_2O)). We note that when the two products in the competition are more different than simple stereoisomers (*ie.,* for all comparisons except between **b** and **c** within each group), the isodesmic comparison is not isoparametric, which means that systematic errors present in all molecular mechanics treatments do not necessarily cancel. Thus, we will also be testing the importance of the systematic errors in our force field for an isodesmic comparison.

$$\Delta\Delta E^{\neq} = E_{TS1} - E_{TS2} - E_{alkene1} + E_{alkene2} \tag{36}$$

5.2.8 Computational Results

The calculated relative rates of dihydroxylation of all alkenes relative to alkene **c** within each group are shown in Table 15.

Table 15 Calculated values for the differences in activation energy within each isomeric group of alkenes (Eq. 36). The c alkene within each group has been used as reference.

	$\Delta\Delta E^{\ddagger}$ *calc* (kJ/mol)			
	in vacuo		H_2O	
Group	**a**	**b**	**a**	**b**
1	12.1	12.3	10.5	9.0
2	12.2	2.9	10.8	2.9
3	4.3	3.7	3.2	2.9
4	4.6	5.6	5.1	2.5

In all cases the **a** and **b** alkenes react faster than the **c** alkenes due to the stabilizing interactions with the ligand environment, which corresponds to the NE and SW corners of the mnemonic device, respectively. As example have been shown the best TS structures for the dihydroxylation of **2a** (Figure 120, left) and **4b** Figure 120, right)

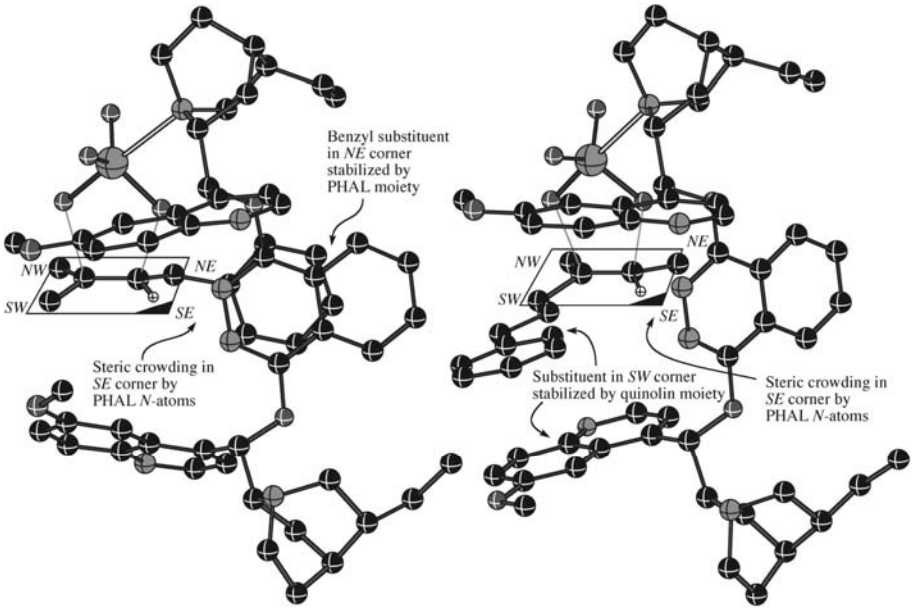

Figure 120 Illustration of the two attractive pockets described by Sharpless (left) and Corey (right). The TS structures of **2a** (left) and **4b** (right) have been oriented in accordance with the Sharpless mnemonic device.

Looking more closely at the results in Table 15, two features are striking. First of all, the differences in reactivity are much larger within groups 1 and 2, than for groups 3 and 4. This is probably due to an increased reactivity of **3c** and **4c** due to the flexibility of the tether allowing the phenyl moiety to achieve stabilizing interactions with other areas of the catalyst. When investigating the structures of the located transitions states, we find that the **a** alkenes can achieve a strong stabilization in the NW corner, where there is a "pocket" created by the primary quinoline and the PHAL linker. With a simple phenyl substituent (group 1) the pocket in the SW corner of the mnemonic between the two quinolines offers slightly better stabilization than NE as illustrated by both experiment and calculations. We are pleased to see that the low reactivity observed for benzyl-substituted alkene **2b** is well reproduced by the computational calculations and will return to this point later (see below). With a two-carbon tether (group 3) the experimental results reveal a small preference for the SW corner, whereas the calculations

suggest the NE as affording the best stabilization. When a three-carbon tether is employed the result is the opposite, with experimental preference for the NE corner and computational results favouring the SW corner. Interestingly, the use of a solvation model changes the preference within group 4, an indication that the differences between SW and NE are very small

Returning to the spurious results obtained for alkene **2b** we decided to investigate the transition states from all four orientations of the alkene in detail. Surprisingly, the "allowed" orientation with the benzyl group in the SW corner is just as bad as the orientation with the benzyl in the empty NW and a methyl group in the sterically crowded SE corner. The pocket in the SW corner exists between two quinoline moieties, which are both co-planar with the alkene double bond. This pocket is well-suited for a phenyl group directly attached to the alkene (**1b**), but due to the sp^3-hybridized carbon atom between the phenyl and the alkene in **2b**, the orientation of the phenyl group now deviates significantly from the plane of the alkene. This increases the steric demands of the phenyl moiety and it now no longer "fits" inside the pocket created by the two quinolines.

A closer look at the calculated energies for the different orientations of alkene **2b** reveals interesting features (Figure 121, left).

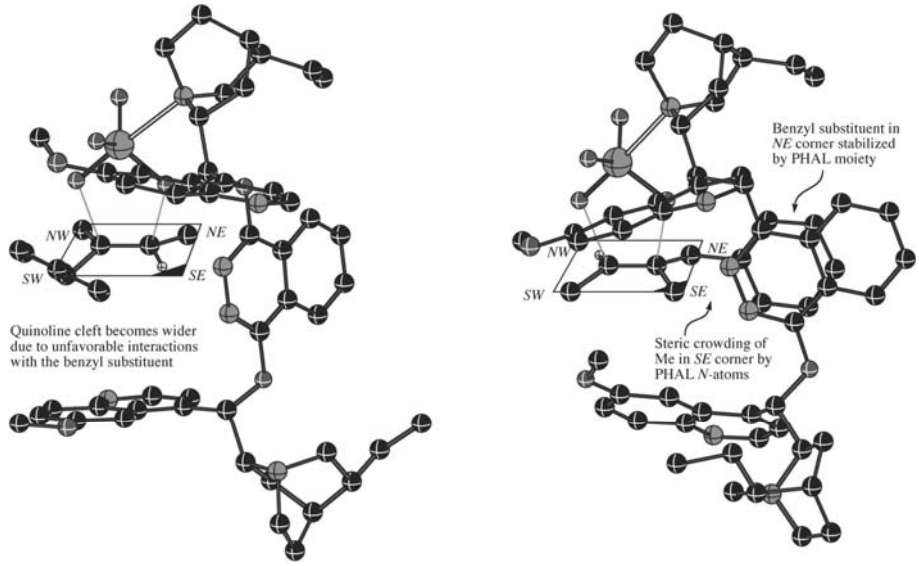

Figure 121 Left: The best SE orientation of **2b**. Right: The best TS structure for **2b**, the NW orientation, with the benzyl group stabilized by the PHAL moiety in the NE corner.

The pocket in the NE corner does not suffer from these harsh geometrical demands, and the favoured orientation of substrate **2b** has the benzyl group pointing towards the NE corner of the

mnemonic, while suffering from steric interactions between the methyl substituent and the PHAL linker (Figure 121, right). This elegantly rationalizes the observed low reactivity of alkene **2b**.

But also the conformer with the benzyl group pointing towards the sterically hindered SE corner has a surprisingly low energy, only 3 kJ/mol higher than for the conformation with the benzyl group in the stabilizing NE corner. Apparently the auxiliary quinoline moiety has changed its orientation in order to accommodate the benzyl substituent in this, otherwise, sterically crowded corner. The lowest energy TS structure for this conformation is shown in Figure 122.

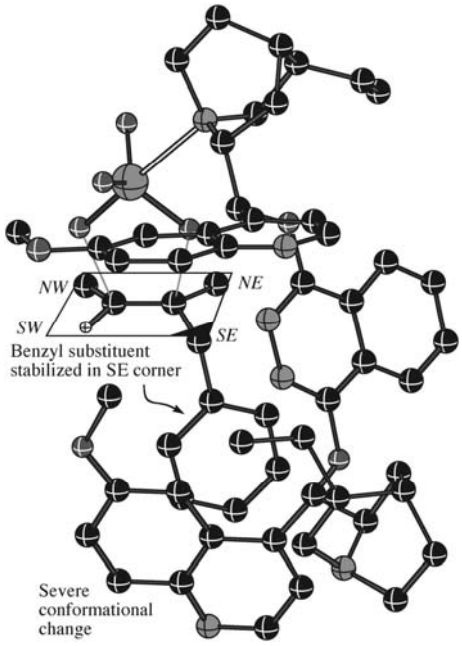

Figure 122 The SW orientation of **2b**, with the benzyl group in the SE corner, crowded by the PHAL moiety.

Upon analyzing the structures of the **c** alkenes we find that none of the four orientations of the alkene within the active catalyst are favoured. The initial designation of a minor steric hindrance in the NW corner can unambiguously be attributed to lack of stabilizing interactions, instead. For groups 3 and 4 where the alkenes contain a two- or three-carbon tether, the experiments suggest slightly better stabilization in the NE corner. The long tethers allow the large substituent to achieve stabilization with other parts of the catalyst, in sharp contrast to the

structures for group 1 where the orientation of the phenyl group is fixed. Use of a solvation model has lead to a small decrease in rate differences, which is in accordance with an increased stabilization of the **c** alkenes, which have the large substituent pointing towards the solvent in the NW corner of the mnemonic device.

Table 16 shows the difference in energy for the formation of enantiomeric diols from each of the twelve alkenes, which can be translated to a predicted selectivity (*%ee*) as discussed previously. In general there is good accordance with the experimental results, *i.e.* high selectivity for all **a** and **b** alkenes except **2b**, and a low selectivity for the **c** alkenes. Impressively, the order of the predicted selectivities within a group is correct for all four groups (*in vacuo*), although for groups 3 and 4 this may be a coincidence as the difference between the **a** and **b** alkenes is minimal. For two of the **c** alkenes the predicted absolute configuration is reversed when using a solvation model, due to the fact that solvation selectively lowers the penalty for having the phenyl moiety in the unstabilized NW corner.

Table 16 Calculated values for the differences in activation energies for the diastereomeric transition states leading to opposite enantiomers.

	$\Delta\Delta E^{\ddagger}$ *calc* (kJ/mol)					
	in vacuo			H_2O		
Group	**a**	**b**	**c**	**a**	**b**	**c**
1	13.1	14.2	3.3	13.0	11.9	2.0
2	4.8	3.1	-1.8	6.9	5.7	0.9
3	7.4	7.4	1.5	8.3	7.2	2.2
4	7.6	7.2	-0.8	8.9	5.2	0.6

5.2.9 Comparison between theory and experiment

Computational results are initially obtained as energies, which can later be converted to reactivities and selectivities for direct comparison to experimental numbers. However, the comparison is usually best carried out in the "energy domain" due to the exponential dependence of the experimental quantities. The data from Table 14 have therefore been converted to relative activation energies for the two competing process, Table 17.

Table 17 The experimental reactivities and selectivities converted to differences in activation energy.

Group	$\Delta\Delta E^{\ddagger}$ *exp* (kJ/mol)						
	toluene		*tBuOH:H_2O*		*ee*		
Isomer	**a**	**b**	**a**	**b**	**a**	**b**	**c**
1	6.2	9.4	6.6	11.9	9.9	>17[a]	4.6
2	5.5	0.8	6.5	0.6	10.9	1.4	1.1
3	2.1	2.3	4.4	6.0	9.4	7.0	2.7
4	3.1	2.8	6.0	5.8	10.1	8.7	2.5

a) Only the major enantiomer was observed and consequently the *ee* was assumed to be at east 99.8%.

The experimental differences in activation energy obtained in toluene were plotted against the theoretical values obtained *in vacuo* (Figure 123).

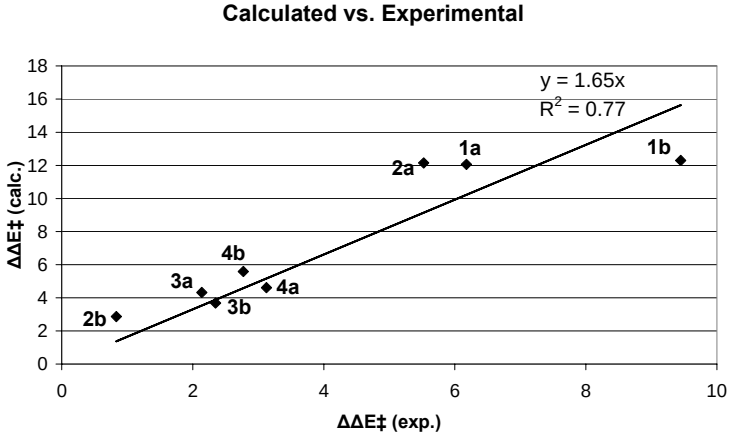

Figure 123 Activation energies relative to the **c** alkenes, computational results in vacuo vs. experimentally determined values in toluene.

In this comparison the reference **c** alkenes are left out, since they have been assigned a relative reactivity of 1 within each group. Unfortunately, the systematic errors present in force fields do not allow a direct comparison between two alkenes from different group, although experimentally the comparison is trivial. The correlation between experiment and theory in Figure 123 is quite good, with only a few data points significantly deviating from the straight

line. The slope of the line is greater than 1, which we attribute to an overestimation of the stabilizing interactions when the calculation is performed without a solvation model.

To verify this proposal, we performed similar comparisons for the experimental selectivities obtained in the two-phase *t*BuOH:H_2O system which are compared to the calculated values *in vacuo* in Figure 124, and to calculated values using a solvation model in Figure 125.

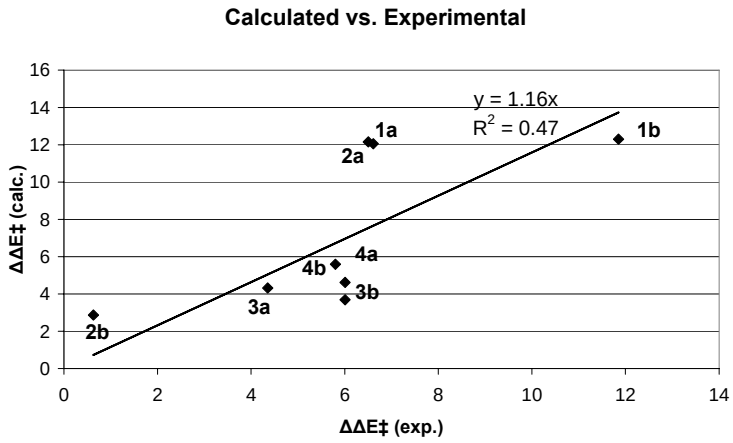

Figure 124 The calculated differences in activation energies (*in vacou*) relative to the **c** alkenes against the experimentally determined values in the two-phase tBuOH:H_2O system.

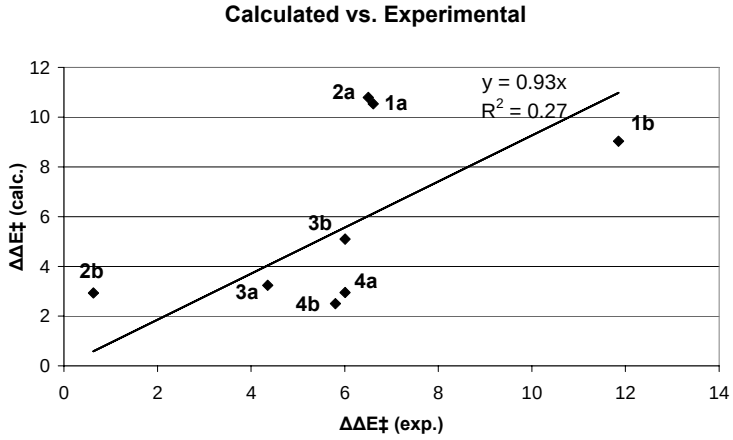

Figure 125 The calculated differences in activation energies (in water) relative to the **c** compounds against the experimentally determined values in the two-phase tBuOH:H_2O system.

In both cases the correlation is worse, which we attribute to "random noise" introduced by use of the solvation model or it could be related to the lack of solvation in the QM calculations used to derive the TSFF.[210] Interestingly, though, the slope is now close to 1, indicating that the previously mentioned overestimation of the stabilizing interactions *is* due to lack of solvation.

Turning to the prediction of selectivity, we envision an even better correlation, since the comparisons are now between diastereomeric structures, which should significantly reduce the intrinsic systematic errors. As mentioned previously, we assume the major enantiomer observed experimentally to arise from an orientation with the vinylic hydrogen close to the PHAL linker. The experimental selectivities have only been obtained in the practical two-phase catalytic system, but are compared to both sets of calculations to estimate the effect of solvation.

When investigating the plot using computational energies obtained *in vacuo* (Figure 126), the predictions are generally quite good, with most being within or close to the estimated computational accuracy of 2 kJ/mol. The dotted line has a slope of 1, thus representing perfect correlation.

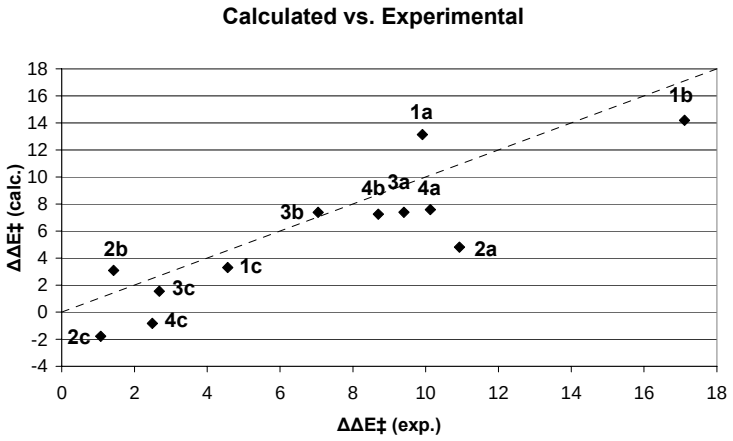

Figure 126 Calculated enantioselectivities in vacuo plotted against the experimentally determined enantioselectivities.

In Figure 127 the same experimental results are shown, but now plotted against the predicted values with the solvation model. As shown previously for the reactivities, we see a slightly worse correlation between experiment and theory, which can probably be attributed to random noise in the solvation model. One of the worst predictions was made for alkene **2a**, which could arise from the fact that benzyl-substituted alkenes were not part of the original development of

the TSFF.[217] As a consequence the potential describing the rotation of the phenyl moiety in the benzyl-substituted alkenes may be subject to significant errors.

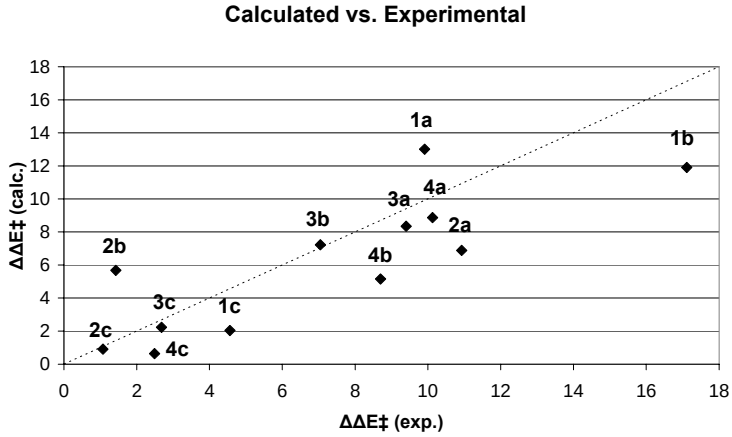

Figure 127 Calculated enantioselectivities using the water model plotted against the experimentally determined enantioselectivities.

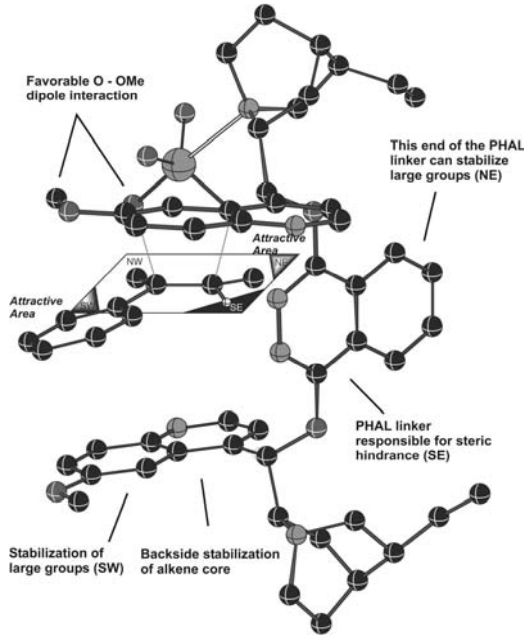

Figure 128 The global minimum structure of alkene **1b** with the phenyl group stabilized in the south-west corner has been overlaid on the revised mnemonic device. The most important stabilizing interactions have been mapped.

The controlling features in the reaction have been summarized in Figure 128, where the best transition state for the dihydroxylation of **1b** has been overlaid on a revised mnemonic device. Compared to the revised mnemonic device suggested by Sharpless and co-workers (Figure 108), this new mnemonic device incorporates an attractive area also in the NE corner in addition to the attractive area already present (SW). Furthermore, the proposed steric hindrance in the NW corner has been removed.

5.2.10 Conclusions

The reactivity- and selectivity-determining features of the osmium-catalyzed asymmetric dihydroxylation were investigated using a combined experimental and theoretical approach. Twelve trisubstituted alkenes were synthesized and used as probes in the kinetic studies. Each individual diol was synthesized and the selectivity (%*ee*) was determined. The obtained experimental results were compared to a computational study using a previously published TSFF, and results were rationalized based on the physical interactions between the substrate and the catalyst in TS. This resulted in a revised mnemonic device along with a mapping of the features of this revised mnemonic device onto a TS structure. In conclusion, the present study has allowed for a better understanding of the controlling features in this important reaction.

6 Concluding Remarks

In the present thesis the focus has been on the combined use of experimental and computational methods for elucidating reaction mechanisms and predicting the selectivity for a selection of homogeneous, asymmetric transition metal-catalyzed reactions. Several synthetically important and mechanistically interesting reactions have been studied, which have resulted in a better understanding of the selectivity-determining features in each of the reactions.

In the mechanistic investigations of the Heck reaction a characterization of the electronic nature of the rate-limiting TS was achieved, which could find use in the development of improved catalytic systems for this reaction.

The palladium-catalyzed allylic alkylation was the subject of several studies; When phenanthroline-type ligands were used the overall selectivity could be described by a sum of ligand-allyl and allyl-nucleophile contributions. This approach allowed the use of an accurate computational method, which would otherwise have been computationally very demanding.

The effect of chloride was studied experimentally and computationally, and it was concluded that the observed "memory effects" are caused specifically by interactions between the chloride ion and palladium resulting in a non-symmetric intermediate. The standard reaction using phosphine ligands was investigated using DFT/B3LYP, and interesting dependencies of the choice of model phosphine was noted. The calculations allowed for a determination of the relative energies of the intermediate allyl complexes, along with the reactivity towards a model cyanide nucleophile. With chloride present the increased reactivity of the anionic $[Pd^0(Cl)PPh_3]$ towards oxidative addition readily explains the "memory effects" observed in experiments as arising from nucleophilic addition *trans* to phosphorus in an neutral, unsymmetrical η^3-allylpalladium complex.

In the intramolecular allylic alkylation developed by Poli and co-workers a small computational study provided a sound explanation for the observed rate increases in absence of Na^+. The prediction from the computational investigation that phase-transfer conditions were not responsible for the observed rate accelerations was confirmed experimentally.

Within the area of transition metal-catalyzed asymmetric oxidations two studies have been carried out. A combined study of reactivity and selectivity using eight methylsubstituted styrenes was used to identify two approach vectors operating in parallel in the Mn(salen)-catalyzed epoxidation. The distinction between two different approach vectors allowed rationalization of the observed low enantioselectivity for substrates which are capable of reacting in both orientations and this concept could be of importance in related organic reactions.

The osmium-catalyzed asymmetric dihydroxylation was investigated using a combination of kinetic studies and computational modelling. The results could be summarized in a revised mnemonic device, which should allow an improved predictability of absolute configuration. For the quantitative determination of enantiomeric excess the TSFF gave results which were in good agreement with experiments. Furthermore, the computational modelling made it possible to map the most important features of the reaction onto a TS structure.

The present thesis serves to illustrate how kinetic studies and/or computational chemistry can be applied in all phases of the development of catalytic asymmetric reactions.

7 References

1 http://www.nobel.se

2 http://nobelprize.org/chemistry/laureates/1909/ostwald-lecture.html

3 Berzelius, J. J. *Edinburgh New Philosophical Journal*, **1836,** *XXI*, 223.

4 Bhaduri, S.; Mukesh, D. *Homogeneous Catalysis: Mechanisms and Industrial Applications*; John Wiley & Sons: New York, 2000.

5 http://www.idsia.ch/~juergen/haberbosch.html

6 Smil, V. *Nature* **1999**, *400*, 415.

7 Smith, B. E. *Science* **2002***, 297*, 1654.

8 Ziegler, K.; Holzkamp, E.; Breil, H.; Martin, H. *Angew. Chem. Int. Ed* **1955**, *67*, 541.

9 Ziegler, K. Nobel lecture, http://nobelprize.org/chemistry/laureates/1963/ziegler-lecture.pdf

10 Kaminsky, W. *J. Polym. Sci Part A: Polym. Chem.* **2004**, *42*, 3911.

11 Farina, V. *Adv. Synth. Catal.* **2004**, *346*, 1553.

12 Eliel, E. L.; Wilen, S. H. *Stereochemistry of Organic Compounds*; Wiley: New York, 1994.

13 a) Cahn, R. S.; Ingold, C. K.; Prelog, V. *Angew. Chem. Int. Ed. Engl.* **1966**, *5*, 385. b) Smith, M. B.; March, J. *March's Advanced Organic Chemistry*; 5th Edition; John Wiley & Sons: New York, 2001, pp. 139-141.

14 Cornforth, J. W. *Chem. Britain* **1975**, *11*, 432.

15 a) *Catalytic Asymmetric Synthesis 2nd Edition;* Ojima, I., Ed.; Wiley-VCH: New York, 2000. b) *Comprehensive Asymmetric Catalysis*; Jacobsen, E. N.; Pfaltz, A.; Yamamoto, H., Eds.; Sprinter-Verlag: Berlin, 2000.

16 Doyle, M. P. In *Catalytic Asymmetric Synthesis*, Ojima, I., Ed.; VCH Publishers: New York, 1993, chapter 3.

17 Nozaki, H.; Moriuti, S.; Takaya, H.; Noyori, R. *Tetrahedron Lett.* **1966**, *43*, 5239.

18 Knowles, W. S.; Sabacky, M. J. *Chem. Commun.* **1968**, *22*, 1445.

19 Knowles, W. S. *Adv. Synth. Catal.* **2003**, *345 No. 1+2*, 3. (Nobel lecture)

20 Patrick, G. L. *An Introduction to Medicinal Chemistry*; 2nd Edition; Oxford University Press: Oxford, 2001.

21 Miyashita, A.; Yasuda, A.; Takaya, H.; Toriumi, K.; Ito, T.; Souchi, T.; Noyori, R. *J. Am. Chem. Soc.* **1980**, *102*, 7932.

22 Noyori, R. *Adv. Synth. Catal.* **2003**, *345 No. 1+2*, 15. (Nobel lecture)

23 http://nobelprize.org/chemistry/laureates/2001/public.html

24 Halpern, J. *Science* **1982**, *217*, 401.

25 a) Schrock, R. R.; Lecture given at Lund University on Wednesday December 14th, 2005. b) Schrock, R. R, Hoveyda, A. H. *Angew. Chem. Int. Ed.* **2003**, *42*, 4592.

26 http://nobelprize.org/chemistry/laureates/2005/

27 Seiders, T. J.; Ward, D.W.; Grubbs, R. H. *Org. Lett.* **2001**, *3*, 3225.

28 Katsuki, T.; Sharpless, K. B. *J. Am. Chem. Soc.* **1980**, *102*, 5974.

29 a) Wei, Z.; Loebach, J. L.; Wilson, S. R.; Jacobsen, E. N. *J. Am. Chem. Soc.* **1990**, *112*, 2801. b) Irie, R.; Noda, K.; Ito, Y.; Matsumoto, N.; Katsuki, T. *Tetrahedron Lett.* **1990**, *31*, 7345.

30 a) Cramer, C. J. *Essentials of Computational Chemistry*; John Wiley Sons Ltd., Chichester, West Sussex, England, 2003. b) Jensen, F. *Introduction to Computational Chemistry*; John Wiley Sons Ltd., Chichester, West Sussex, England, 1999. c) Serway, R. A.; Moses, C. J.; Moyer, C. A. *Modern Physics*; 2nd Edition; Saunders College Publishing: Fort Worth, USA, 1989.

31 http://nobelprize.org/chemistry/laureates/1998/index.html

32 a) Allinger, N. L.; Chang, S. H.-M.; Glaser, D. H.; Honig, D. *Israel J. Chem.* **1980**, *20*, 51. b) Burkert, U.; Allinger, N. L. *Molecular Mechanics*; American Chemical Society: Washington DC, 1982. c) Allinger, N. L.; Yuh, Y. H.; Lii, J.-H. *J. Am. Chem. Soc.* **1989**, *111*, 8551. d) Allinger, N. L.; Rahman, M.; Lii, J. H. *J. Am. Chem. Soc.* **1990**, *112*, 8293.

33 MacroModel v. 8.0 from Schrodinger Inc.: Mohamadi, F.; Richards, N. G. J.; Guida, W. C.; Liskamp, R.; Lipton, M.; Caulfield, C.; Chang, G.; Hendrickson, T.; Still, W. C. *J. Comput. Chem.* **1990**, *11*, 440. For current versions, see: http://www.schrodinger.com

34 a) Menschutkin, N. *Z. Physik. Chem.* **1890**, *5*, 589. b) Menschutkin, N. *Z. Physik. Chem.* **1890** ,*6,* 41.

35 Eliel, E. L.; Wilen.; S. H. *Stereochemistry of Organic Compounds*; Wiley: New York, 1994, chapter 10.5.

36 For a more elaborate discussion, see: Atkins, P. W. *Physical Chemistry*; 6th Edition; Oxford University Press: Oxford, 1998, chapter 27.

37 a) Bohr, N. *Phil. Mag.* **1913**, *26*, 1. b) Bohr, N. *Nature* **1913**, *92*, 231.

38 Hohenberg, P.; Kohn, W. *Phys. Rev.* **1964**, *136*, B864.

39 Becke, A. D. *J. Chem. Phys.* **1993**, *98*, 5648.

40 Stephens, P. J.; Devlin, J. F.; Chabalowski, C. F.; Frisch, M. J. *J. Phys. Chem.* **1994**, *98*, 11623.

41 Ziegler, T.; Autschbach, J. *Chem. Rev.* **2005**, *105*, 2695.

42 a) Tannor, D. J.; Marten, B.; Murphy, R.; Friesner, R. A.; Sitkoff, D.; Nicholls, A.; Ringnalda, M.; Goddard III, W. A.; Honig, B. *J. Am. Chem. Soc.* **1994**, *116*, 11875. b) Marten, B.; Kim, K.; Cortis, C.; Friesner, R. A.; Murphy, R. B.; Ringnalda, M. N.; Sitkoff, D.; Honig, B. *J. Phys. Chem.* **1996**, *100*, 11775.

43 Ahlquist, M.; Kozuch, S.; Shaik, S.; Tanner, D.; Norrby, P.-O. *Organometallics* **2006**, *25*, 45.

44 Still, W. C.; Tempczyk, A.; Hawley, R. C.; Hendrickson, T. *J. Am. Chem. Soc.* **1990**, *112*, 6127.

45 Young, D. C. *Computational Chemistry: A Practical Guide for Applying Techniques to Real-World Problems*; John Wiley & Sons: New York, 2001, Chapter 23.

46 Gao, J. *Acc. Chem. Res.* **1996**, *29*, 298.

47 a) Warshel, A.; Lewitt, M. *J. Mol. Biol.* **1976**, *103*, 227. b) Åqvist, J.; Warshel, A. *Chem. Rev.* **1993**, *93*, 2523.

48 Maseras, F.; Morokuma, K. *J. Comput. Chem.* **1995**, *16*, 1170.

49 a) Ujaque, G.; Maseras, F.; Lledós, A. *J. Am. Chem. Soc.* **1999**, *121*, 1317. b) Drudis-Solé, G.; Ujaque, G.; Maseras, F.; Lledós, A. *Chem. Eur. J.* **2005**, *11*, 1017.

50 *Combined Quantum and Molecular Mechanics Methods*; Gao, J.; Thompson, M., Eds.; American Chemical Society: Washington, 1998.

51 a) Eksterowicz, J. E.; Houk, K. N. *Chem. Rev.* **1993**, *93*, 2439. b) Houk, K. N.; Li, Y., Evanseck, J. D. *Angew. Chem. Int. Ed. Engl.* **1992**, *31*, 682.

52 Raimondi, L.; Brown, F. K.; Gonzalez, J.; Houk, K. N. *J. Am. Chem. Soc.* **1992**, *114*, 4796.

53 Spellmeyer, D. C.; Houk, K. N. *J. Org. Chem.* **1987**, *52*, 959.

54 Wu, Y.-D.; Houk, K. N.; Florez, J.; Trost, B. M. *J. Org. Chem.* **1991**, *56*, 3656.

55 Bernardi, A.; Capelli, A. M.; Gennari, C.; Goodman, J. M.; Paterson, I. *J. Org. Chem.* **1990**, *55*, 3576.

56 Norrby, P.-O. *J. Mol. Struct. (Theochem)* **2000**, *506*, 9.

57 a) Jensen, F. *J. Am. Chem. Soc.* **1992**, *114*, 1596. b) Olsen, P. T.; Jensen, F. *J. Chem. Phys.* **2003**, *118*, 3523.

58 *Handbook of Organopalladium Chemistry for Organic Synthesis*; Negishi, E., Ed.; John Wiley & Sons: New York, 2002.

59 Tsuji, J. *Acc. Chem. Res.* **1969,** *2*, 144.

60 Suzuki-type: Saito, S.; Oh-tani, S.; Miyaura, N. *J. Org. Chem.* **1997**, *62*, 8024. Sonogashira-type: Wang, L.; Li, P.; Zhang, Y. *Chem. Commun.* **2004**, 514. Aminations: Lipschutz, B. H.; Ueda, H. *Angew. Chem. Int. Ed. Engl.* **2000**, *39*, 4492.

61 a) Littke, A. F.; Fu, G. C. *J. Org.Chem.* **1999**, *64*, 10. b) Shaughnessy, K. H.; Kim, P.; Hartwig, J. F. *J. Am. Chem. Soc.* **1999**, *121*, 2123. c) Littke, A. F.; Fu, G. C. *J. Am. Chem. Soc.* **2001**, *123*, 6989.

62 a) Miyaura, N.; Yanagi, T.; Suzuki, A. *Synth. Commun.* **1981**, *11*, 513. b) Suzuki, A. *Acc. Chem. Res.* **1982**, *15*, 178. c) Miyaura, N.; Suzuki, A. *Chem. Rev.* **1995**, *95*, 2457. d) Suzuki, A. In *Handbook of Organopalladium Chemistry for Organic Synthesis*; Negishi, E., Ed.; John Wiley & Sons: New York, 2002, Chapter III.2.2.

63 a) Milstein, D.; Stille, J. K. *J. Am. Chem. Soc.* **1979**, *101*, 4992. b) Stille, J. K. *Angew. Chem. Int. Ed. Engl.* **1986**, *25*, 508 c) Kosugi, M; Fugami, K. In *Handbook of Organopalladium Chemistry for Organic Synthesis*; Negishi, E., Ed.; John Wiley & Sons: New York, 2002, Chapter III.2.3.

64 a) King, A. O.; Okukado, N.; Negishi, E. I. *J. Chem. Soc., Chem. Commun.* **1977**, *19*, 683. b) Negishi, E.-I. In *Handbook of Organopalladium Chemistry for Organic Synthesis*; Negishi, E., Ed.; John Wiley & Sons: New York, 2002, Chapter III.2.1.

65 Kumada, M. *Pure Appl. Chem.* **1980**, *52*, 669.

66 a) Sonogashira, K.; Tohda, Y.; Hagihara, N. *Tetrahedron Lett.* **1975**, *50*, 4467. b) Sonogashira, K. *J. Organomet. Chem.* **2002**, *653*, 46. c) Sonogashira, K. In *Handbook of Organopalladium*

Chemistry for Organic Synthesis; Negishi, E., Ed.; John Wiley & Sons: New York, 2002, Chapter III.2.8.1.

67 a) Guram, A. S.; Rennels, R. A.; Buchwald, S. L. *Angew. Chem. Int. Ed. Engl.* **1995**, *34*, 1348. b) Louie, J.; Hartwig, J. F. *Tetrahedron Lett.* **1995**, *36*, 3609. c) Driver, M. S.; Hartwig, J. F. *J. Am. Chem. Soc.* **1996**, *30*, 7217. c) Hartwig, J. F. *Acc. Chem. Res.* **1998**, *31*, 852. d) Hartwig, J. F. In *Handbook of Organopalladium Chemistry for Organic Synthesis*; Negishi, E., Ed.; John Wiley & Sons: New York, 2002, Chapter III.3.2.

68 Mizoroki, T.; Mori, K.; Ozaki, A. *Bull. Chem. Soc. Jpn.* **1971**, *44*, 581

69 a) Heck, R. F.; Nolley, J. P. *J. Org. Chem.* **1972**, *37*, 2320. b) Heck, R. F. *Acc. Chem. Res.* **1979**, *12*, 146.

70 a) Beletskaya, I. P.; Cheprakov, A. V. *Chem. Rev.* **2000**, *100*, 3009 b) De Meijere, A., Meyer, F. E. *Angew. Chem Int. Ed. Engl.* **1994**, *33*, 2379.

71 Jeffery, T. *J. Chem. Soc, Chem. Commun.* **1984**, 1287.

72 Amatore, C.; Azzabi, M.; Jutand A. *J. Am. Chem. Soc.* **1991**, *113*, 8375.

73 a) Hagiwara, H.; Sugawara, Y.; Hoshi, T.; Suzuki, T. *Chem. Commun.* **2005**, 2942. b) Bhanage, B. M.; Shirai, M.; Arai, M. *J. Mol. Cat. A: Chem.* **1999**, *145*, 69.

74 Herrmann, W. A.; Brossmer, C.; Öfele, K.; Reisinger, C.-P., Priermeier, T.; Beller, M.; Fischer, H. Beller, M.; Fischer, H. *Angew. Chem., Int. Ed. Engl.* **1995**, *34*, 1844. b) Beller, M.; Fischer, H.; Herrmann, W. A., Öfele, K.; Brossmer, C. *Angew. Chem., Int. Ed. Engl.* **1995**, *34*, 1848.

75 a) Herrmann, W. A.; Reisinger, C.-P.; Spiegler, M. *J. Organomet.Chem.* **1998**, *557*, 93. b) Selvakumar, K.; Zapf, A.; Beller, M. *Org. Lett.* **2002**, *4*, 3031.

76 Astruc, D.; Lu, F.; Aranzaes, J. R. *Angew. Chem. Int. Ed.* **2005**, *44*, 7852

77 a) Djakovitch, L.; Wagner, M.; Hartung, C. G.; Beller, M.; Koehler, K. *J. Mol. Cat. A.: Chem.* **2004**, *219*, 121. b) Christmann, U.; Vilar. R. *Angew. Chem. Int. Ed.* **2005**, *44*, 366.

78 Capri, W.; Candiani, I.; Bedeschi A.; Santi, R. *Tetrahedron Lett.* **1991**, *32***,** 1753.

79 a) Cabri, W.; Candiani, I.; Debernardinis, S.; Francalanci, F.; Penco, S.; Santi, R. *J. Org. Chem.* **1991**, *56*, 5796. b) Cabri, W.; Candiani, I.; Bedeschi, A.; Penco, S. *J. Org. Chem.* **1992**, *57*, 1481.

80 Hayashi, T.; Kubo, A.; Ozawa, F. *Pure. Appl. Chem.* **1992**, *64*, 421.

81 Abelman, M. M.; Oh, T.; Overman, L. E. *J. Org. Chem.* **1987**, *52*, 4130. b) Karabelas, K.; Westerlund, C.; Hallberg, A. *J. Org. Chem.* **1985**, *50*, 3896.

82 Ludwig, M.; Strömberg, S.; Svensson, M.; Åkermark, B. *Organometallics*, **1999**, *18*, 970.

83 Deeth, R. J.; Smith, A.; Brown, J. M. *J. Am. Chem. Soc.* **2004**, *126*, 7144.

84 Sato, Y.; Sodeoka, M.; Shibasaki, M. *J. Org. Chem.* **1989**, *54*, 4738.

85 Carpenter, N. E.; Kucera, D. J.; Overman, L. E. *J. Org. Chem.* **1989**, *54*, 5846.

86 Overman, L. E.; Poon, D. J. *Angew. Chem. Int. Ed. Engl.* **1997**, *36*, 518.

87 a) Shibasaki, M; Vogl, E. M, Ohshima, T. *Adv. Synth. Catal.* **2004**, *346*, 1533. b) Shibasaki, M; Vogl, E. M. *J. Organomet. Chem.* **1999**, 1. c) Shibasaki, M.; Miyazaki, F. In *Handbook of*

Organopalladium Chemistry for Organic Synthesis; Negishi, E., Ed.; John Wiley & Sons: New York, 2002, Chapter IV.2.3.

88 Dounay, A. B.; Overman, L. E. *Chem. Rev.* **2003**, *103*, 2945.

89 Hammett, L. P. *J. Am. Chem. Soc.* **1937**, *59*, 96.

90 Jaffé, H. H. *Chem. Rev.* **1953**, *53*, 191.

91 Clayden, J.; Greeves, N.; Warren, S.; Wothers, P. *Organic Chemistry*; Oxford University Press: Oxford, 2001, pp. 1090-1100.

92 Hansch, C.; Leo, A.; Taft, R. W. *Chem. Rev.* **1991**, *91*, 165.

93 Smith, M. B.; March, J. *March's Advanced Organic Chemistry*; 5th Edition; John Wiley & Sons: New York, 2001, p. 375.

94 Schreck, J. O. *J. Chem. Educ.* **1971**, *48*, 103.

95 Trost, B. M.; Crawley, M. L. *Chem. Rev.* **2003**, *103*, 2921.

96 a) Consiglio, G.; Waymouth, R. M. *Chem. Rev.* **1989**, *89*, 257. b) Frost, C. G.; Howarth, J.; Williams, J. M. J. *Tetrahedron: Asymmetry* **1992**, *3*, 1089. c) Trost, B. M.; Van Vranken, D. L. *Chem. Rev.* **1996**, *96*, 395. d) Helmchen, G. *J. Organomet. Chem.* **1999**, *576*, 203.

97 a) Trost, B. M.; Verhoeven, T. R. In *Comprehensive Organometallic Chemistry*; Wilkinson, G., Ed.; Pergamon Press: Oxford, 1982, Vol. 8, Chapter 57. b) Hayashi, T. In *Catalytic Asymmetric Synthesis*; Ojima, I., Ed.; VCH Publishers: New York, 1993. Chapter 7.1 c) Pfaltz, A.; Lautens, M. In *Comprehensive Asymmetric Catalysis I-III*; Jacobsen, E. N.; Pfaltz, A.; Yamamoto, H., Eds.; Springer Verlag: Berlin, 2000, Chapter 24. d) Trost, B. M.; Lee, C. In *Catalytic Asymmetric Synthesis*; Ojima, I., Ed.; Wiley-VCH: New York, 2000, Chapter 8E. e) Acemoglu, L.; Williams, J. M. J. In *Handbook of Organopalladium Chemstry for Organic Synthesis*; Negishi, E.-I., Ed.; Wiley-Interscience: New York, 2002, Vol. 2, Chapter V.2.4.

98 a) Tsuji, J. *Pure Appl. Chem.* **1986,** *58,* 869. b) Tsuji, J. *Tetrahedron* **1986,** *42,* 4361. c) Tsuji, J. *J. Organomet. Chem.* **1986**, *300*, 281.

99 Trost, B. M.; Murphy, D. J. *Organometallics* **1985**, *4*, 1143.

100 Sennhenn, P.; Gabler, B.; Helmchen, G. *Tetrahedron Lett.* **1994**, *35,* 8595.

101 Trost, B. M.; Organ, M. G. *J. Am. Chem. Soc.* **1994**, *116,* 10320.

102 Trost, B. M.; Toste, F. D. *J. Am. Chem. Soc.* **1998**, *120*, 815.

103 Eichelmann, H.; Gais, H.-J. *Tetrahedron Asymmetry* **1995**, *6,* 643.

104 Johannsen, M.; Jørgensen, K. A. *Chem. Rev.* **1998**, *98*, 1689.

105 a) Tsuji, J.; Takahashi, H.; Morikawa, M. *Tetrahedron Lett.* **1965**, 4387. b) Tsuji, J. *New J. Chem.* **2000**, *24*, 127.

106 a) Oslinger, M.; Powell, S. *Can. J. Chem.* **1973**, *96*, 274. b) Trost, B. M.; Fullerton, T. J. *J. Am. Chem. Soc.* **1973**, *95*, 292.

107 Vrieze, K. *Dynamic Nuclear Magnetic Resonance Spectroscopy*; Jackman, L. M.; Cotton, F. A., Eds.; Academic Press: New York, 1975, chapter 11. b) Pregosin, P. S.; Salzmann, R. *Coord. Chem. Rev.* **1996**, *155*, 35.

108 a) Sprinz, J.; Kiefer, M.; Helmchen, G.; Huttner, G.; Walter, O.; Zsolnai, L.; Reggelin, M. *Tetrahedron Lett.* **1994**, *35*, 1523. b) Pregosin, P. S.; Salzmann, R.; Togni, A. *Organometallics* **1995**, *14*, 842.

109 a) Mackenzie, P. B.; Whelan, J.; Bosnich, B. *J. Am. Chem. Soc.* **1985,** *107,* 2046. b) Takahashi, T.; Jinbo, Y.; Kitamura, K.; Tsuji, J. *Tetrahedron Lett.* **1984**, *25,* 5921. c) Granberg, K. L.; Bäckvall, J.-E. *J. Am. Chem. Soc.* **1992**, *114*, 6858.

110 a) Hansson, S.; Norrby, P.-O.; Sjögren, M. P. T.; Åkermark, B.; Cucciolito, M. E.; Giordano, F.; Vitagliano, A. *Organometallics* **1993**, *12*, 4940. b) Burckhardt, U.; Baumann, M.; Trabesinger, G.; Gramlich, V.; Togni, A. *Organometallics* **1997**, *16,* 5252. c) Burckhardt, U.; Baumann, M.; Togni, A. *Tetrahedron Asymmetry* **1997**, *8*, 155.

111 Brown, J. M.; Hulmes, D. I.; Guiry, P. J. *Tetrahedron* **1994**, *50*, 4493.

112 Martin, J. T.; Oslob, J. D.; Åkermark, B.; Norrby, P.-O. *Acta Chem. Scand.* **1995**, *49*, 888.

113 a) Bosnich, B.; Mackenzie, P. B. Pure Appl. Chem. **1982**, *54*, 189. b) Auburn, P. R.; Mackenzie, P. B.; Bosnich, B. *J. Am. Chem. Soc.* **1985**, *107*, 2033. c) Auburn, P. R.; Mackenzie, P. B.; Bosnich, B. *J. Am. Chem. Soc.* **1985**, *107*, 2046.

114 a) Kazmaier, U.; Zumpe, F. L. *Angew. Chem. Int. Ed.* **2000**, *39*, 802. b) Kazmaier, U.; Zumpe, F. L. *Eur. J. Org. Chem.* **2001**, *4067*.

115 Trost, B. M.; Dietsche, T. J. *J. Am. Chem. Soc.*, **1973**, *95*, 8200.

116 Trost, B. M.; Strege, P. E. *J. Am. Chem. Soc.* **1977**, *99*, 1650.

117 a) Hayashi, T.; Yamamoto, A.; Hagihara, T.; Ito, Y. *Tetrahedron Lett*. **1986**, *27*, 191. b) Hayashi, T.; Yamamoto, A.; Ito, Y. *Chem. Lett.* **1987**, 177. c) Hayashi, T. *Pure and Appl. Chem.* **1988**, *60*, 7.

118 Trost, B. M.; Van Vranken, D. L. *Angew. Chem., Int. Ed. Engl.* **1992**, *31*, 228.

119 Trost, B. M.; Van Vranken, D. L.; Bingel, C. *J. Am. Chem. Soc.* **1992**, *114*, 9327.

120 von Matt, P.; Pfaltz, A. *Angew. Chem. Int. Ed. Engl.* **1993**, *32,* 566.

121 Sprinz, J.; Helmchen, G. *Tetrahedron Lett*. **1993**, *34,* 1769.

122 a) Dawson, G. J.; Frost, C. G.; Williams, J. M. J.; Coote, S. J. *Tetrahedron Lett*. **1993**, *34,* 3149. b) Coote, S. J.; Dawson, G. J.; Frost, C. G.; Williams, J. M. J.; Coote, S. J. *Synlett* **1993**, 509.

123 a) Åkermark, B.; Krakenberger, B. Hansson, S. *Organomettalics* **1987**, *6*, 620.

124 For NMR studies, see: a) Steinhagen, H.; Reggelin, M.; Helmchen, G. *Angew. Chem. Int. Ed. Engl.* **1997**, *36*, 2108. b) Togni, A.; Burckhardt, U.; Gramlich, V.; Pregosin, P.; Salzmann, R. *J. Am. Chem. Soc.* **1996**, *118*, 1031.

125 For Computational studies, see: a) Blöchl, P. E.; Togni, A. *Organometallics* **1996**, *15,* 4125. b) Ward, T. R. *Organometallics* **1996**, 15, 2836. c) Goldfuss, B.; Kazmaier, U. *Tetrahedron* **2000**, *56*, 6493.

126 Helmchen, G.; Pfaltz, A. *Acc. Chem. Res.* **2000**, *33*, 336.

127 Lloyd-Jones, G. C.; Pfaltz, A. *Angew. Chem., Int. Ed.* **1995**, *34*, 462.

128 a) Janssen, J. P.; Helmchen, G. *Tetrahedron Lett.* **1997**, *38*, 8025. b) Lipowsky, G.; Miller, N.; Helmchen, G. *Angew. Chem. Intl. Ed.* **2004**, *43*, 4595.

129 Trost, B. M.; Hachiya, I. *J. Am. Chem. Soc.* **1998**, *120*, 1104.

130 Chelucci, G.; Thummel, R. P. *Chem. Rev.* **2002**, *102*, 3129.

131 Sjögren, M. ; Hansson, S.; Norrby, P.-O.; Åkermark, B.; Cucciolito, M. E.; Vitagliano, A. *Organometallics* **1992**, *11*, 3954.

132 Sjögren, M. P. T.; Hansson, S.; Åkermark, B.; Vitagliano, A. *Organometallics* **1994**, *13*, 1963.

133 Hagelin, H.; Åkermark, B.; Norrby, P.-O. *Chem. Eur. J.* **1999**, *5*, 902.

134 Sjögren, M. P. T. *Selectivity Control in Transition Metal-Catalyzed Nucleophilic Substitution of Allylic Leaving Groups*, Ph.D. Thesis, Royal Institute of Technology, Stockholm, Sweden, 1993.

135 Pedersen, T. M.; Hansen, E. L.; Kane, J.; Rein, T., Helquist, P.; Norrby, P.-O., Tanner, D. *J. Am. Chem. Soc.* **2001**, *123*, 9738.

136 a) Strand, D.; Rein. T., *Org. Lett.* **2005**, *7*, 199. b) Strand, D.; Rein, T. *Org. Lett.* **2005**, *7*, 2779. c) Strand, D.; Norrby, P.-O.; Rein, T. *J. Org. Chem.* **2006**, ASAP.

137 Jaguar 4.2, Schrödinger, Inc., Portland, OR, **1991-2000**, see http://schrodinger.com.

138 Hay, P. J.; Wadt, W. R. *J. Chem. Phys.* **1985**, *82*, 299.

139 a) Norrby, P.-O.; Åkermark, B.; Hæffner, F.; Hansson, S.; Blomberg, M. *J. Am. Chem. Soc.* **1993**, *115*, 4859. b) Hagelin, H.; Åkermark, B.; Norrby, P.-O. *Organometallics* **1999**, *18*, 2884.

140 Oslob, J. D.; Åkermark, B.; Helquist, P.; Norrby, P.-O. *Organometallics* **1997**, *16*, 3015.

141 Fiaud, J.-C.; Malleron, J. L. *Tetrahedron Lett.* **1981**, *22*, 1399.

142 Trost, B. M.; Schmuff, N. R. *Tetrahedron Lett.* **1981**, *22*, 2999.

143 Hayashi, T.; Kishi, K.; Yamamoto, A.; Ito, Y. *Tetrahedron Lett.* **1990**, *31*, 1743.

144 Blacker, A. J.; Clarke, M. L.; Loft, M. S.; Williams, J. M. J. *Org. Lett.* **1999**, *12*, 1969.

145 a) Lloyd-Jones, G. C.; Stephen, S. C. *Chem. Eur. J.* **1998**, *4,* 2539. b) Lloyd-Jones, G. C.; Stephen, S. C.; Murray, M.; Butts, C. P.; Vyskocil, S.; Kocovsky, P. *Chem. Eur. J.* **2000**, *6,* 4348. c) Lloyd-Jones, G. C. *Synlett* **2001**, *2*, 161. d) Fairlamb, I. J. S.; Lloyd-Jones, G. C.; Vyskocil, S.; Kocovsky, P. *Chem. Eur. J.* **2002**, *8,* 4443. e) Gouriou, L.; Lloyd-Jones, G. C.; Vyskovil, S.; Kocovsky, P. *J. Organomet. Chem.* **2003**, *687*, 525.

146 Trost, B. M.; Bunt, R. C. *J. Am. Chem. Soc.* **1996**, *118*, 235.

147 Butts, C. P.; Crosby, J.; Lloyd-Jones, G. C.; Stephen, S. C. *Chem. Commun.* **1999**, 1707.

148 Fagnou, K.; Lautens, M. *Angew. Chem. Int. Ed.* **2002**, *41*, 26.

149 a) Amatore, C.; Jutand, A.; M'Barki, M. A.; Meyer, G.; Mottier, L. *Eur. J. Inorg. Chem.* **2001**, 873. b) Jutand, A. *Eur. J. Inorg. Chem.* **2003**, 2017.

150 Landis, C. R.; Halpern, J. *J. Am. Chem. Soc.* **1987**, *109*, 1746.

151 a) Amatore, C.; Azzabi, M.; Jutand. A. *J. Am. Chem. Soc.* **1991**, *113*, 8375. b) Mosleh, A.; Jutand, A. *Organometallics* **1995**, *14*, 1810. c) Roy, A. H.; Hartwig, J. F. *Organometallics* **2004**, *23*, 194.

152 Kozuch, S.; Shaik, S.; Jutand, A.; Amatore, *C. Chem. Eur. J.* **2004**, *10*, 3072.

153 Searle, M. S.; Westwell, M. S.; Williams, D. H. *J. Chem. Soc., Perkin Trans. 2* **1995**, 141.

154 a) Szabo, M. J.; Galea, N. M.; Michalak, A.; Yang, S.-Y.; Groux, L. F.; Piers, W. E.; Ziegler, T. *J. Am. Chem. Soc.* **2005**, *127*, 14692. b) Woo, T. K.; Blöchl, P. E.; Ziegler, T. *J. Phys. Chem. A* **2000**, *104*, 121.

155 Ahlquist, M.; Kozuch, S.; Shaik, S.; Tanner, D.; Norrby, P.-O. *Organometallics* **2005**, *25*, 45.

156 Ahlquist, M.; Fabrizi, G.; Cacchi, S.; Norrby, P.-O. *Chem. Commun.* **2005**, *33*, 4196.

157 a) Senn, H. M.; Ziegler, T. *Organometallics* **2004**, *23*, 2980. b) Ahlquist. M.; Fristrup. P.; Tanner D.; Norrby P.-O. *Organometallics* **2006**, *accepted*.

158 Popp, B. V.; Thorman, J. L.; Morales, C. M.; Landis, C. R.; Stahl, S. S. *J. Am. Chem. Soc.* **2004**, *126*, 14832.

159 a) Szabo, K. J. *Chem. Eur. J.* **2000**, *6*, 4413. b) Solin, N.; Kjellgren, J.; Szabo, K. J. *Angew. Chem. Int. Ed.* **2003**, *42*, 3656. c) Solin, N.; Kjellgren, J.; Szabo, K. J. *J. Am. Chem. Soc.* **2004**, *126*, 7026.

160 a) Giambastiani, G.; Pacini, B.; Porcelloni, M.; Poli, G. *J. Org. Chem.* **1998**, *63*, 804. b) Poli, G.; Giambastiani, G. *J. Org. Chem.* **2002**, *67*, 9456. c) Thorimbert, S.; Giambastiani, G.; Commandeur, C.; Vitale, M.; Poli, G.; Malacria, M. *Eur. J. Org. Chem.* **2003**, 2702. d) Lemaire, S.; Giambastiani, G.; Prestat, G.; Poli, G. *Eur. J. Org. Chem.* **2004**, 2840.

161 Norrby, P.-O.; Mader, M. M.; Vitale, M.; Prestat, G.; Poli, G. *Organometallics*, **2003**, *22*, 1849.

162 Madec, D.; Prestat, G.; Martini, E.; Fristrup, P.; Poli, G.; Norrby, P.-O. *Org. Lett.* **2005**, *7*, 995.

163 Caron, M.; Sharpless, K. B. *J. Org. Chem.* **1985**, *50*, 1557.

164 Meunier, B.; de Visser, S. P.; Shaik, S. *Chem. Rev.* **2004**, *104*, 3947

165 Groves, J. T.; Nemo, T. E. *J. Am. Chem. Soc.* **1983**, *105*, 5786.

166 Samsel, E. G.; Srinivasan, K.; Kochi, J. K. *J. Am. Chem. Soc.* **1985**, *107*, 7606.

167 Srinivasan, K.; Kochi, J. K. *Inorg. Chem.* **1985**, *24*, 4671.

168 Srinivasan, K.; Michaud, P.; Kochi, J. K. *J. Am. Chem. Soc.* **1986**, *108*, 2309.

169 Groves, J. T.; Nemo, T. E.; Myers, R. S. *J. Am. Chem. Soc.* **1979**, *101*, 1032.

170 Ferringer, D.; Plattner, D. A. *Angew. Chem., Int. Ed. Engl.* **1997**, *36*, 1718.

171 For recent reviews, see a) McGarrigle, E. M.; Gilheany, D. G. *Chem. Rev* **2005**, *105*, 1563. b) Xia, Q.-H.; Ge, H.-Q.; Ye, C.-P.; Liu, Z.-M.; Su, K.-X. *Chem. Rev.* **2005**, *105*, 1603.

172 Jacobsen, E. N.; Zhang, W.; Muci, A. R.; Ecker, J. R.; Deng, L. *J. Am. Chem. Soc.* **1991**, *113*, 7063.

173 http://www.sigmaaldrich.com/Brands/Fluka___Riedel_Home/Miscellaneous/Reagent_of_the_Year/1994.html

174 Skarzewski, J.; Gupta, A.; Vogt, A. *J. Mol. Cat. A* **1995**, *103*, L63.

175 Finney, N. S.; Pospisil, P. J.; Chang, S.; Palucki, M.; Konsler, R. G.; Hansen, K. B.; Jacobsen, E. N. *Angew. Chem. Int. Ed. Engl.* **1997**, *36*, 1720.

176 Miura, K.; Katsuki, T. *Synlett* **1999**, 783.

177 Chang, S.; Galvin, J. M.; Jacobsen, E. N. *J. Am. Chem. Soc.* **1994**, *116*, 6937.

178 Norrby, P.-O.; Linde, C.; Åkermark, B. *J. Am. Chem. Soc.* **1995**, *117*, 11035.

179 Sharpless, K. B.; Teranishi, A. Y.; Bäckvall, J.-E. *J. Am. Chem. Soc.* **1977**, *99*, 3120

180 Jørgensen, K. A.; Schiøtt, B. *Chem. Rev.* **1990**, *90*, 1483.

181 Hamada, T.; Fukuda, T.; Imanishi, H.; Katsuki, T. *Tetrahedron* **1996**, *52*, 515.

182 Linde, C.; Arnold, M.; Norrby, P.-O.; Åkermark, B. *Angew. Chem. Int. Ed. Engl.* **1997**, *36*, 1723.

183 Palucki, M.; Finney, N. S.; Pospisil, P. J.; Guler, M. L.; Ishida, T.; Jacobsen, E. N. *J. Am. Chem. Soc.* **1998**, *120*, 948.

184 Smith, M. B.; March, J. *March's Advanced Organic Chemistry*; 5th Edition; John Wiley & Sons, New York, 2001, pp. 284-285.

185 Cavallo, L.; Jacobsen, H. *J. Org. Chem.* **2003**, *68*, 6202.

186 a) Linde, C.; Åkermark, B.; Norrby, P.-O.; Svensson, M. *J. Am. Chem. Soc.* **1999**, *121*, 5083. b) Schröder, D.; Shaik, S.; Schwarz, H. *Acc. Chem. Res.* **2000**, *33*, 139.

187 For a review, see: Limberg, C. *Angew. Chem., Int. Ed.* **2003**, *42*, 593

188 Linde, C.; Koliaï, N.; Norrby, P.-O.; Åkermark, B. *Chem. Eur. J.* **2002**, *8*, 2568.

189 Kolb, H. C.; Sharpless, K. B. *Tetrahedron* **1992**, *48*, 10515.

190 Tu, Y.; Wang, Z. X.; Shi, Y. *J. Am. Chem. Soc.* **1996**, *118*, 9806.

191 Kolb, H. C.; VanNieuwenzhe, M. S.; Sharpless, K. B. *Chem. Rev.* **1994**, *94*, 2483.

192 Fukuda, T.; Irie, R.; Katsuki, T. *Synlett* **1995**, 197.

193 Brandes, B. D.; Jacobsen, E. N. *J. Org. Chem.* **1994**, *59*, 4378.

194 Schröder, M. *Chem. Rev*., **1980**, *80*, 187.

195 Hofmann, K. A. *Chem. Ber*. **1912**, *45*, 3329.

196 Criegee, R.; Marchand, B. ; Wannowius, H. *Justus Liebigs Ann. Chem.* **1942**, *550*, 99.

197 Hentges, S. G. ; Sharpless, K. B. *J. Am. Chem. Soc.* **1980**, *102*, 4263.

198 Markó, I. E.; Svendsen, J. S. In *Comprehensive Asymmetric Catalysis I-III*; Jacobsen, E. N.; Pfaltz, A.; Yamamoto, H.; Eds.; Springer Verlag: Berlin, 2000, Chapter 20.

199 Crispino, G. A.; Sharpless, K. B. *Tetrahedron Lett.* **1992**, *33*, 4273.

200 Johnson, R. A.; Sharpless, K. B. In *Catalytic Asymmetric Synthesis*; 2nd Edition; Ojima, I., Ed.; Wiley-VCH, New York, 2000, chapter 6D.

201 Becker, H.; Sharpless, K. B.; *Angew. Chem. Int. Ed.* **1996**, *35*, 448.

202 Bolm, C.; Hildebrand, J. P.; Muñiz, K. In *Catalytic Asymmetric Synthesis*; 2nd Edition; Ojima, I., Ed.; Wiley-VCH, New York, 2000, Chapter 6E.

203 Jacobsen, E. N. ; Markó, I. ; Mungall, W. S. ; Schröder, G. ; Sharpless, K. B. *J. Am. Chem. Soc.* **1988**, *110,* 1968.

204 Van Rheenen, V. ; Kelly, R. C.; Cha, D. Y. *Tetrahedron Lett.*, **1976**, 1973.

205 Minato, M.; Yamamoto, K.; Tsuji, J. *J. Org. Chem.* **1990**, *55,*766.

206 Wai, J. S. M.; Markó, I.; Jacobsen, E. N.; Pulla Rao, C.; Bott., S.; Sharpless, K. B. *J. Org. Chem.* **1989**, *111*, 1123.

207 Böseken, J. *Rec. Trav. Chim*. **1922**, *41*, 199.

208 Göbel, T.; Sharpless, K. B. *Angew. Chem., Int. Ed. Engl.* **1993**, *32*, 1329.

209 Corey, E. J.; Noe, M. C. *J. Am. Chem. Soc.* **1996**, *118*, 11038.

210 Corey, E. J.; Noe, M. C. *J. Am. Chem. Soc.* **1996**, *118*, 319.

211 Kolb, H. C.; Andersson, P. G.; Sharpless, K. B. *J. Am. Chem. Soc.* **1994**, *116*, 1278.

212 Corey, E. J.; Noe, M. C.; Grogan, M. J. *Tetrahedron Lett.* **1996**, *37*, 4899.

213 Delmonte, A. J.; Haller, J.; Houk, K. N.; Sharpless, K. B.; Singleton, D. A.; Strassner, T.; Thomas, A. A. *J. Am. Chem. Soc.* **1997**, *119*, 9907.

214 Veldkamp, A.; Frenking, G. *J. Am. Chem. Soc.* **1994**, *116*, 4937.

215 Dapprich, S.; Ujaque, G.; Maseras, F.; Lledós, A.; Musaev, D. G.; Morokuma, K. *J. Am. Chem. Soc.* **1996**, *118*, 11660.

216 Torrent, M.; Deng, L. Q.; Duran, M.; Sola, M.; Ziegler, T. *Organometallics* **1997**, *16*, 13.

217 Norrby, P.-O.; Rasmussen, T.; Haller, J.; Strassner, T.; Houk, K. N. *J. Am. Chem. Soc.* **1999**, *121*, 10186.

218 a) Sharpless, K. B.; Amberg, W.; Beller, M.; Chen, H.; Hartung, J.; Kawanami, Y.; Lübben, D.; Manoury, E.; Ogino, Y.; Shibata, T.; Ukita, T. *J. Org. Chem.* **1991**, *56*, 4585. b) Sharpless, K. B.; Amberg, W.; Bennani, Y. L.; Crispino, G. A.; Hartung, J.; Jeong, K.-S.; Kwong, H.-L.; Morikawa, K.; Wang, Z.-M.; Xu, D.; Zhang, X.-L. *J. Org. Chem.* **1992**, *57*, 2768.

219 Berrisford, D. J.; Bolm, C.; Sharpless, K. B. *Angew. Chem., Int. Ed. Engl.* **1995**, *34*, 1059.

220 Pearlstein R. M.; Blackburn, B. K.; Davis, W. M.; Sharpless K. B. *Angew. Chem. Int. Ed. Engl.* **1990**, *29*, 639.

221 a) Corey, E. J.; Noe, M. C.; Sarshar, S. *Tetrahedron Lett.* **1994**, *35*, 2861. b) Corey, E. J.; Noe, M. C.; Grogan, M. J. *Tetrahedron Lett.* **1994**, *35*, 6427. c) Corey, E. J.; Noe, M. C. *J. Am. Chem. Soc.* **1996**, *118*, 11038. d) Corey, E. J.; Zhang, J. *Org. Lett.* **2001**, *3*, 3211.

222 Norrby, P.-O.; Kolb, H. C.; Sharpless, K. B. *J. Am. Chem. Soc.* **1994**, *116*, 8470.

223 Goodman, J. M.; Still, W. C. *J. Comput. Chem.* **1991**, *12*, 1110.

224 Chang, G.; Guida, W. C.; Still, W. C. *J. Am. Chem. Soc.* **1990**, *112*, 1419.

225 Kolossvary, I.; Guida, W. C. *J. Am. Chem. Soc.* **1996**, *118*, 5011.